Chapter 5
TEST PROBLEMS AND NUMERICAL RESULTS

In this chapter, numerical experiments of the simple and high order continuum traffic flow models simulated by the high resolution schemes have been carried out. First we tested and compared the numerical accuracies and stabilities of WENO finite volume (FV), TVD slope-limiter finite difference (FD), and other simple numerical schemes, including the Upwind, Lax-Friedrichs, Leapfrog, Beam-Warming, Lax-Wendroff, MacCormack, Godunov, for the Riemann problems in the LWR model. Four test problems in the LWR model were conducted against the exact solutions. Then the method which has the most accurate LWR solutions was applied to solve three test problems of high order continuum models. In these examples, WENO scheme was found to be numerically stable and dominantly accurate, but cost more execution time. The programming jobs were run on a PC equipped with AMD Duron^{TM} 600 MHz processor, 128 MB (PC-100) SDRAM, and 15GB (5,400 RPM) hard drive. Detailed descriptions of these test problems were given as follows.

5.1 Numerical Examples for LWR Model

In this section, numerical solutions of Riemann problems, including shocks and rarefaction waves, traffic signal, and square wave problem in LWR model were presented.

5.1.1 Shock Problems

The shock problem, which is a class of Riemann problems, was formulated as follows:

Greenshieds flow-density relationship: $q = ku_f(1-\frac{k}{k_j})$

LWR model: $\frac{\partial k(x,t)}{\partial t}+\frac{\partial q(x,t)}{\partial x}=0$

Free-flow speed u_f = 90 km/hr

Jam density k_j = 180 veh/km

Length of road section = 30 km

The road section is discretized into 99 segments (100 nodes), each segment 303m long. The initial condition for the Riemann problem can be given as follows:

$$k(x,0)=\begin{cases}k_l, & x<0\\ k_r, & x>0\end{cases}$$

where k_l and k_r are upstream and downstream densities, respectively.

5.1.1.1 Case I

For case I of the shock problems, the initial condition was assumed as follows:

$$k(x,0)=\begin{cases}10, & 0\le x<15\\ 70, & 15\le x\le 30\end{cases}.$$

The numerical results of these schemes are presented in Figure 5.1-5.18.

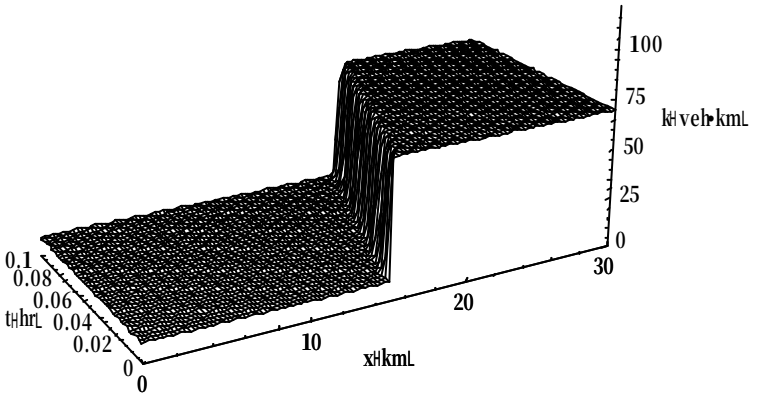

Figure 5.1. The density behavior for case I of shocks simulated by the Upwind scheme.

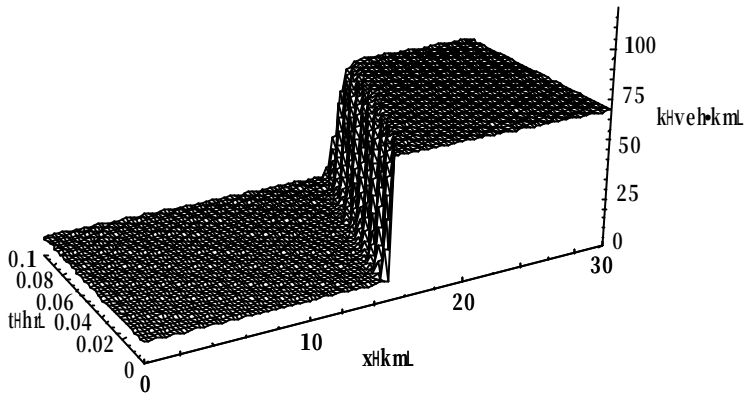

Figure 5.2. The density behavior for case I of shocks simulated by the Lax-Friedrichs scheme.

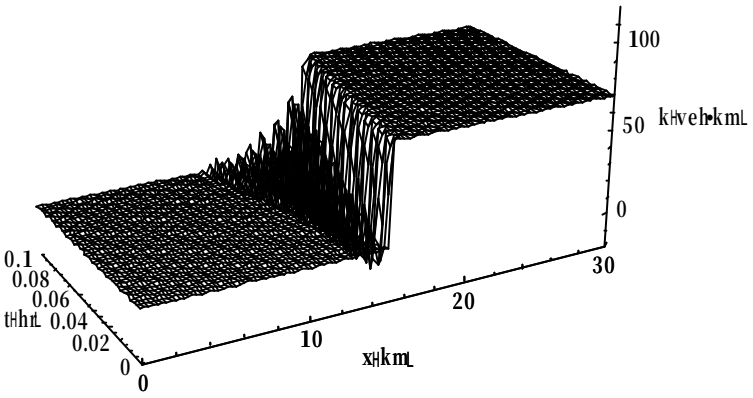

Figure 5.3. The density behavior for case I of shocks simulated by the Leapfrog scheme.

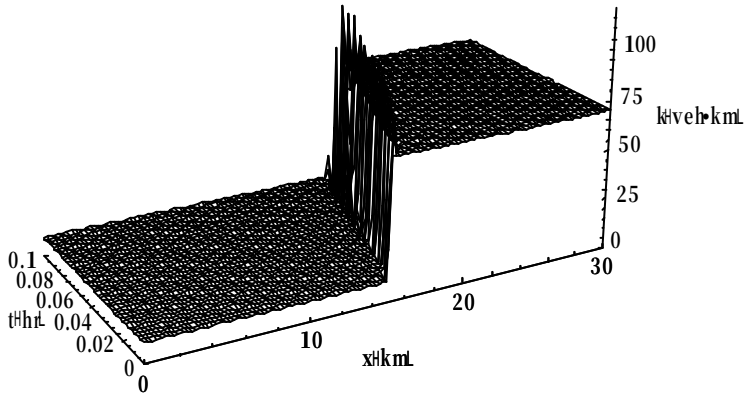

Figure 5.4. The density behavior for case I of shocks simulated by the Beam-Warming scheme.

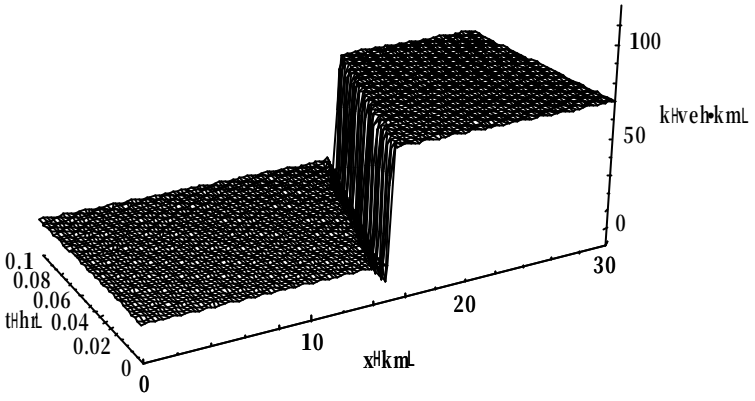

Figure 5.5. The density behavior for case I of shocks simulated by the Lax-Wendroff scheme.

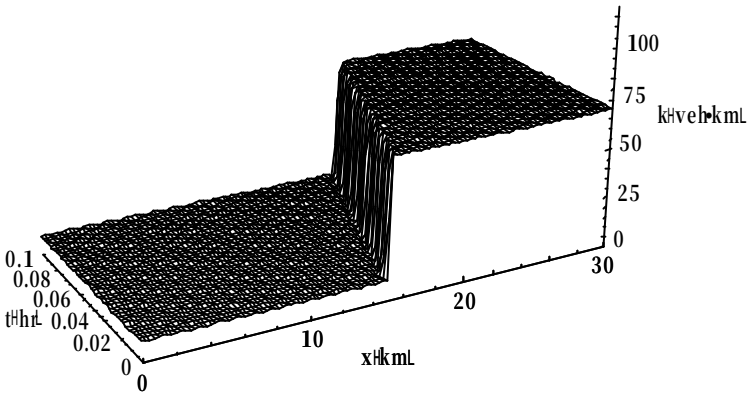

Figure 5.6. The density behavior for case I of shocks simulated by the MacCormack scheme.

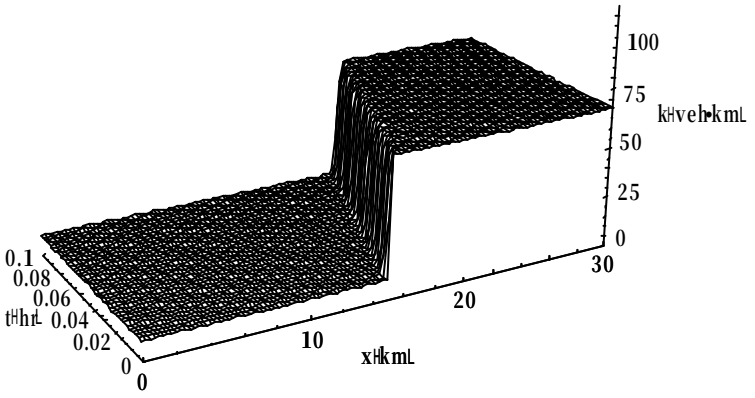

Figure 5.7. The density behavior for case I of shocks simulated by the Godunov scheme.

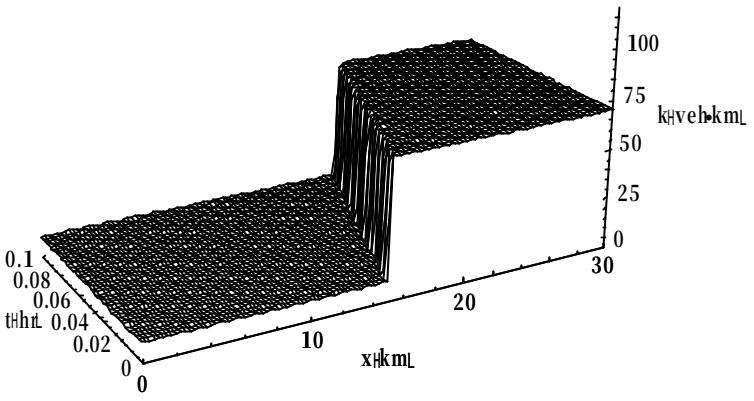

Figure 5.8. The density behavior for case I of shocks simulated by TVD slope-limiter scheme.

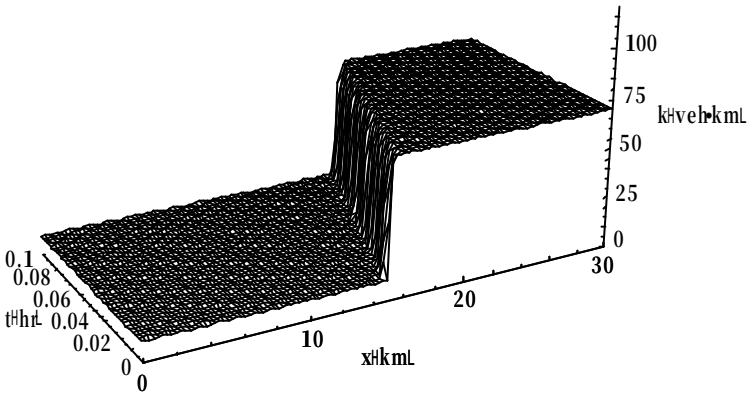

Figure 5.9. The density behavior for case I of shocks simulated by WENO FV scheme.

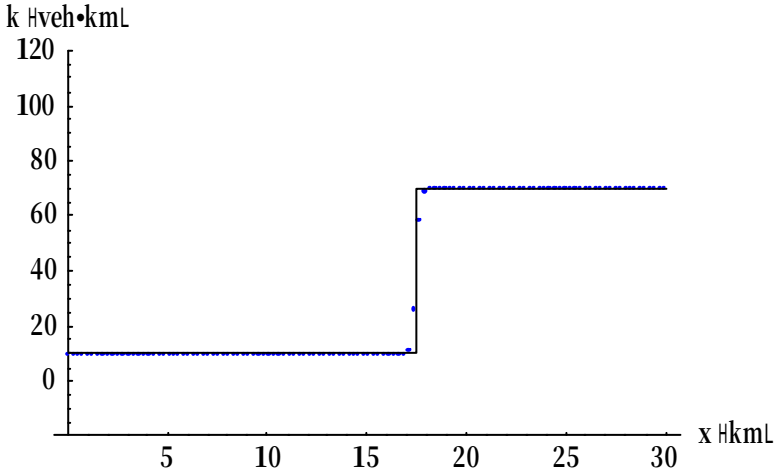

Figure 5.10. The density profile at t = 0.05hr for case I of shocks simulated by the Upwind scheme.

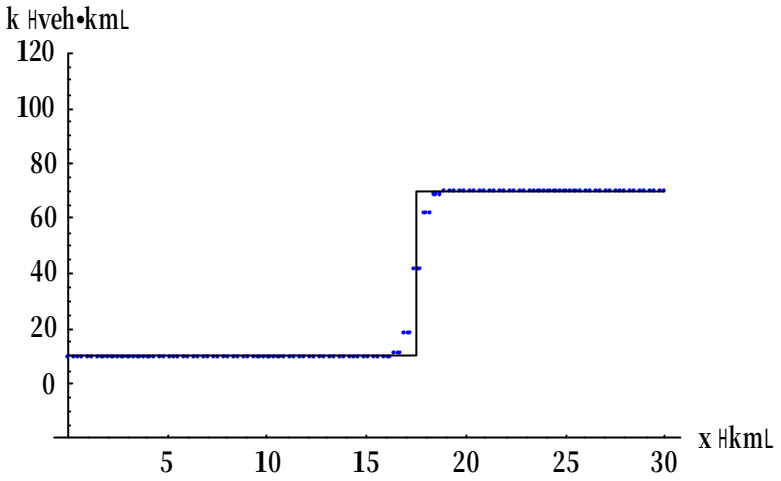

Figure 5.11. The density profile at t = 0.05hr for case I of shocks simulated by the Lax-Friedrichs scheme.

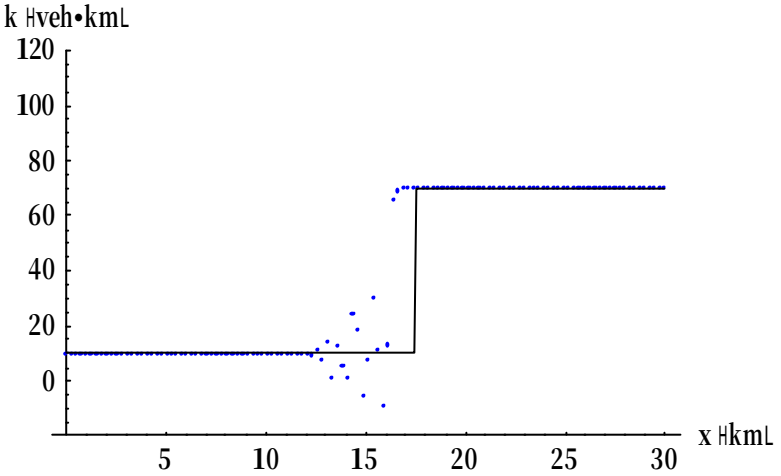

Figure 5.12. The density profile at t = 0.05hr for case I of shocks simulated by the Leapfrog scheme.

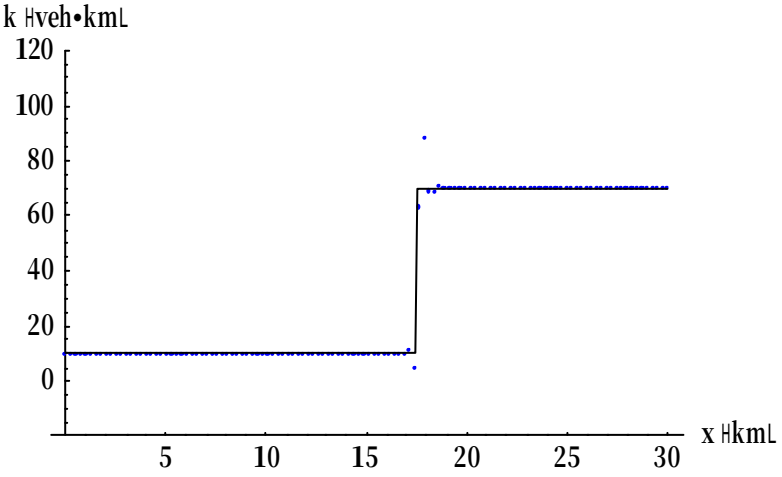

Figure 5.13. The density profile at t = 0.05hr for case I of shocks simulated by the Beam-Warming scheme.

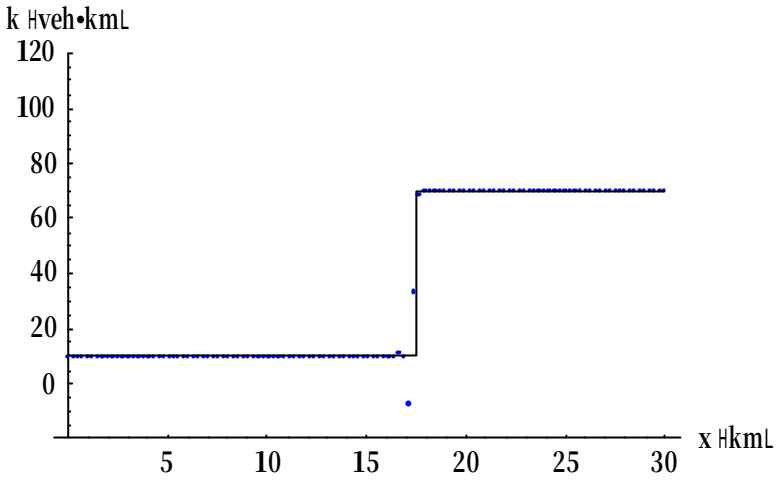

Figure 5.14. The density profile at t = 0.05hr for case I of shocks simulated by the Lax-Wendroff scheme.

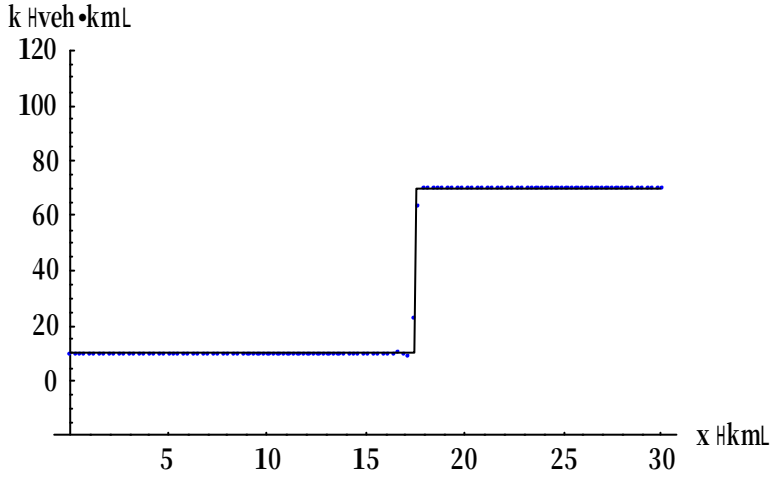

Figure 5.15. The density profile at t = 0.05hr for case I of shocks simulated by the MacCormack scheme.

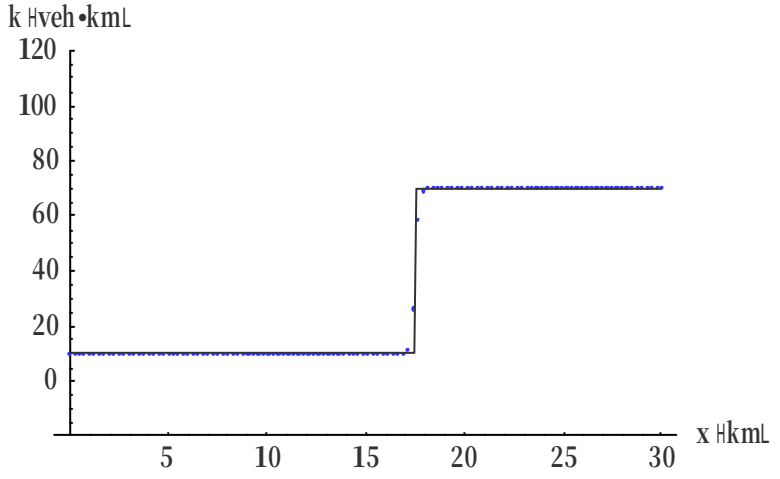

Figure 5.16. The density profile at t = 0.05hr for case I of shocks simulated by the Godunov scheme.

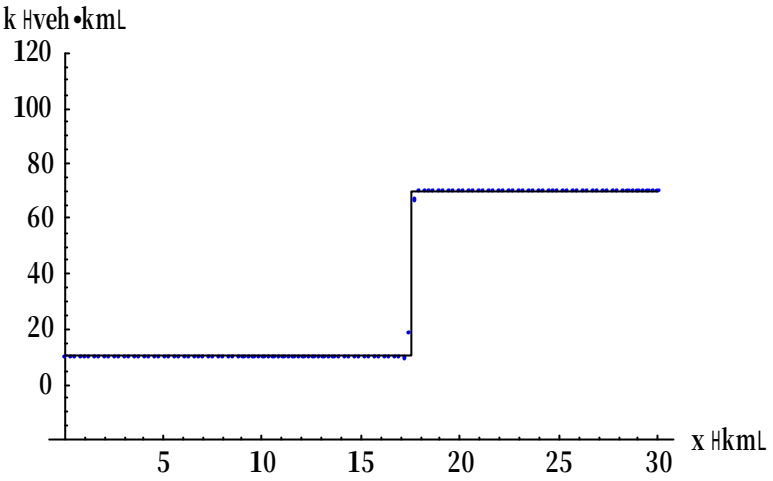

Figure 5.17. The density profile at t = 0.05hr for case I of shocks simulated by TVD slope-limiter scheme.

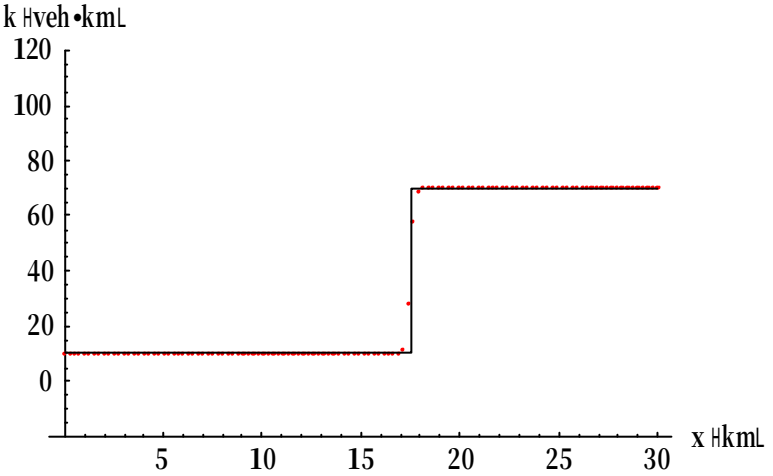

Figure 5.18. The density profile at t = 0.05hr for case I of shocks simulated by WENO FV scheme.

Obviously, the results indicate that the Leapfrog and Beam-Warming schemes have poor numerical stability.

5.1.1.2 Case II

For case II of the shock problems, the initial condition was assumed as follows:

$$k(x,0)=\begin{cases}10, & 0\le x<15\\ 110, & 15\le x\le 30\end{cases}.$$

The numerical results of these schemes are presented in Figure 5.19-5.26.

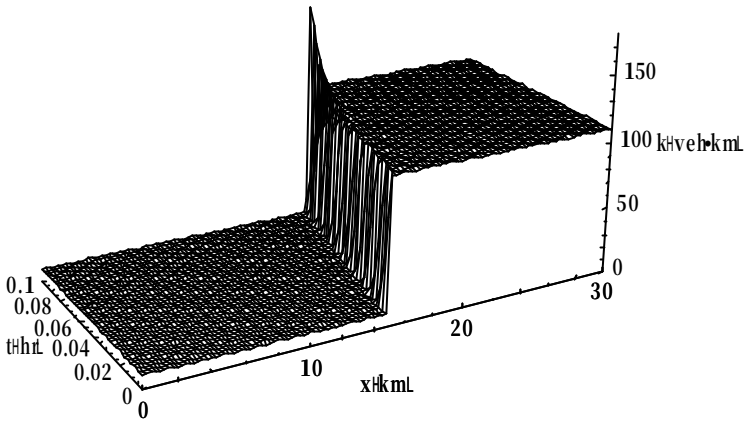

Figure 5.19. The density behavior for case II of shocks simulated by the Upwind scheme.

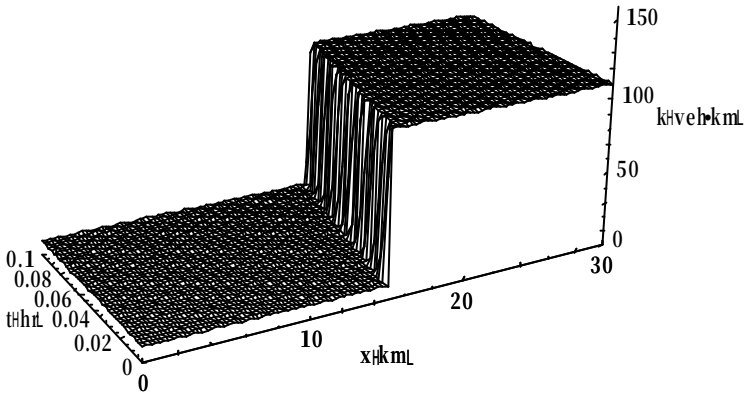

Figure 5.20. The density behavior for case II of shocks simulated by the Godunov scheme.

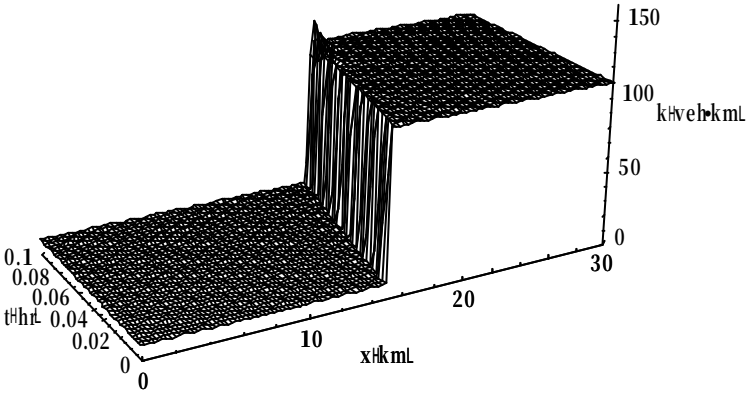

Figure 5.21. The density behavior for case II of shocks simulated by TVD slope-limiter scheme.

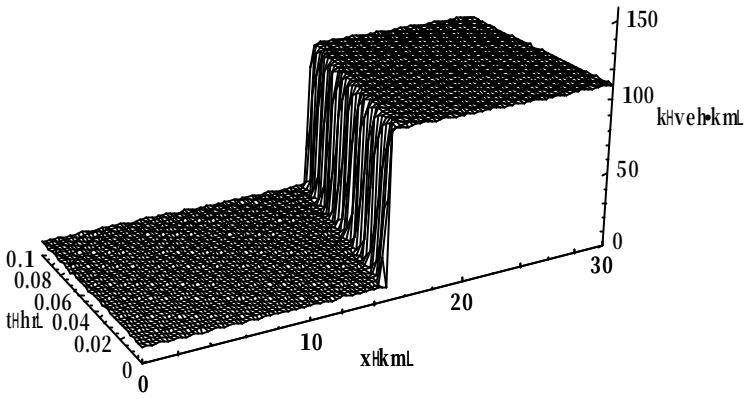

Figure 5.22. The density behavior for case II of shocks simulated by WENO FV scheme.

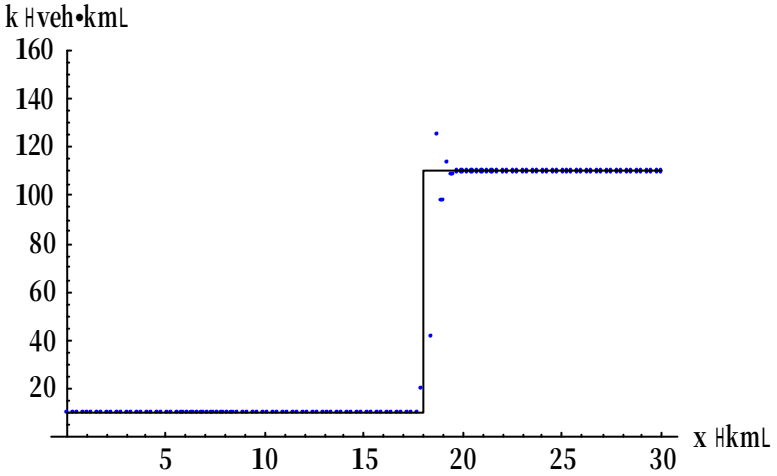

Figure 5.23. The density profile at t = 0.05hr for case II of shocks simulated by the Upwind scheme.

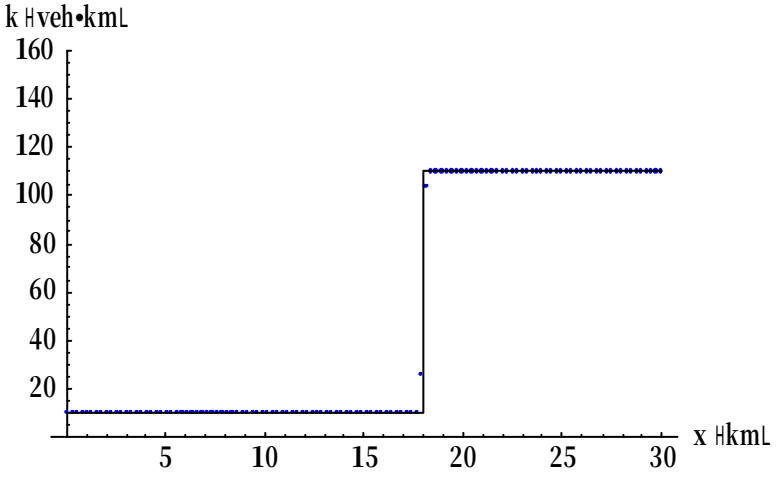

Figure 5.24. The density profile at t = 0.05hr for case II of shocks simulated by the Godunov scheme.

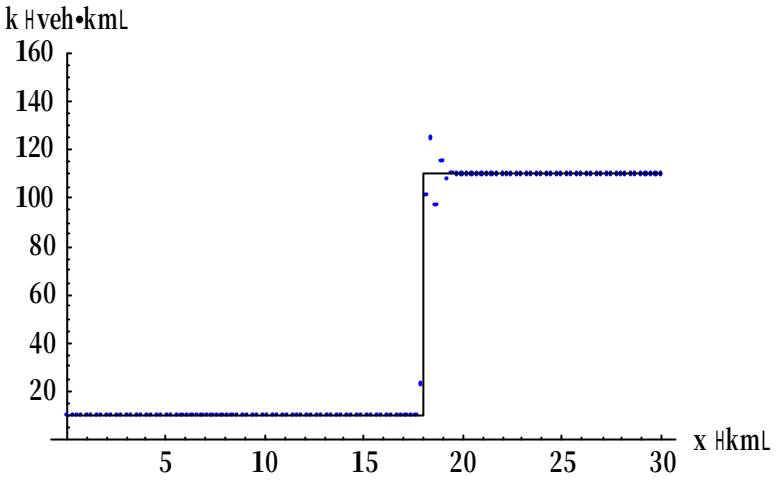

Figure 5.25. The density profile at t = 0.05hr for case II of shocks simulated by TVD slope-limiter scheme.

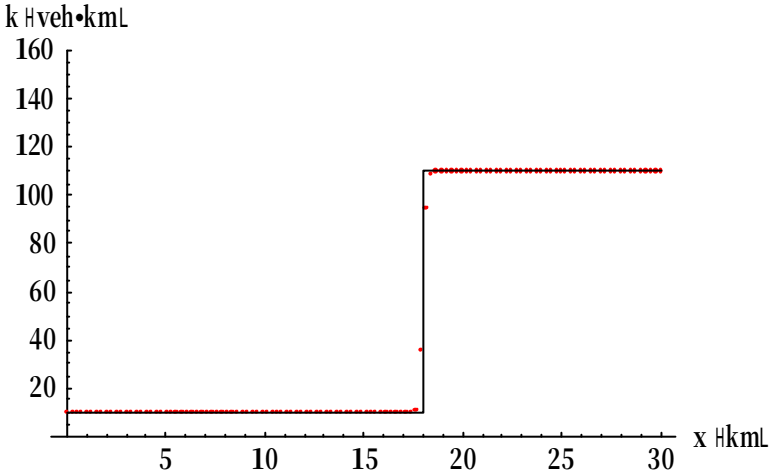

Figure 5.26. The density profile at t = 0.05hr for case II of shocks simulated by WENO FV scheme.

In case II, the Upwind scheme loses its accuracy after t = 0.05 hr and then becomes worse and worse. Only the Godunov and WENO FV schemes have the desirable accuracy.

5.1.2 Rarefaction Wave Problems

In the rarefaction wave problems, all the formulations were the same as the shock problems except the initial conditions.

5.1.2.1 Case I

For case I of the rarefaction wave problems, the initial condition was assumed as follows:

$$k(x,0)\begin{cases}80, & 0 \le x < 15\\ 20, & 15 \le x \le 30\end{cases}.$$

The numerical results of these schemes are presented in Figure 5.27-5.44.

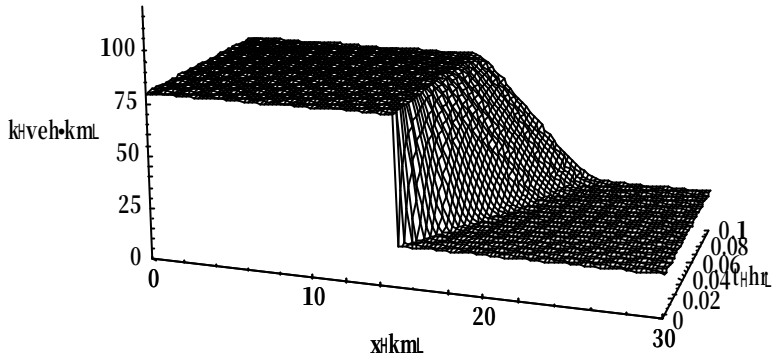

Figure 5.27. The density behavior for case I of rarefaction waves simulated by the Upwind scheme.

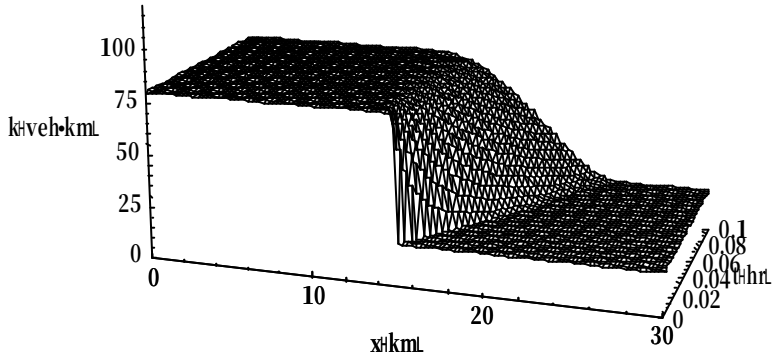

Figure 5.28. The density behavior for case I of rarefaction waves simulated by the Lax-Friedrichs scheme.

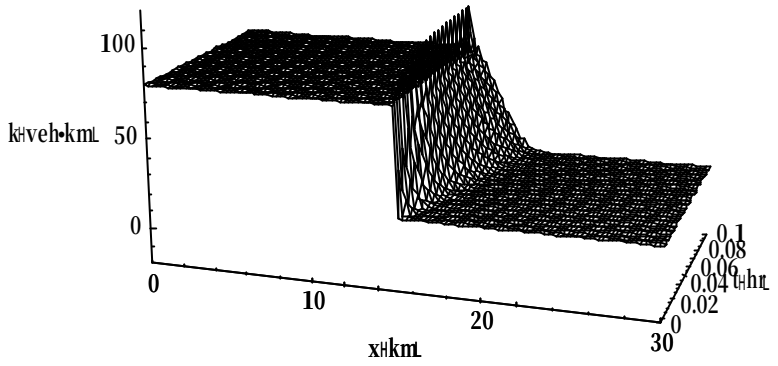

Figure 5.29. The density behavior for case I of rarefaction waves simulated by the Leapfrog scheme.

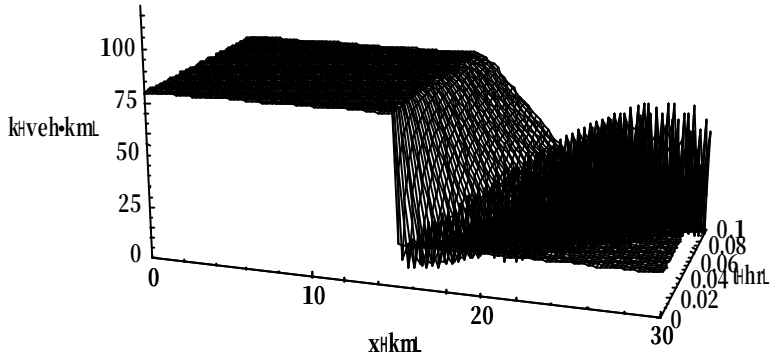

Figure 5.30. The density behavior for case I of rarefaction waves simulated by the Beam-Warming scheme.

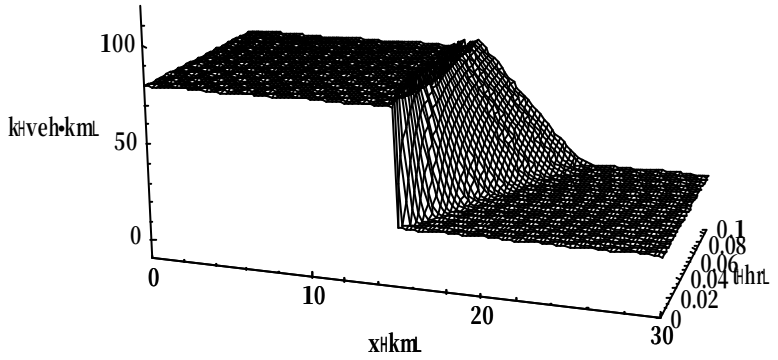

Figure 5.31. The density behavior for case I of rarefaction waves simulated by the Lax-Wendroff scheme.

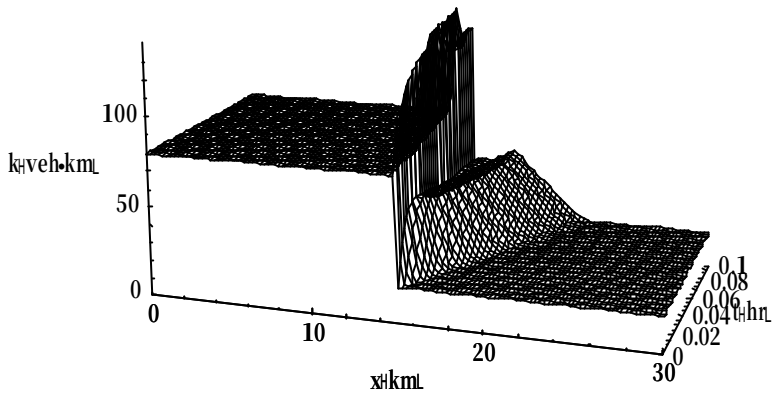

Figure 5.32. The density behavior for case I of rarefaction waves simulated by the MacCormack scheme.

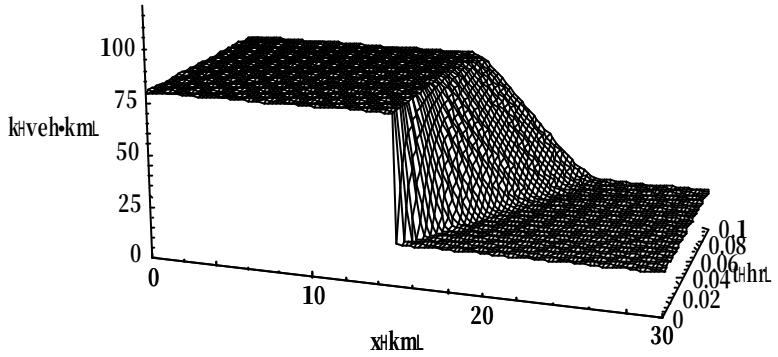

Figure 5.33. The density behavior for case I of rarefaction waves simulated by the Godunov scheme.

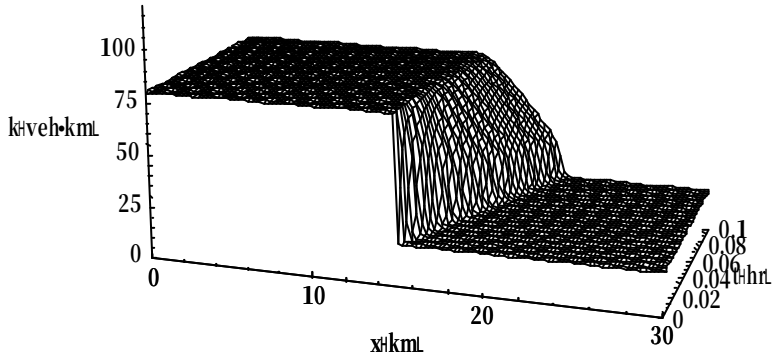

Figure 5.34. The density behavior for case I of rarefaction waves simulated by TVD slope-limiter scheme.

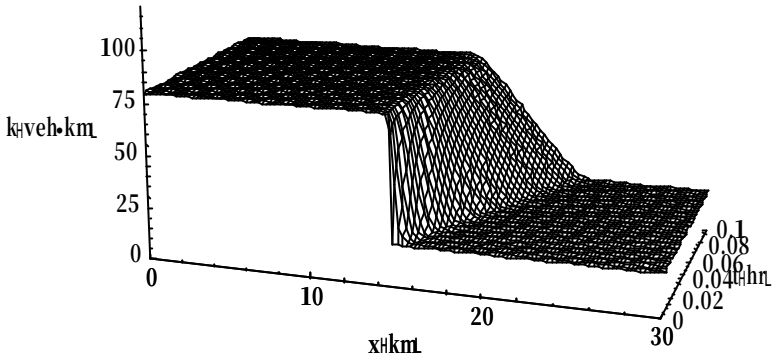

Figure 5.35. The density behavior for case I of rarefaction waves simulated by WENO FV scheme.

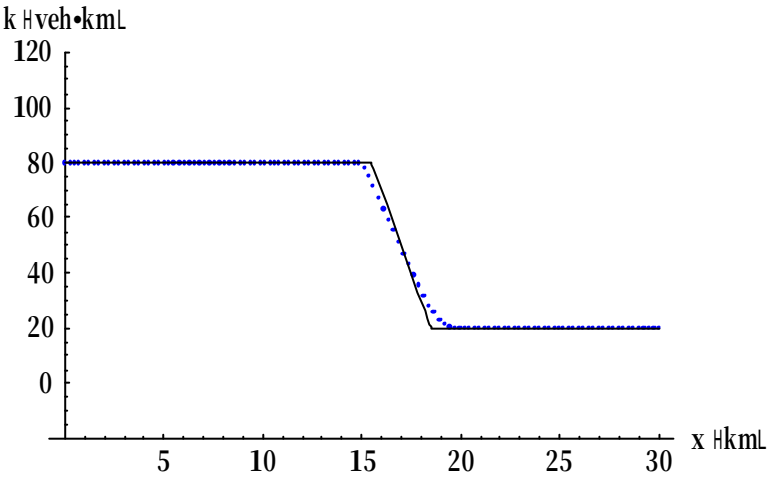

Figure 5.36. The density profile at t = 0.05hr for case I of rarefaction waves simulated by the Upwind scheme.

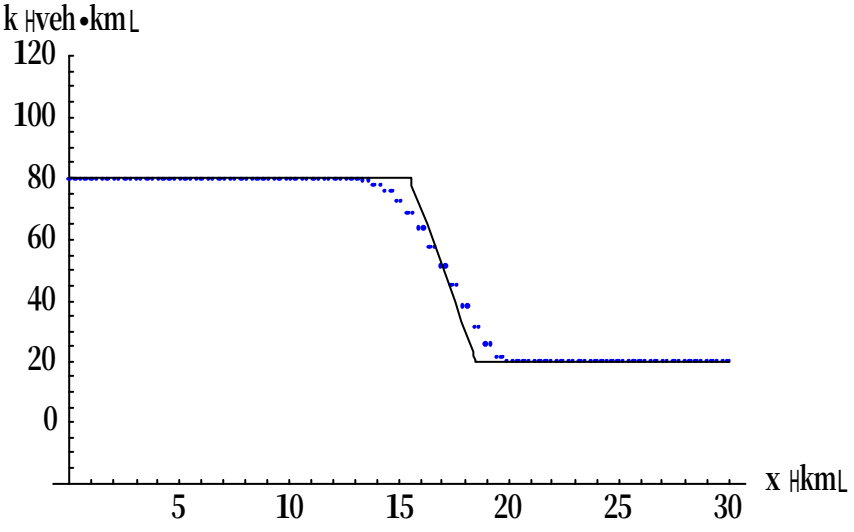

Figure 5.37. The density profile at t = 0.05hr for case I of rarefaction waves simulated by the Lax-Friedrichs scheme.

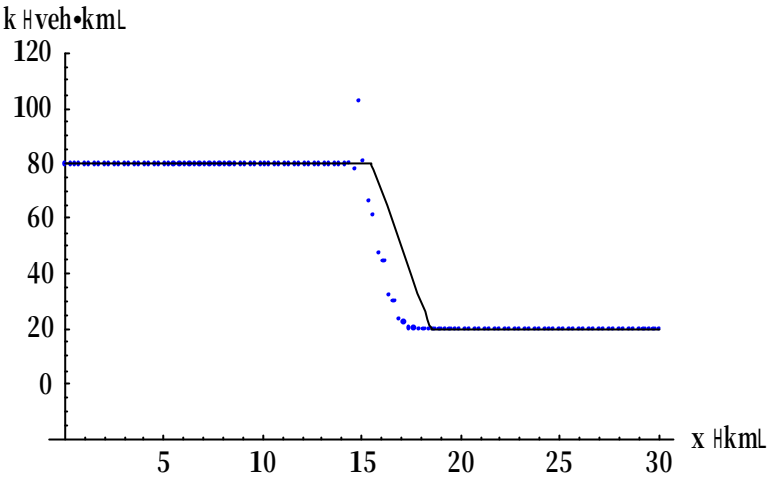

Figure 5.38. The density profile at t = 0.05hr for case I of rarefaction waves simulated by the Leapfrog scheme.

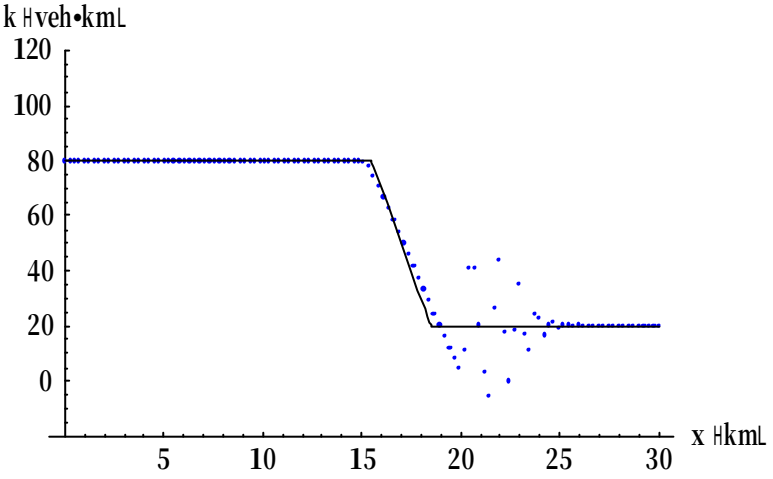

Figure 5.39. The density profile at t = 0.05hr for case I of rarefaction waves simulated by the Beam-Warming scheme.

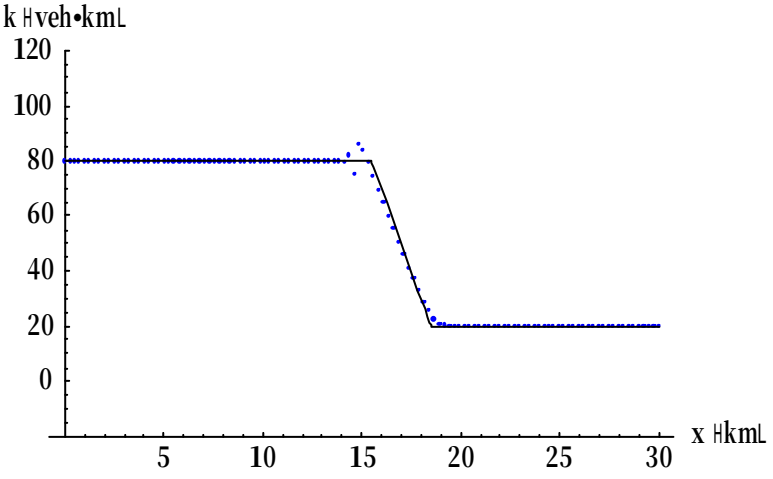

Figure 5.40. The density profile at t = 0.05hr for case I of rarefaction waves simulated by the Lax-Wendroff scheme.

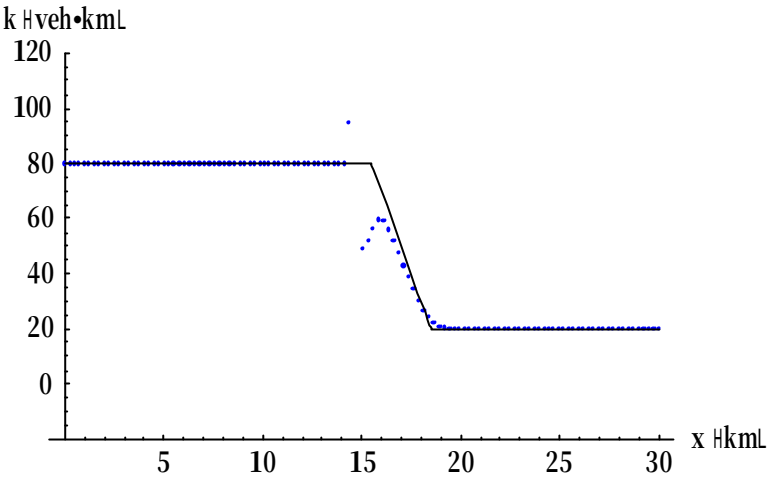

Figure 5.41. The density profile at t = 0.05hr for case I of rarefaction waves simulated by the MacCormack scheme.

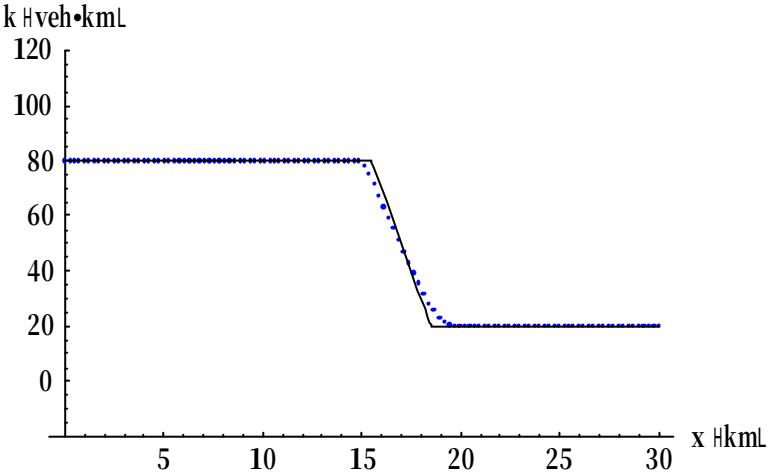

Figure 5.42. The density profile at t = 0.05hr for case I of rarefaction waves simulated by the Godunov scheme.

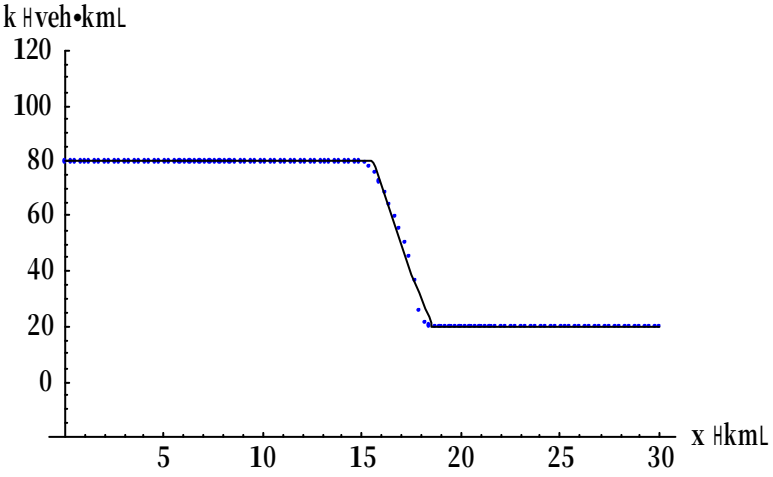

Figure 5.43. The density profile at t = 0.05hr for case I of rarefaction waves simulated by TVD slope-limiter scheme.

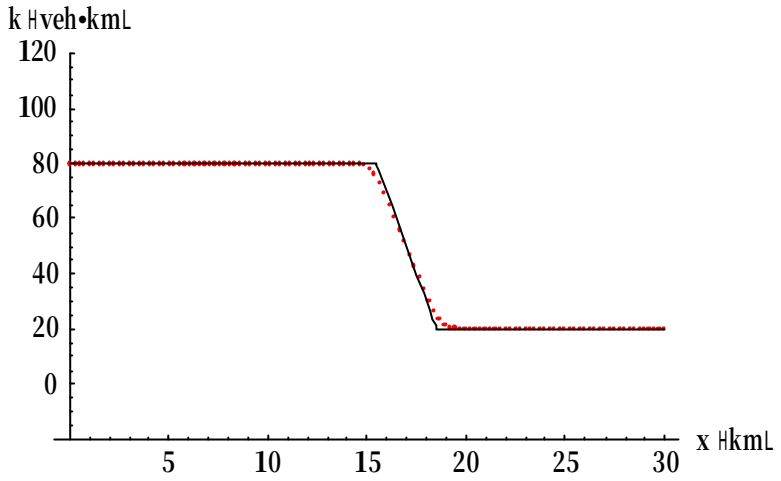

Figure 5.44. The density profile at t = 0.05hr for case I of rarefaction waves simulated by WENO FV scheme.

In case I of the rarefaction wave problems, the Leapfrog and Beam-Warming scheme shows their ill numerical stabilities again. The Lax-Wendroff and MacCormack also don't have the satisfactory accuracy.

5.1.2.2 Case II

In case II of the rarefaction wave problems, the initial condition was assumed as follows:

$$k(x,0)=\begin{cases}100, & 0\le x<15\\ 20, & 15\le x\le 30\end{cases}.$$

The numerical results of these schemes are presented in Figure 5.45-5.52.

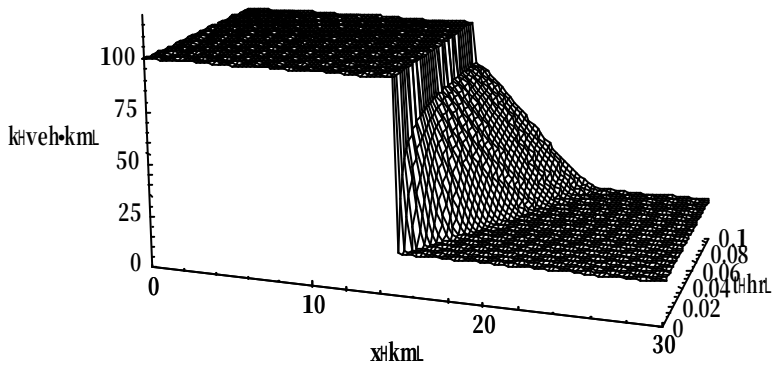

Figure 5.45. The density behavior for case II of rarefaction waves simulated by the Upwind scheme.

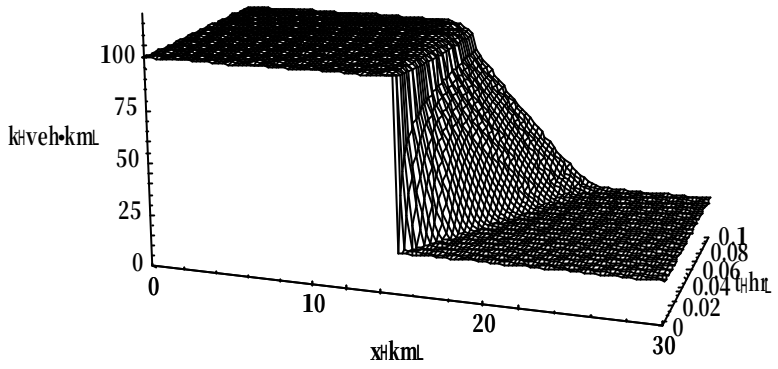

Figure 5.46. The density behavior for case II of rarefaction waves simulated by the Godunov scheme.

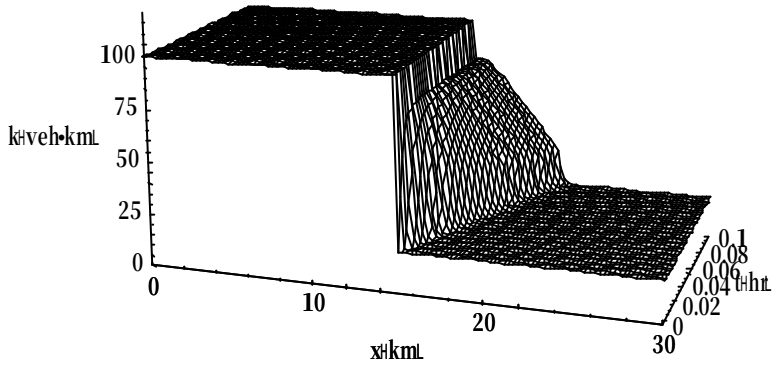

Figure 5.47. The density behavior for case II of rarefaction waves simulated by TVD slope-limiter scheme.

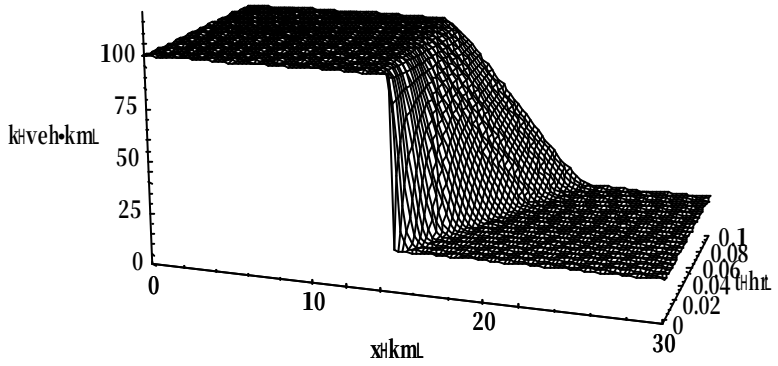

Figure 5.48. The density behavior for case II of rarefaction waves simulated by WENO FV scheme.

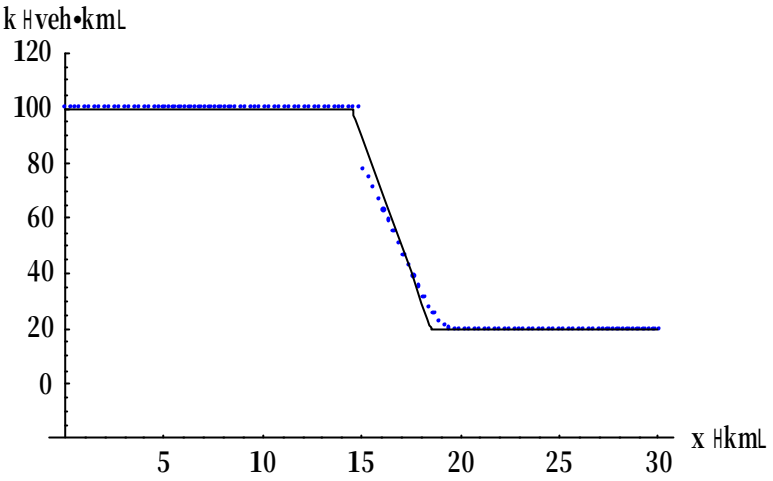

Figure 5.49. The density profile at t = 0.05hr for case II of rarefaction waves simulated by the Upwind scheme.

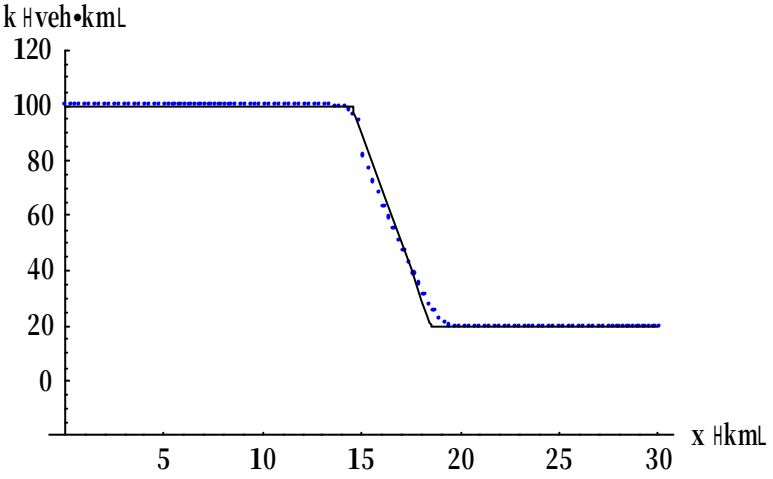

Figure 5.50. The density profile at t = 0.05hr for case II of rarefaction waves simulated by the Godunov scheme.

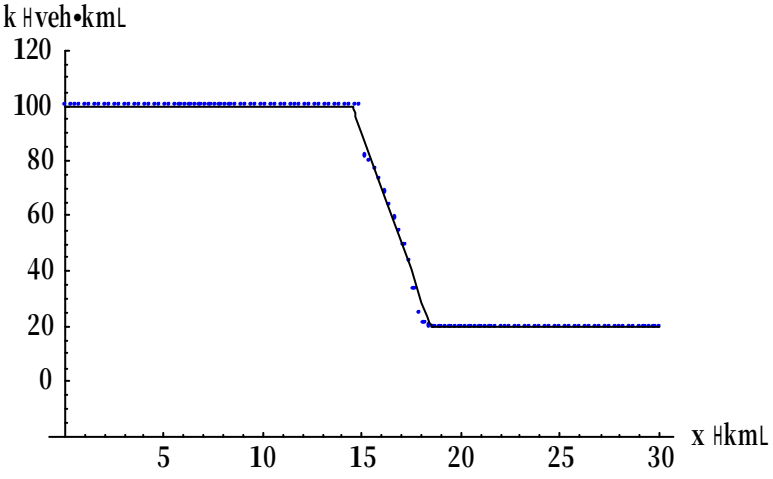

Figure 5.51. The density profile at t = 0.05hr for case II of rarefaction waves simulated by TVD slope-limiter scheme.

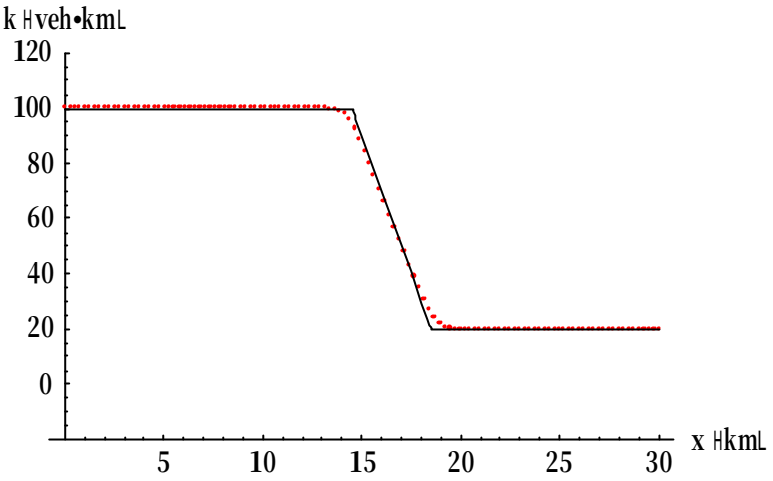

Figure 5.52. The density profile at t = 0.05hr for case II of rarefaction waves simulated by WENO FV scheme.

In case II of the rarefaction wave problems, WENO FV scheme demonstrates the dominant accuracy among these applied schemes.

5.1.3 Traffic Signal Switching from Red to Green

The traffic signal example in this study is a road section with a signal shown in Figure 5.53. The situation that a traffic signal switches from red to green at that time the traffic is lined up behind the red light is simulated. In this example, the numerical errors were analyzed to acquire the most accurate scheme. Based on the results from Sections 5.1.1 and 5.1.2, Godunov-type TVD slope-limiter, which combines TVD sloper-limiter with Godunov, and WENO FV schemes had better accuracies and thus were compared in this section. This numerical example was formulated as follows:

Greenshieds density-speed relationship: $u = u_f (1 - \frac{2k}{k_j})$

LWR model: $\frac{\partial k(x,t)}{\partial t} + u_f (1 - \frac{2k}{k_j}) \frac{\partial k(x,t)}{\partial x} = 0$

Initial condition: $k(x,0) = \begin{cases} 70, & 0 \le x < 10 \\ 0, & 10 \le x \le 20 \end{cases}$

Boundary condition: $k(0,t) = 70 - 120t$

where free-flow speed u_f = 80 kph and jam density k_j = 160 veh/km. The length of street section is 20 km, and observed time period is 0.25 hr. The exact solution is shown as follows:

$$k(x,t)=\begin{cases} 75-60t-\sqrt{(60t-5)^2-120(x-10t)} & 10\le x<10t \\ 70 & 10t\le x\le 10t+10 \\ 80-\dfrac{x-10}{t} & 10t+10<x\le 80t+10 \\ 0 & 80t+10<x\le 20 \end{cases}$$

To check accuracy at a given time level, the L_1 and L_∞ error are measured.

$$L_1 \text{ error} = \int_a^b \left|u(x)_{\text{exact}} - u(x)_{\text{computed}}\right| dx \cong \sum_{i=1}^{N} \left|u(x_i)_{\text{exact}} - u(x_i)_{\text{computed}}\right| (x_i - x_{i-1})$$

$$L_\infty \text{ error} = \sup_i \left|u(x_i)_{\text{exact}} - u(x_i)_{\text{computed}}\right|$$

The simulated result of WENO FV scheme is shown in Figure 5.54, which illustrates the rarefaction waves corresponding to the gradual initiation of the traffic flow when traffic light at x = 0 turns from red to green at t = 0. Figure 5.55 presents the numerical comparison of accuracy between WENO FV and Godunov-type TVD slope-limiter FD methods. Table 5.1 and 5.2 demonstrate the numerical accuracy and CPU timing of WENO FV and Godunov-type TVD slope-limiter FD methods separately. The results show that WENO FV scheme is more accurate than Godunov-type TVD slope-limiter FD method, but requires more execution time.

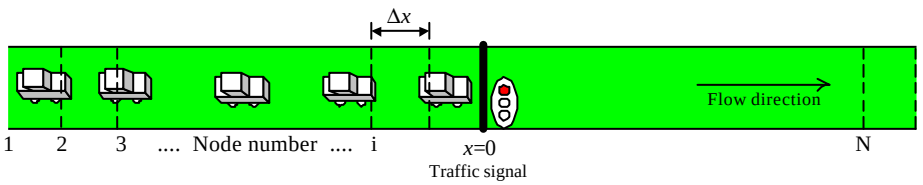

Figure 5.53. A road section with a traffic signal.

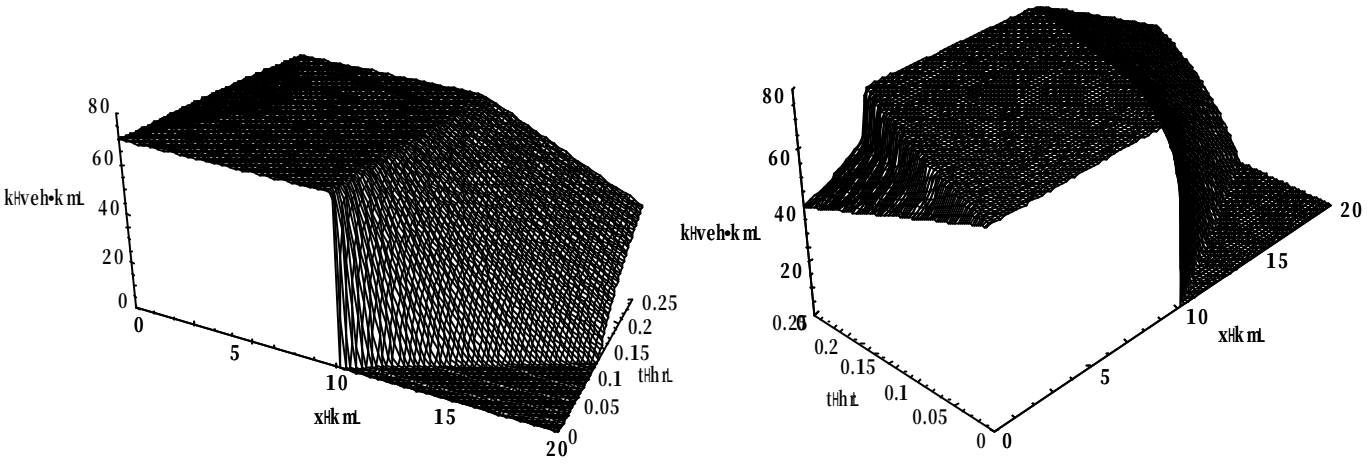

Figure 5.54. The density behavior with a traffic signal turning from red to green simulated by WENO FV scheme.

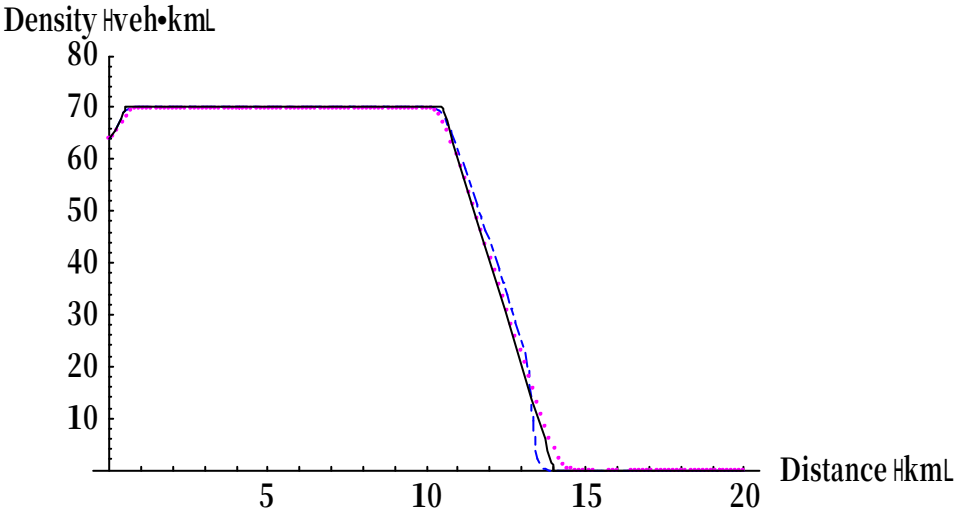

Figure 5.55. The density profile at t = 0.05 hr for traffic signal problem (Solid line: exact solution; Dashes: solution of Godunov-type TVD slope-limiter FD scheme; Dots: solution of WENO FV scheme).

Table 5.1. Numerical accuracy in density at t = 0.05hr for traffic signal problem with infinity-norm and one-norm errors (unit: veh/km).

Scheme	L_∞ error	L_1 error
WENO FV	4.144	7.054
Godunov-type TVD Slope-limiter FD	8.417	12.71

Table 5.2. Execution times for simulation of traffic signal problem (unit: CPU sec.).

Mesh (M×N) / Schemes	75×100	75×200	150×200	300×400
WENO FV	6	12	16	45
Godunov-type TVD Slope-limiter FD	1	1	2	3

5.1.4 Square Wave Problem

In order to demonstrate both shock and rarefaction waves, the test case of square wave was examined. The square wave problem was formulated as follows:

Equilibrium density-speed relationship: $u(k) = u_f e^{-9k/k_j}$

LWR model: $\frac{\partial k(x,t)}{\partial t} + \frac{\partial k(x,t) \cdot u(k)}{\partial x} = 0$

Initial condition: $k(x,0) = \begin{cases} 110, & 10 \le x \le 20 \\ 0, & otherwise \end{cases}$

Neumann boundary condition: $\frac{\partial k(0,t)}{\partial t} = 0$

where free-flow speed u_f = 140 kph and jam density k_j = 220 veh/km. The length of street section is 60 km, and observed time period is 1hour.

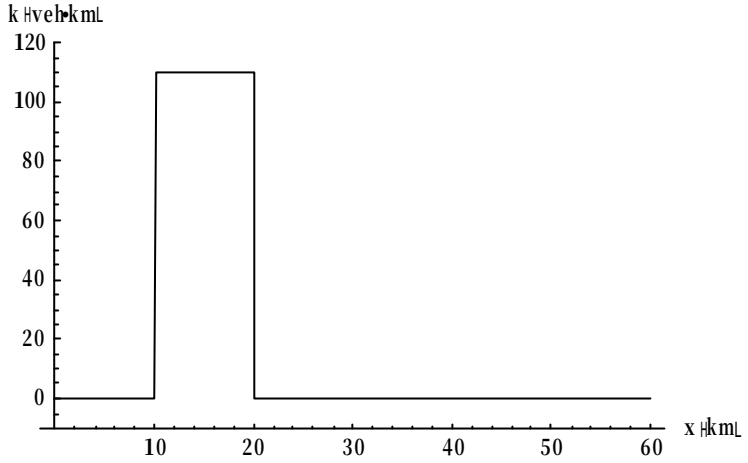

Figure 5.56. The initial condition of density profile in square wave problem.

First, the analytical solution shall be derived to be the benchmark of the numerical accuracy. The exact solutions are obtained using the method of characteristics. With the equilibrium density-velocity function

$$u(k) = u_f e^{-9k/k_j}, \tag{5.1}$$

so that the flow-density relationship, i.e. the flux function, is

$$q(k) = k u_f e^{-9k/k_j}. \tag{5.2}$$

From

$$\frac{\partial k}{\partial t} + \frac{\partial q(k)}{\partial x} = \frac{\partial k}{\partial t} + a(k)\frac{\partial k}{\partial x} = 0, \tag{5.3}$$

the wave speed can be obtained

$$a(k) = \frac{dq}{dk} = q'(k) = u_f (1 - 9k/k_f) e^{-9k/k_j}. \tag{5.4}$$

Using the chain rule

$$\frac{dk}{dt} = \frac{\partial k}{\partial t} + \frac{dx}{dt}\frac{\partial k}{\partial x},$$

and substituting $\frac{\partial k}{\partial t}$ in Eqn. (5.3), the acquired forms are shown as follows:

$$\frac{dk}{dt} - \frac{dx}{dt}\frac{\partial k}{\partial x} + a(k)\frac{\partial k}{\partial x} = 0,$$

and

$$\frac{dk}{dt} - \frac{\partial k}{\partial x}\left(\frac{dx}{dt} - a(k)\right) = 0.$$

Therefore, $\frac{dk}{dt} = 0$ on the lines indicates

$$\frac{dx}{dt} = a(k), \tag{5.5}$$

which implies that k and hence $a(k)$ is constant along these lines. These are the characteristics, which are straight lines in this case given by

$$x = x_0 + at, \tag{5.6}$$

where x_0 is the value of x at $t = 0$, and

$$a = a(k(x_0,0)) = u_f(1 - 9k(x_0,0)/k_f)e^{-9k(x_0,0)/k_j}. \tag{5.7}$$

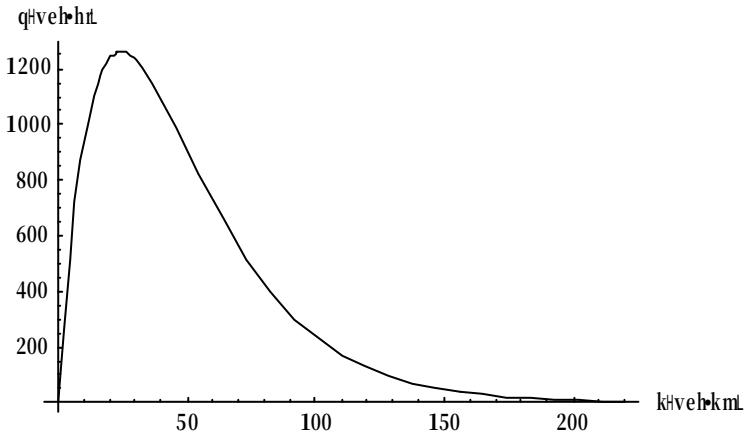

Figure 5.57. The flow-density relationship used in square wave problem.

In order to obtain the exact solution at (x,t), we trace the characteristic that passes through that point back to the initial density profile, where k has the same value on the characteristic, i.e.

$$k(x,t) = k(x_0,0) = k_0.$$

When characteristics cross, however, the solution becomes multiply defined and contravenes physical phenomena. This is encountered immediately when considering the square wave at x = 10. Using the Rankine-Hugoniot jump condition, a shock moving with speed

$$s = \frac{[q]}{[k]} = \frac{q_r - q_l}{k_r - k_l} = \frac{110 u_f e^{-9/2} - 0}{110 - 0} = u_f e^{-9/2} \tag{5.8}$$

is formed. By checking the entropy condition

$$\frac{q(k_r) - q(k)}{k_r - k} \le s \le \frac{q(k_l) - q(k)}{k_l - k}, \quad \forall k , \tag{5.9}$$

a shock is confirmed.

It is a different scenario for the discontinuity at x = 20. The characteristics to the left of discontinuity have negative speed $a(k_l) = -\frac{7}{2} u_f e^{-9/2}$, whereas to the right the characteristics have positive speed $a(k_r) = u_f$. Therefore these characteristics do not meet, Eqn. (5.9) would not be satisfied, and hence there is no single shock connecting these states. With the non-convex flux function $q(k)$, however, there is a point of inflection. Provided that k_l and k_r are both to the left or right of the point of inflection, then the void created between the characteristics is filled in with a rarefaction fan. When the convex hull of the flux function is the same as the flux function itself between k_l and k_r, the solution is purely an expansion fan. Therefore it is needed to check where k_l and k_r are relative to the point of inflection.

The point of inflection of the flux function (5.2) is at $k = k_I$, where

$$q''(k_I) = u_f (81 k_I / k_j^2 - 18 / k_j) e^{-9 k_I / k_j} = 0 ,$$

and consequently,

$$k_I = 2 k_j / 9 . \tag{5.10}$$

Since at x = 20, $k_r < k_I < k_l$, k_l and k_r are on opposite sides of the point of inflection, the

flux function and its convex hull are not the same. The discontinuity therefore comprises of a shock and an expansion fan, separated at k_T, the point where the tangent to the flux function passes through (k_l, q_l). This ensures the correct entropy-satisfying weak solution. The point (k_T, q_T) can be found by equating the derivative of the flux function at k_T to the slope of the line between (k_T, q_T) and (k_l, q_l), i.e.

$$q'(k_T) = \frac{q_T - q_l}{k_T - k_l}. \tag{5.11}$$

Multiplying by $(k_T - k_l)$,

$$q_T - q_l - (k_T - k_l)q'(k_T) = 0 \tag{5.12}$$

is obtained.

Substituting for the flux function (5.2), we obtain

$$(9k_T^2 / k_j - 9k_T k_l / k_j + k_l)e^{-9k_T/k_j} - k_l e^{-9k_l/k_j} = 0, \tag{5.13}$$

where k_l = 110, and k_T can be calculated by using Newton' s method.

Once k_T is found, the speed of the shock (5.8) can be calculated from

$$s = \frac{q_T - q_l}{k_T - k_l} = u_f(1 - 9k_T / k_j)e^{-9k_T/k_j}$$

and since k_l is unchanged while the shock is moving, k_T is constant, and thus so is the speed until the shocks collide.

In order to derive the expansion fan to the right of the shock, between k_T and k_r = 0, the slope of the characteristic A ($q'(k_T) \le A \le q'(k_r)$) is found from Eqn. (5.6), i.e.

$$A = \frac{x - 20}{t} \tag{5.14}$$

with the given (x, t).

Then k can be found again with A using Newton iteration, from

$$q'(k) = u_f(1-9k/k_j)e^{-9k/k_j} = A,$$

and

$$u_f(1-9k/k_j)e^{-9k/k_j} - A = 0. \tag{5.15}$$

When the shocks cross, an expansion fan is followed by a discontinuity of height k_T. This new discontinuity is a shock whose speed can be calculated using Eqn. (5.8), where $k_l = 0$ and k_r is given by k_T. The shock therefore moves with positive speed and hence, as it moves, its height decreases, thus changing the shock speed. The shock path will therefore no longer be a straight line in the characteristic diagram. The shape of the shock can be calculated numerically using Euler's method. The instantaneous shock speed is calculated by starting at the initial position of the colliding shocks and moving a distance $\ddot{a}x$ in time $\ddot{a}t$. This new position (x, t) crosses a characteristic from the expansion fan, and then A can be calculated using Eqn. (5.14). So can the new k_r by Eqn. (5.15), and hence the new shock speed by Eqn. (5.8). The resulting density profile would be a shock moving with positive but decreasing speed, with decreasing height, followed by an expansion fan of increasing width.

Figure 5.62-5.65 present the numerical comparison of accuracy between WENO FV and Godunov-type TVD slope-limiter FD methods on various mesh sizes. Table 5.3 and 5.4 demonstrate the numerical accuracy and CPU timing of WENO FV and Godunov-type TVD slope-limiter FD methods separately. The results also show that WENO FV scheme is still more accurate than Godunov-type TVD slope-limiter FD method, but requires more execution time.

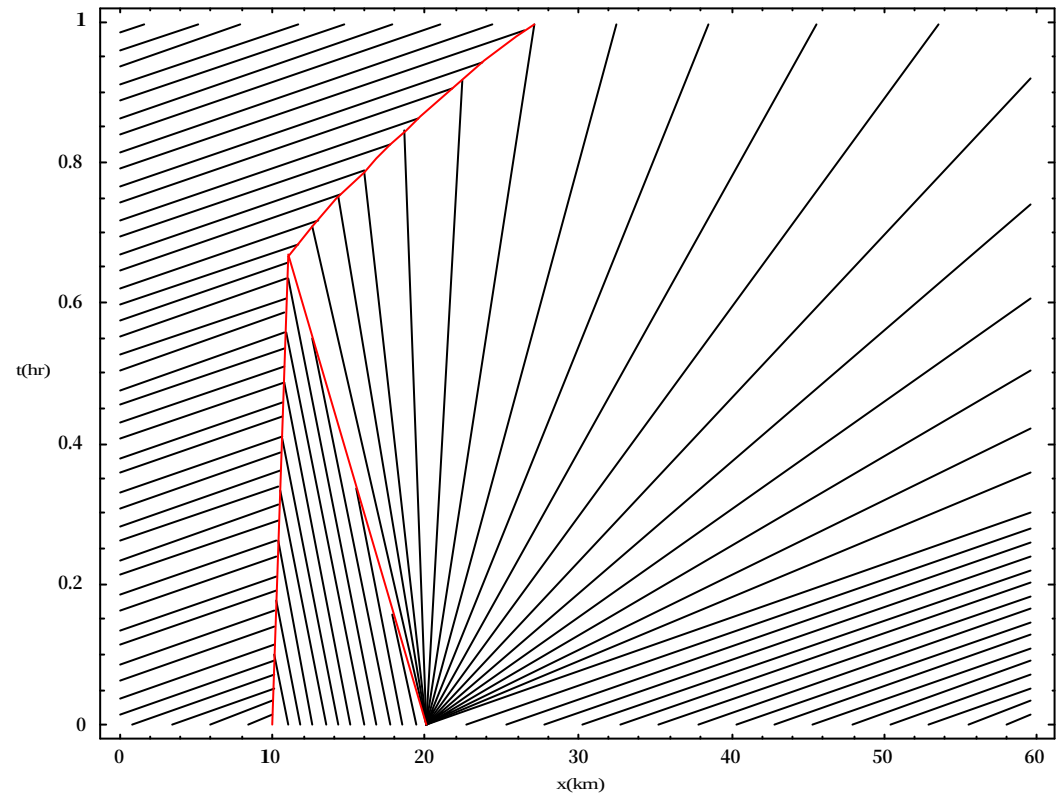

Figure 5.58. Characteristics diagram for square wave problem.

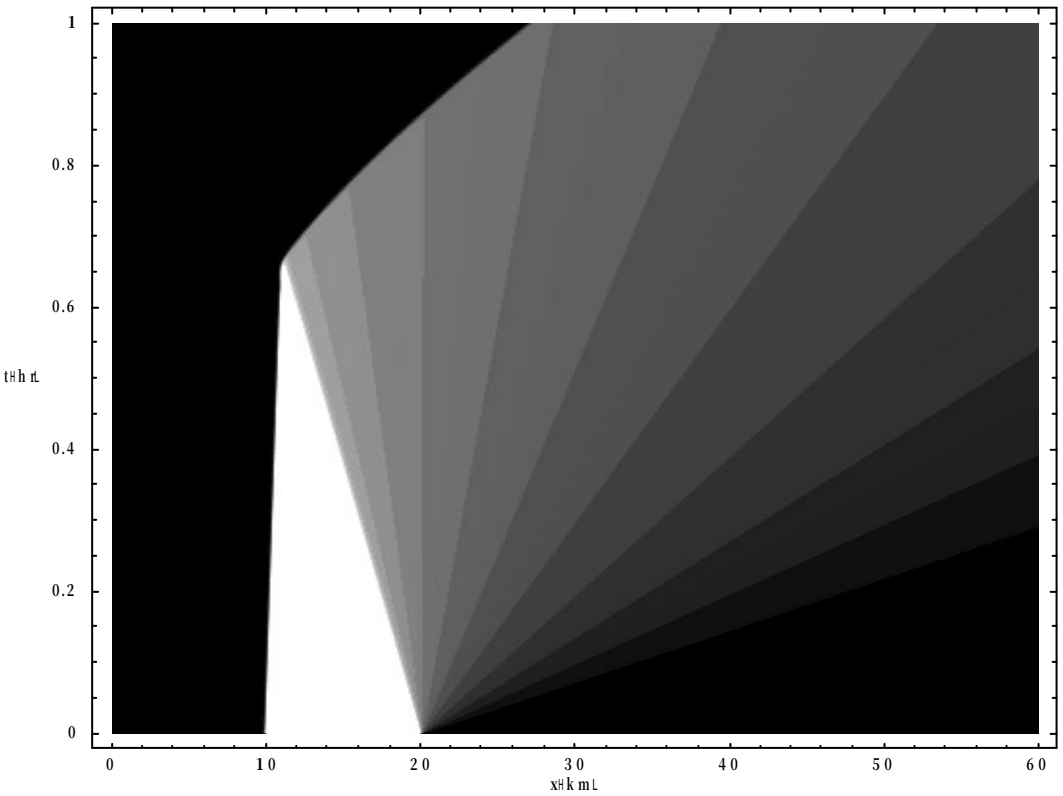

Figure 5.59. Characteristics for square wave problem simulated by WENO FV scheme.

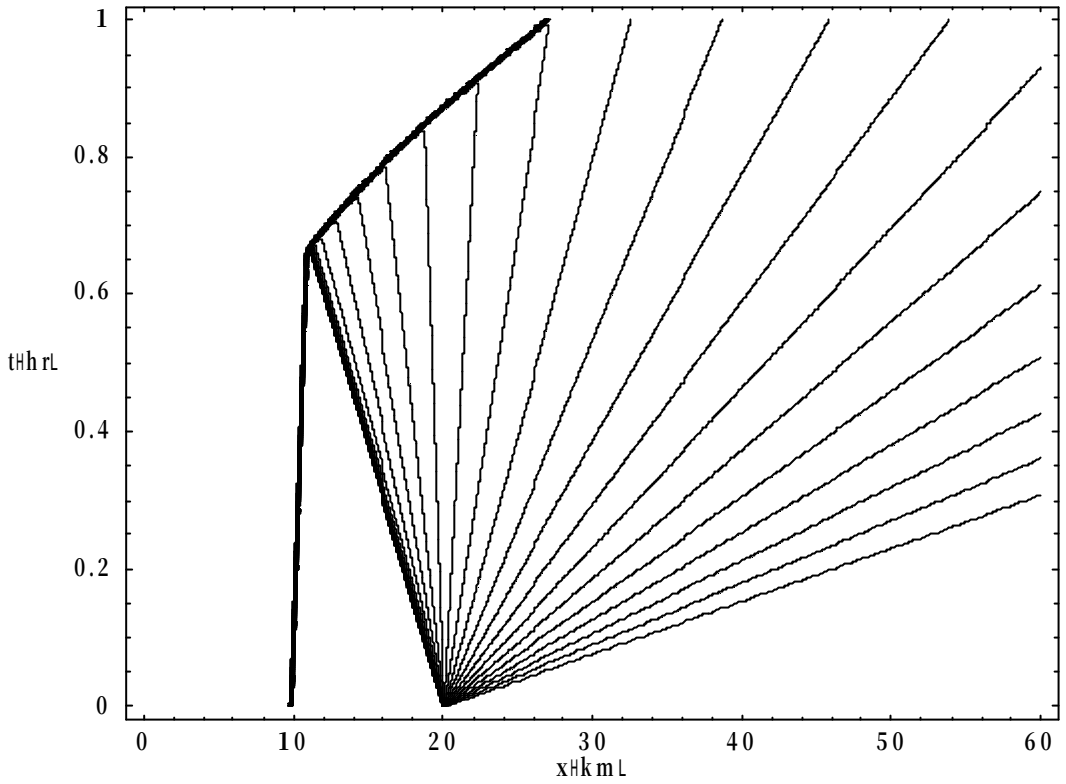

Figure 5.60. Contours of density for square wave problem simulated by WENO FV scheme.

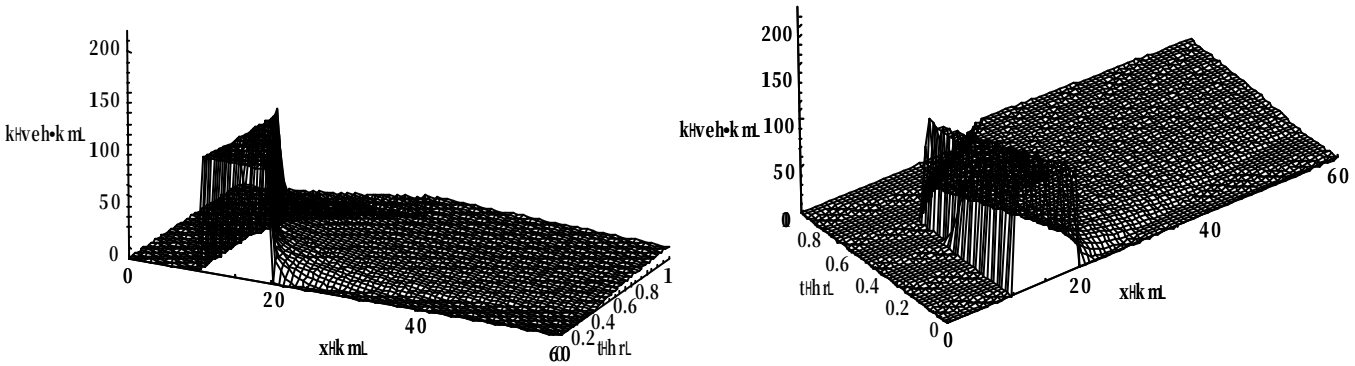

Figure 5.61. The density behavior for square wave problem simulated by WENO FV scheme.

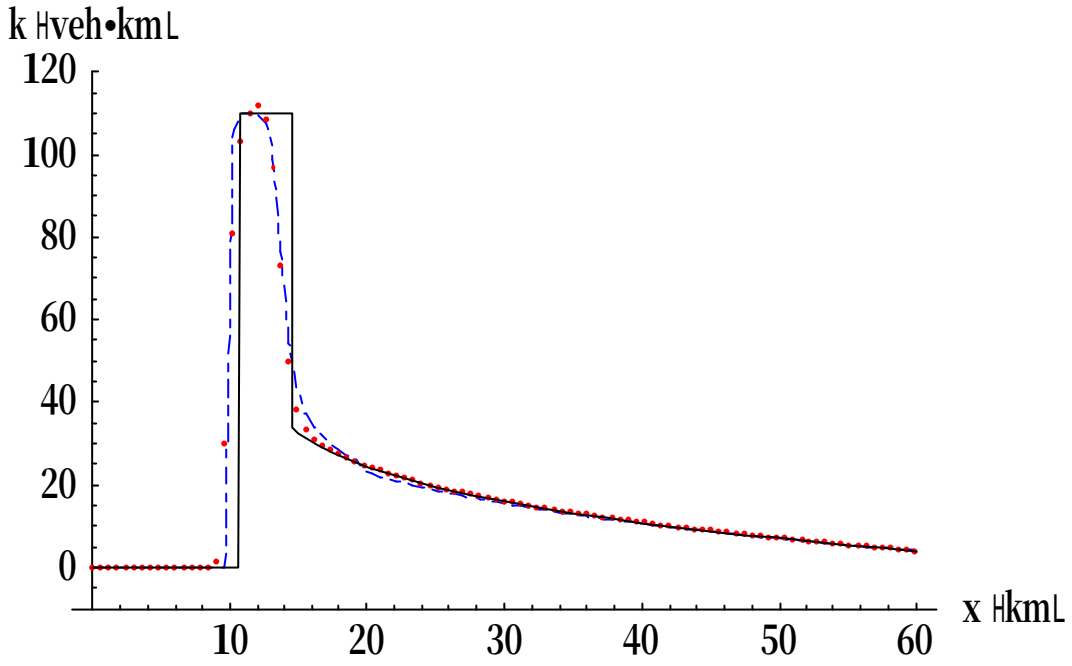

Figure 5.62. The density profile at t = 0.4 hr for square wave problem (Mesh: 100×100; Solid line: exact solution; Dashes: solution of Godunov-type TVD slope-limiter FD scheme; Dots: solution of WENO FV scheme).

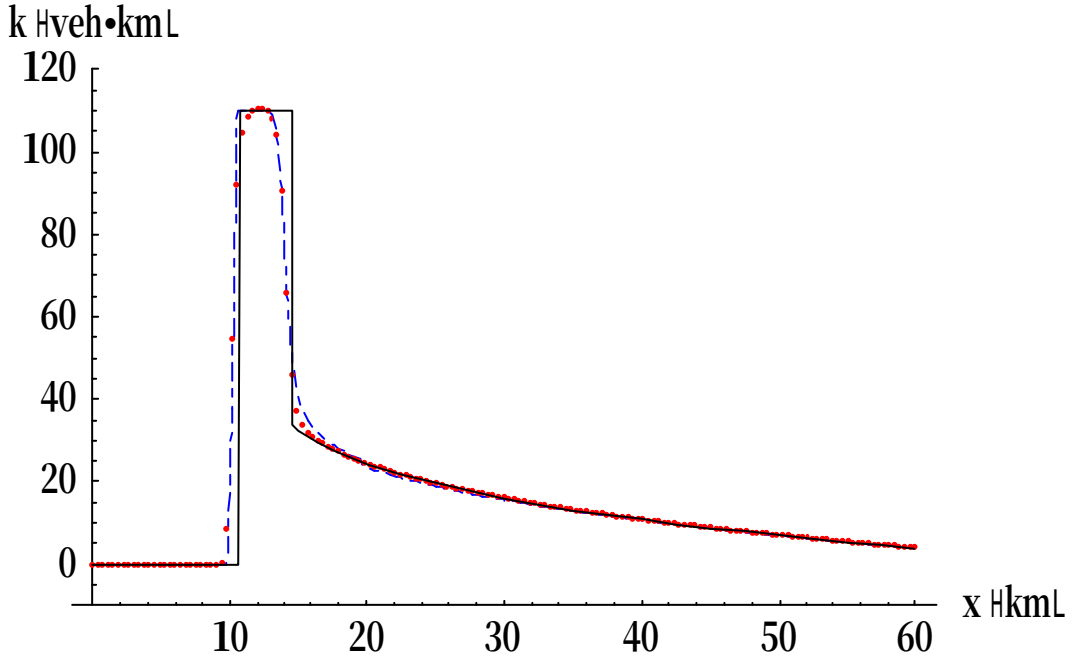

Figure 5.63. The density profile at t = 0.4 hr for square wave problem (Mesh: 160×160; Solid line: exact solution; Dashes: solution of Godunov-type TVD slope-limiter FD scheme; Dots: solution of WENO FV scheme).

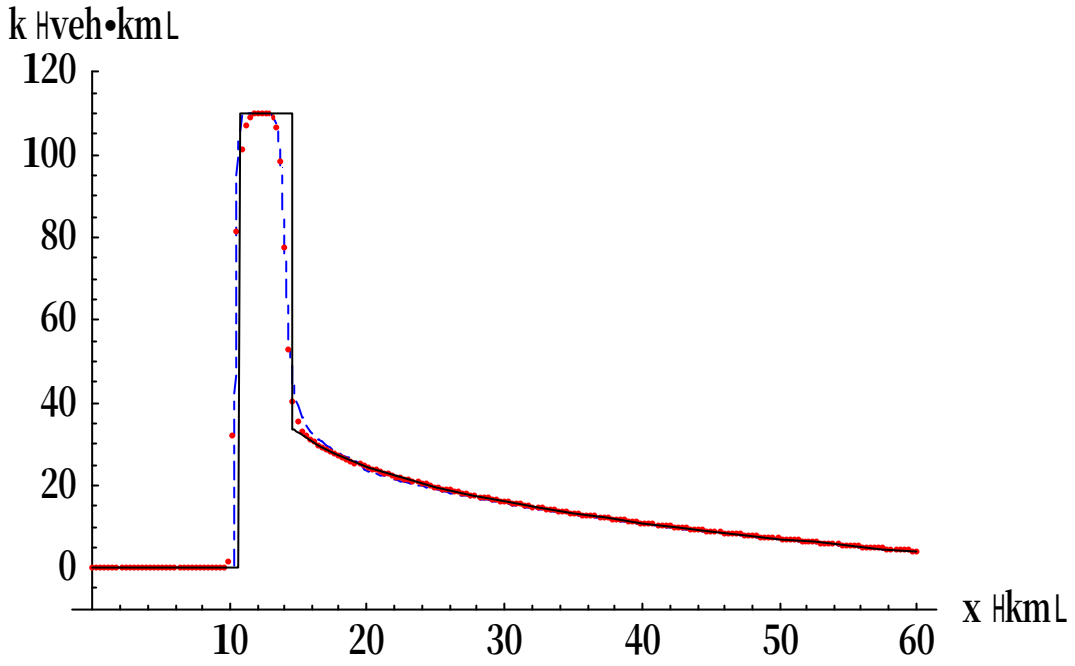

Figure 5.64. The density profile at t = 0.4 hr for square wave problem (Mesh: 200×200; Solid line: exact solution; Dashes: solution of Godunov-type TVD slope-limiter FD scheme; Dots: solution of WENO FV scheme).

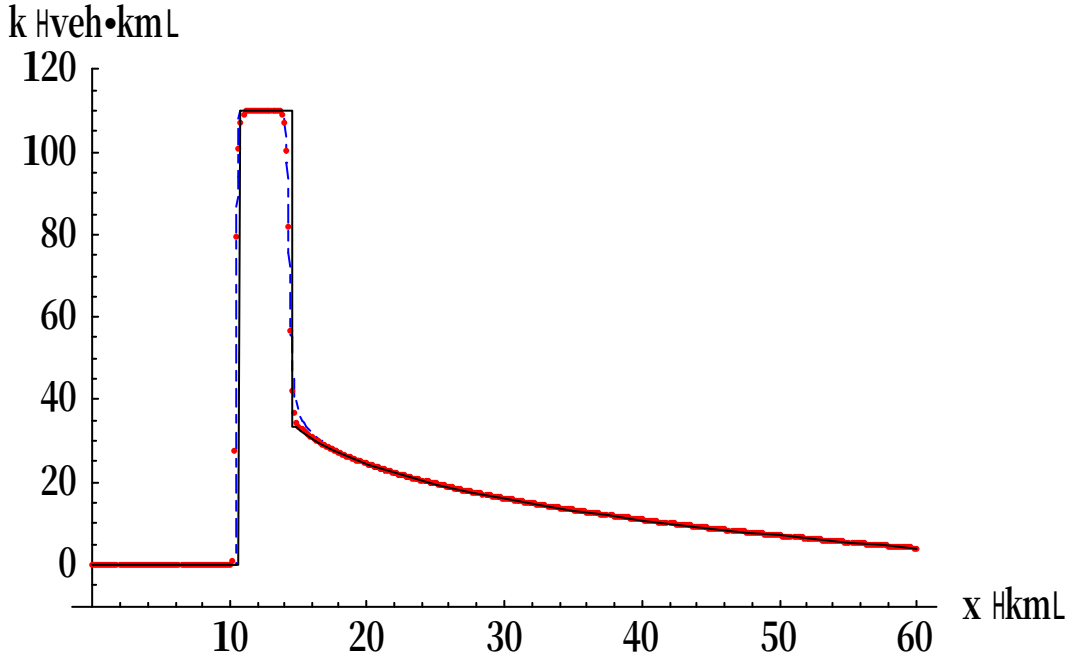

Figure 5.65. The density profile at t = 0.4 hr for square wave problem (Mesh: 400×400; Solid line: exact solution; Dashes: solution of Godunov-type TVD slope-limiter FD scheme; Dots: solution of WENO FV scheme).

Table 5.3. Numerical accuracy in density at t = 0.4 hr for square ware problem with infinity-norm and one-norm errors (unit: veh/km).

Scheme	Mesh (M×N)	L_∞ error	L_1 error
WENO FV	100×100	80.99	147.00
	160×160	91.96	116.61
	200×200	81.39	75.54
	400×400	79.29	35.76
Godunov-type TVD Slope-limiter FD	100×100	105.95	157.95
	160×160	110.00	126.99
	200×200	101.90	84.10
	400×400	93.79	42.55

Table 5.4. Execution times for simulation of square ware problem (unit: CPU sec.).

Schemes \ Mesh (M×N)	100×100	160×160	200×200	400×400
WENO FV	6	19	24	95
Godunov-type TVD Slope-limiter FD	1	2	3	5

5.2 Numerical Examples for PW and Jiang's Improved Models

In this section, WENO FV scheme was utilized to solve two classes of high order continuum traffic flow models. The PW model, i.e. the original high order model, and the novel Jiang's improved model, which was presented in 2002, were selected for the following test pronlems. The equilibrium speed-density relationship developed by Del Castillo and Benitez (1995) was applied in both models.

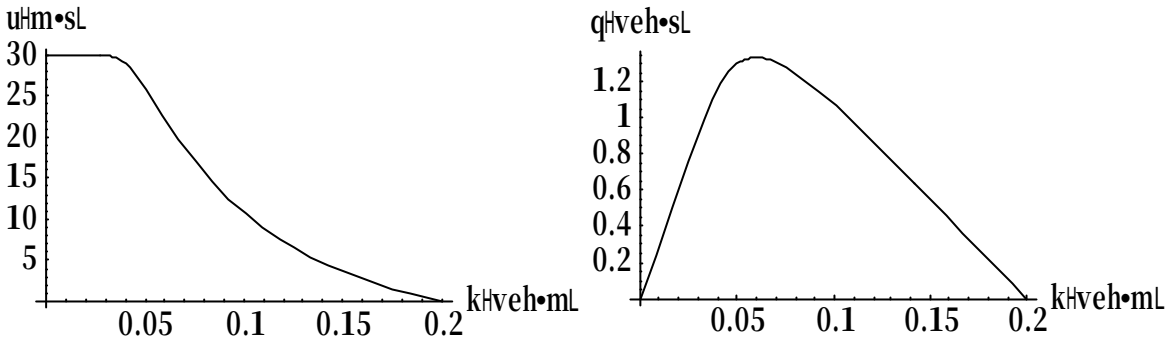

Figure 5.66. The equilibrium speed-density and flow-density relationships developed by Del Castillo and Benitez.

The PW and Jiang's improved models were introduced in Chapter 2 and formulated for numerical discretization in Chapter 3. These numerical examples were formulated as follows:

Del Castillo and Benitez' s density-speed relationship: $u = u_f \left[1 - \exp\left(1 - \exp\left(\frac{c_m}{u_f} \left(\frac{k_j}{k} - 1 \right) \right) \right) \right]$

PW model: $\begin{cases} \dfrac{\partial k}{\partial t} + \dfrac{\partial ku}{\partial x} = 0 \\ \dfrac{\partial u}{\partial t} + u\left(\dfrac{\partial u}{\partial x} \right) = -\dfrac{c_0^2}{k} \dfrac{\partial k}{\partial x} + \dfrac{1}{\boldsymbol{t}} \left(u_e(k) - u \right) \end{cases}$

Jiang' s improved model: $\begin{cases} \dfrac{\partial k}{\partial t} + \dfrac{\partial ku}{\partial x} = 0 \\ \dfrac{\partial u}{\partial t} + u\left(\dfrac{\partial u}{\partial x} \right) = \dfrac{1}{\boldsymbol{t}} \left(u_e(k) - u \right) + c \dfrac{\partial u}{\partial x} \end{cases}$

Initial condition: $k(x,0) = \begin{cases} k_l, & 0 < x < 10 \\ k_r, & 10 < x < 20 \end{cases}$

where free-flow speed u_f = 30 m/s, jam density k_j = 0.2 veh/m, relaxation time $\boldsymbol{t}$ = 2 sec, the kinematic wave speed under the jam density c_m = 11 m/s, and the propagation speed of the disturbance c = 11 m/s . The length of street section is 20 km, and observed time period is 10 min.

5.2.1 Shock Problems

In the shock problems, three cases are shown as follows.

5.2.1.1 Case I

In case I of the shock problems, the situation $k_l < k_r$ and $q_l > q_r$ was considered. There are two conditions satisfying the situation, as shown in Figure 5.67.

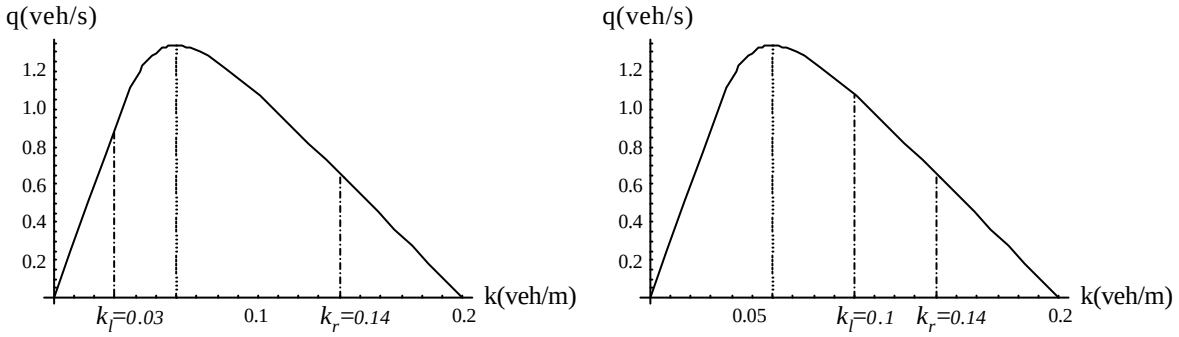

(a) (b)

Figure 5.67. Two conditions in case I of shock problems: (a) k_l = 0.03 veh/m and k_r = 0.14 veh/m; (b) k_l = 0.1 veh/m and k_r = 0.14 veh/m.

Condition (a)

$$k(x,0) = \begin{cases} 0.03, & 0 \le x < 10 \\ 0.14, & 10 \le x \le 20 \end{cases}$$

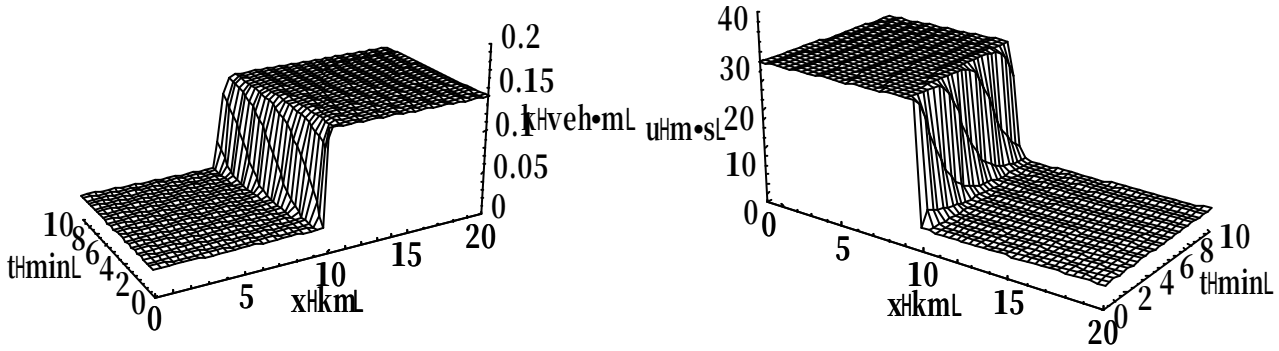

Figure 5.68. The density and velocity behaviors for condition (a) in case I of shock problems simulated by Jiang' s FD scheme with PW model.

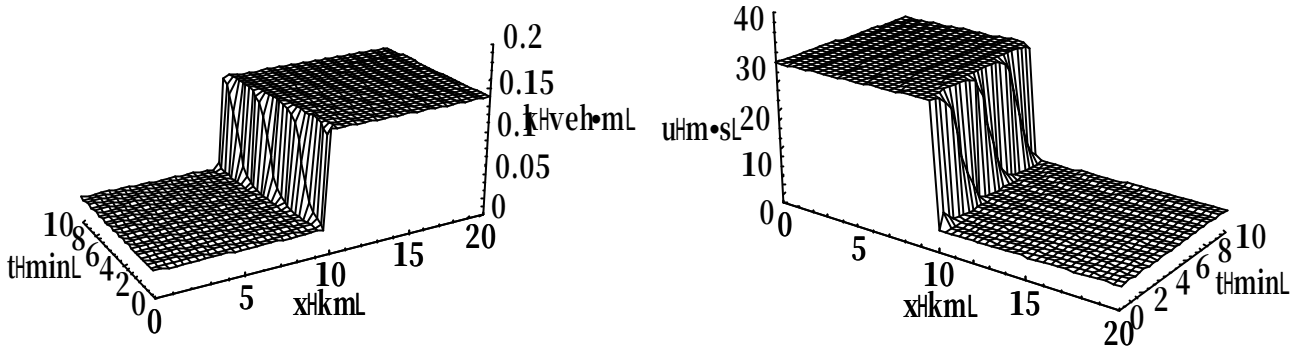

Figure 5.69. The density and velocity behaviors for condition (a) in case I of shock problems simulated by WENO FV scheme with PW model.

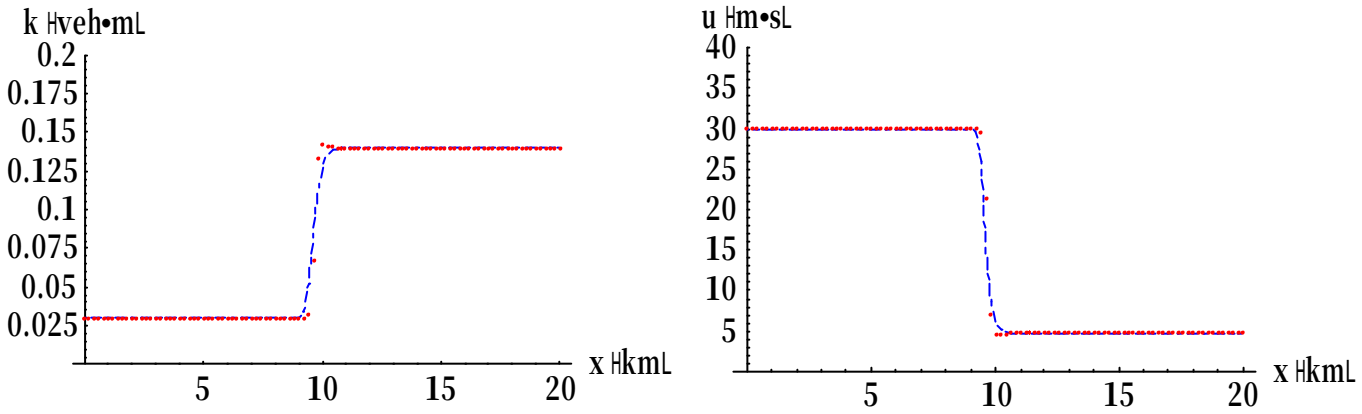

Figure 5.70. The density and velocity profiles at t = 2 min for condition (a) in case I of shock problems simulated with PW model (Dashes: solution of Jiang' s FD scheme; Dots: solution of WENO FV scheme).

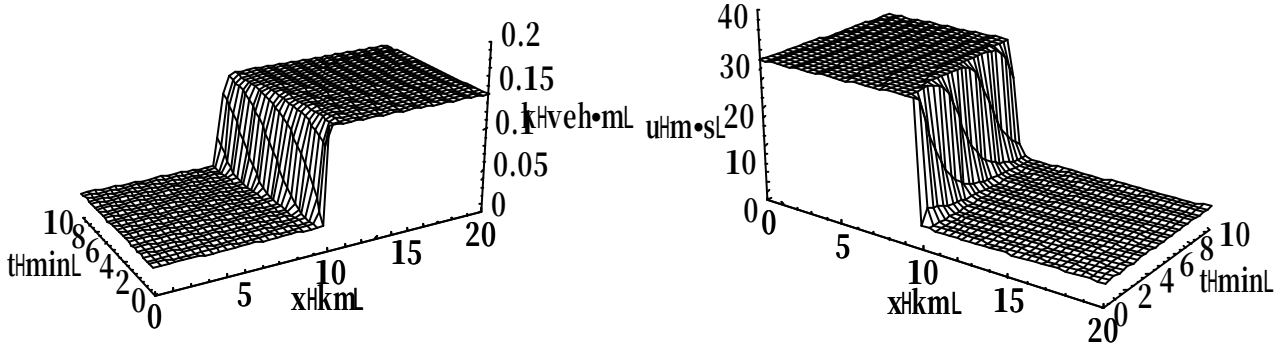

Figure 5.71. The density and velocity behaviors for condition (a) in case I of shock problems simulated by Jiang' s FD scheme with Jiang' s improved model.

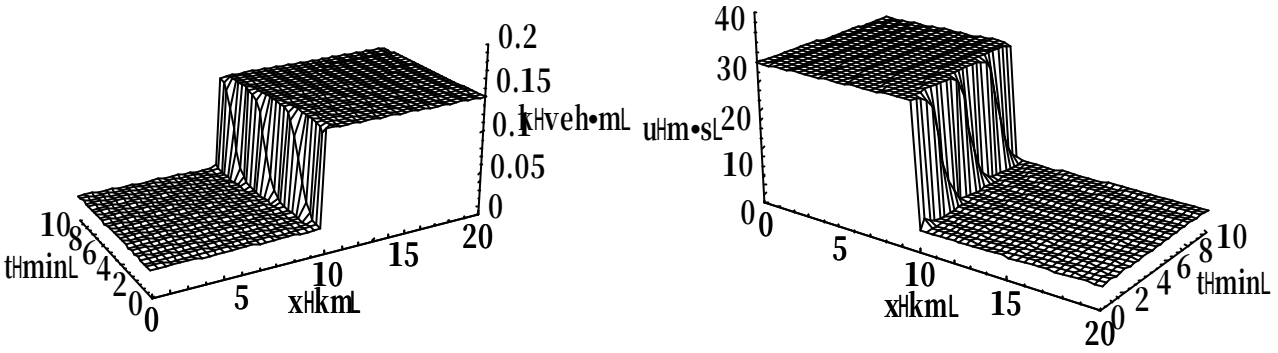

Figure 5.72. The density and velocity behaviors for condition (a) in case I of shock problems simulated by WENO FV scheme with Jiang' s improved model.

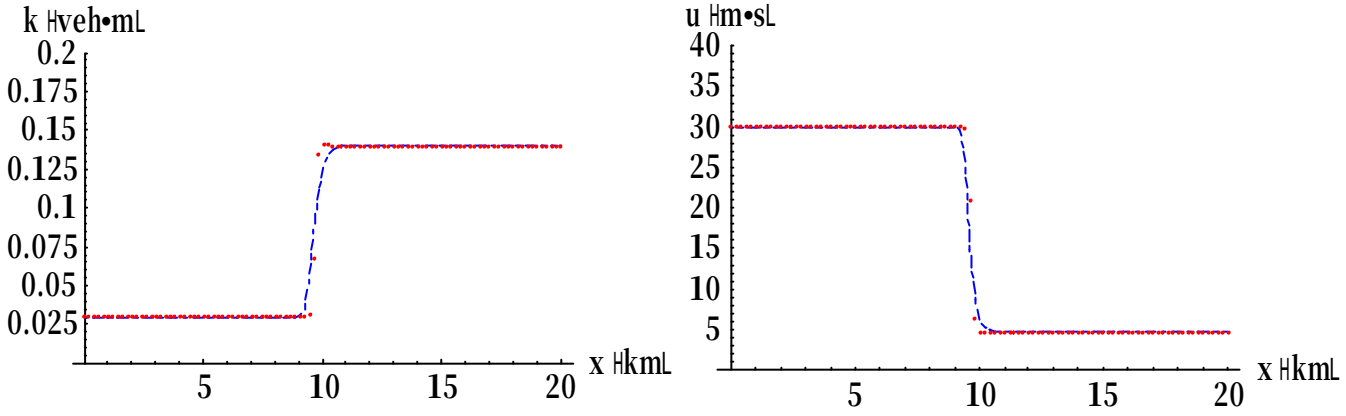

Figure 5.73. The density and velocity profiles at t = 2 min for condition (a) in case I of shock problems simulated with Jiang' s improved model (Dashes: solution of Jiang' s FD scheme; Dots: solution of WENO FV scheme).

Condition (b)

$$k(x,0)=\begin{cases}0.1, & 0\le x<10\\ 0.14, & 10\le x\le 20\end{cases}$$

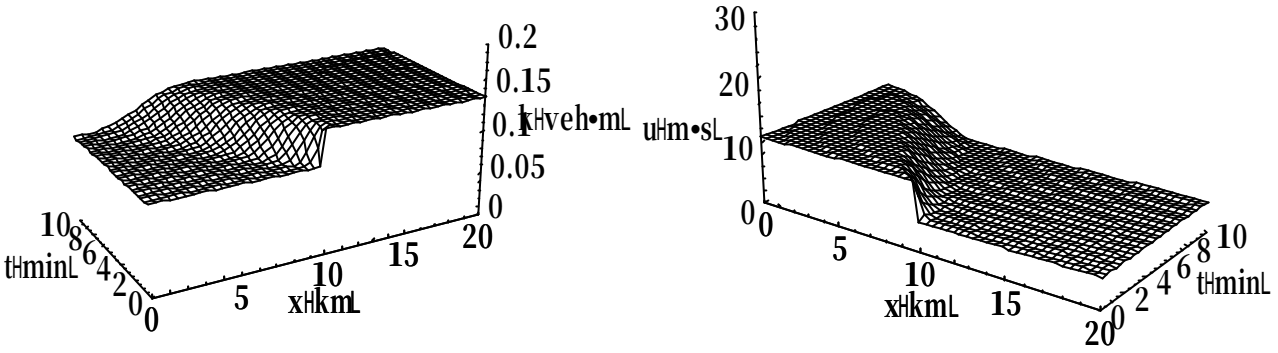

Figure 5.74. The density and velocity behaviors for condition (b) in case I of shock problems simulated by Jiang' s FD scheme with PW model.

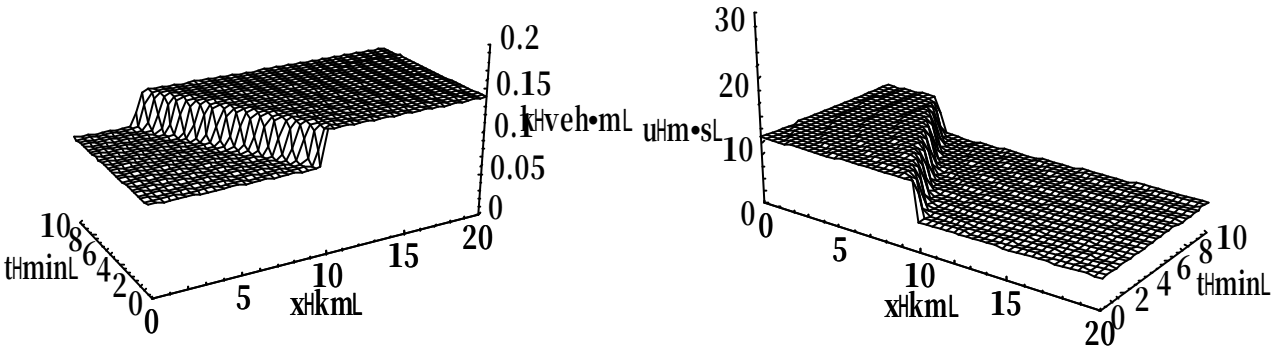

Figure 5.75. The density and velocity behaviors for condition (b) in case I of shock problems simulated by WENO FV scheme with PW model.

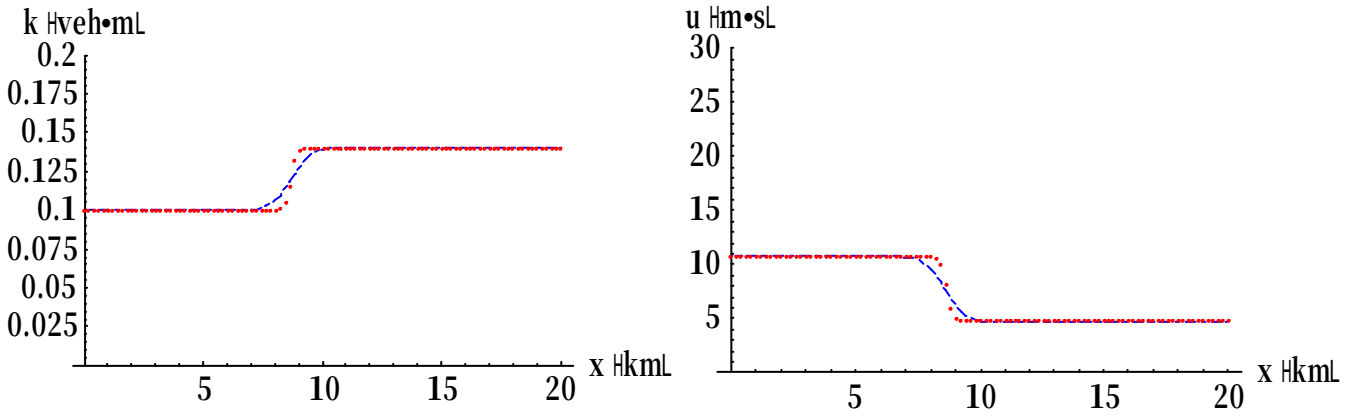

Figure 5.76. The density and velocity profiles at t = 2 min for condition (b) in case I of shock problems simulated with PW model (Dashes: solution of Jiang' s FD scheme; Dots: solution of WENO FV scheme).

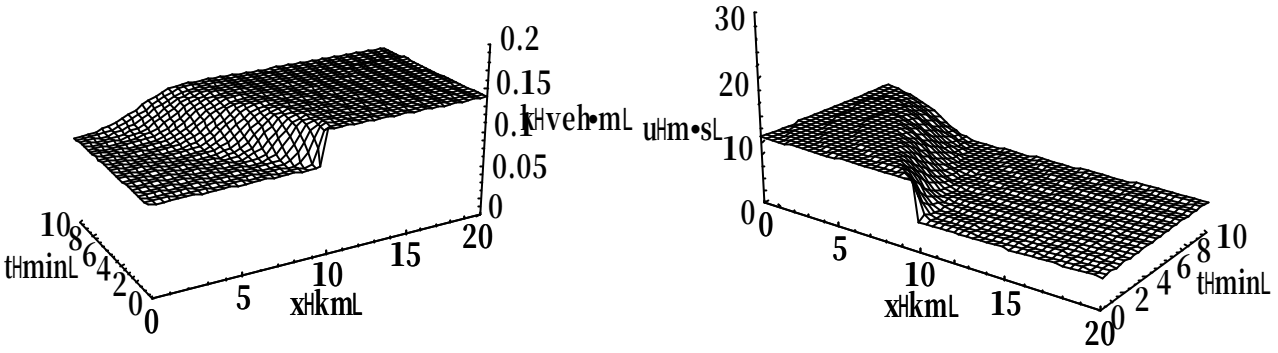

Figure 5.77. The density and velocity behaviors for condition (b) in case I of shock problems simulated by Jiang' s FD scheme with Jiang' s improved model.

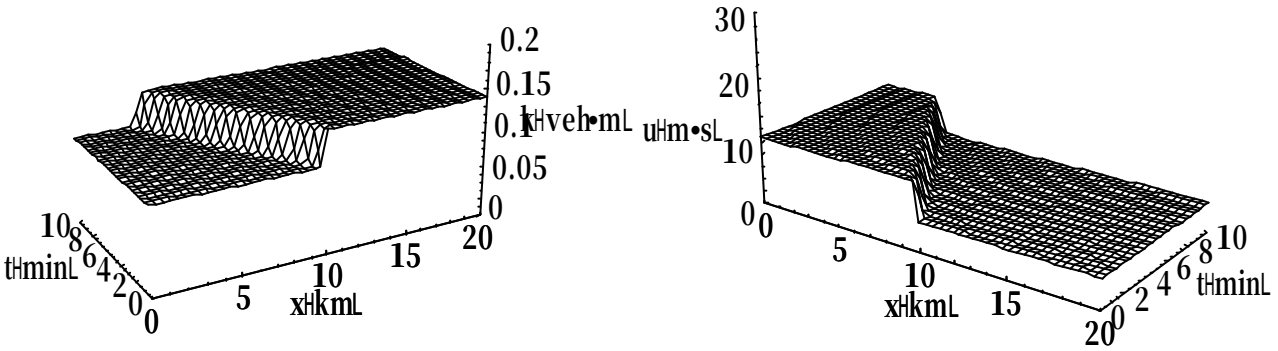

Figure 5.78. The density and velocity behaviors for condition (b) in case I of shock problems simulated by WENO FV scheme with Jiang' s improved model.

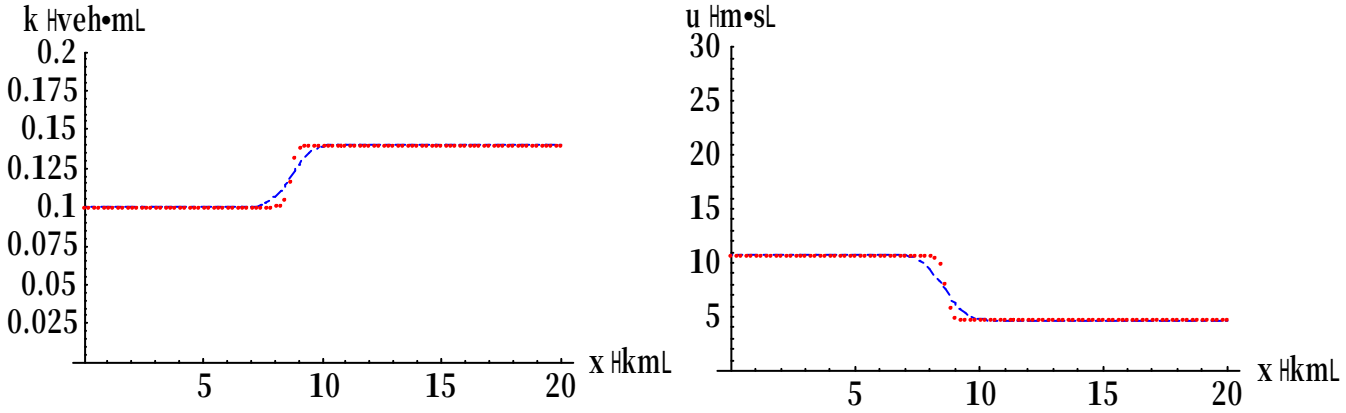

Figure 5.79. The density and velocity profiles at t = 2 min for condition (b) in case I of shock problems simulated with Jiang' s improved model (Dashes: solution of Jiang' s FD scheme; Dots: solution of WENO FV scheme).

5.2.1.2 Case II

In case II of the shock problems, the situation $k_l < k_r$ and $q_l < q_r$ was considered. There are two conditions satisfying the situation, as shown in Figure 5.80.

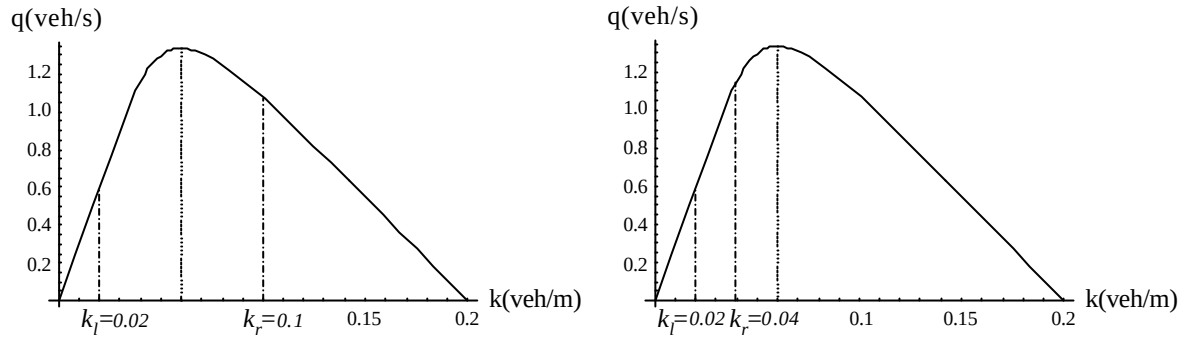

(a) (b)

Figure 5.80. Two conditions in case II of shock problems: (a) k_l = 0.02 veh/m and k_r = 0.1 veh/m; (b) k_l = 0.02 veh/m and k_r = 0.04 veh/m.

Condition (a)

$$k(x,0)=\begin{cases}0.02, & 0 \le x < 10\\ 0.1, & 10 \le x \le 20\end{cases}$$

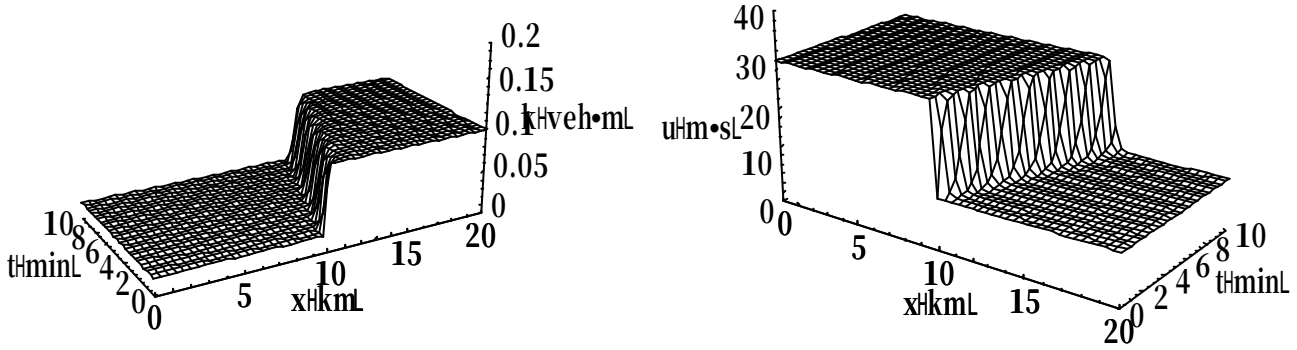

Figure 5.81. The density and velocity behaviors for condition (a) in case II of shock problems simulated by Jiang' s FD scheme with PW model.

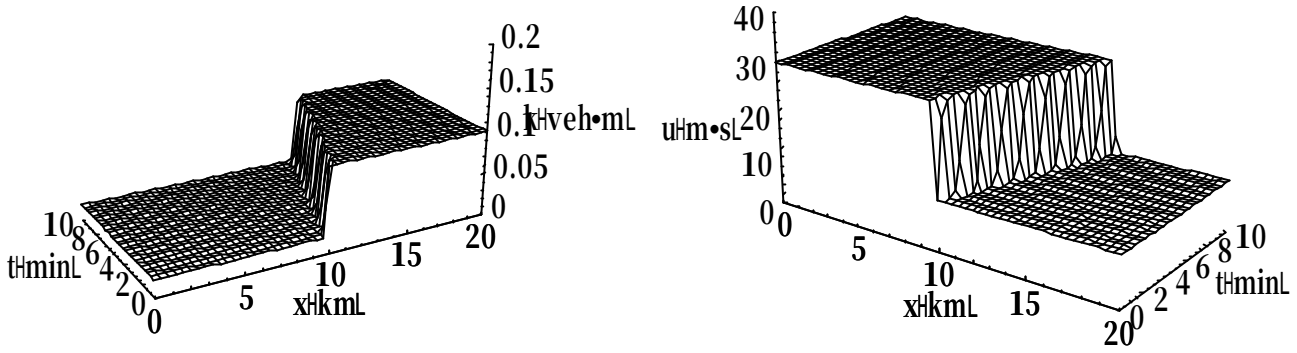

Figure 5.82. The density and velocity behaviors for condition (a) in case II of shock problems simulated by WENO FV scheme with PW model.

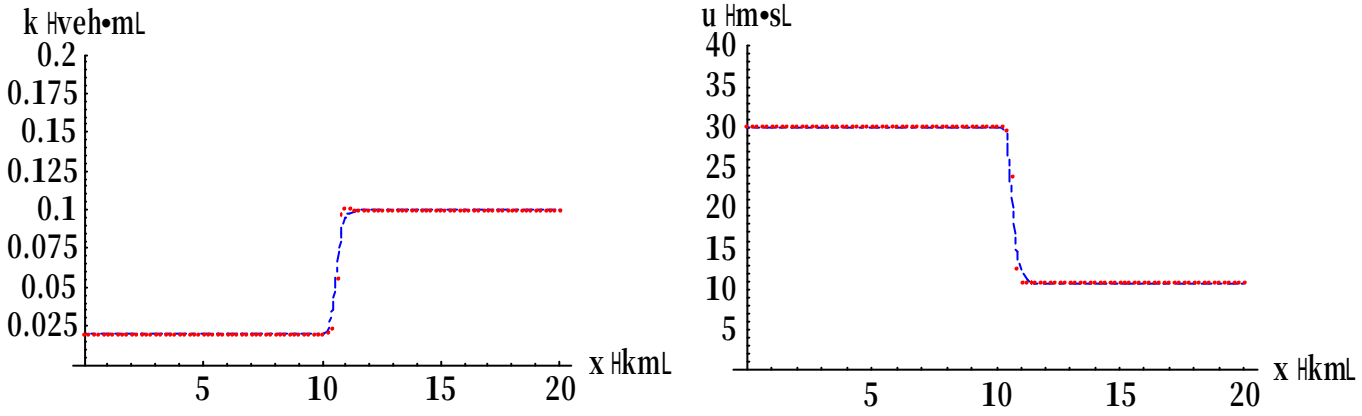

Figure 5.83. The density and velocity profiles at t = 2 min for condition (a) in case II of shock problems simulated with PW model (Dashes: solution of Jiang' s FD scheme; Dots: solution of WENO FV scheme).

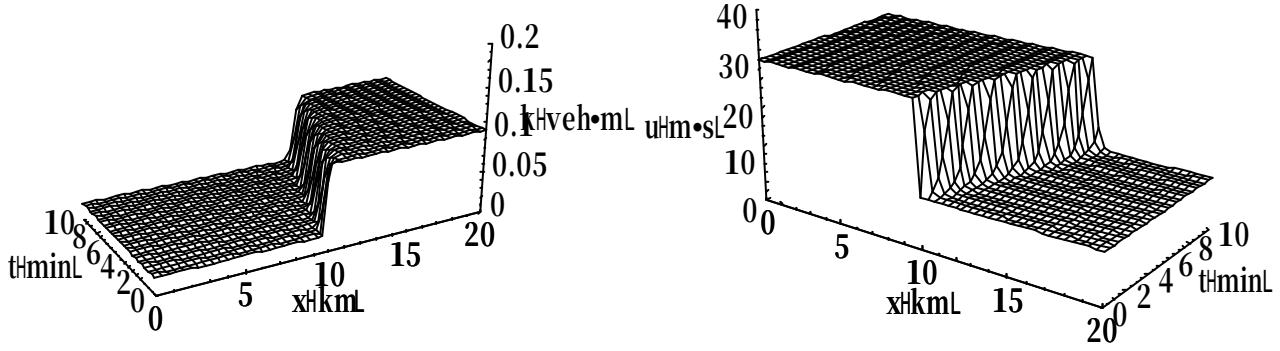

Figure 5.84. The density and velocity behaviors for condition (a) in case II of shock problems simulated by Jiang' s FD scheme with Jiang' s improved model.

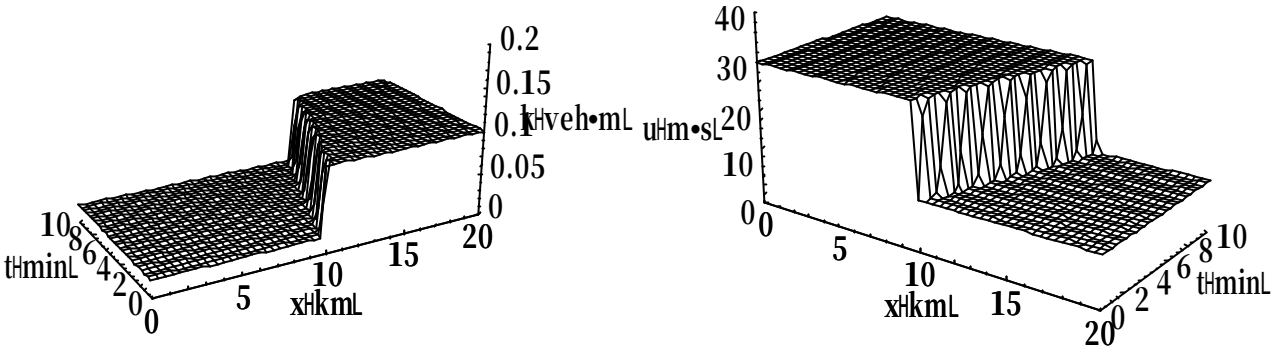

Figure 5.85. The density and velocity behaviors for condition (a) in case II of shock problems simulated by WENO FV scheme with Jiang' s improved model.

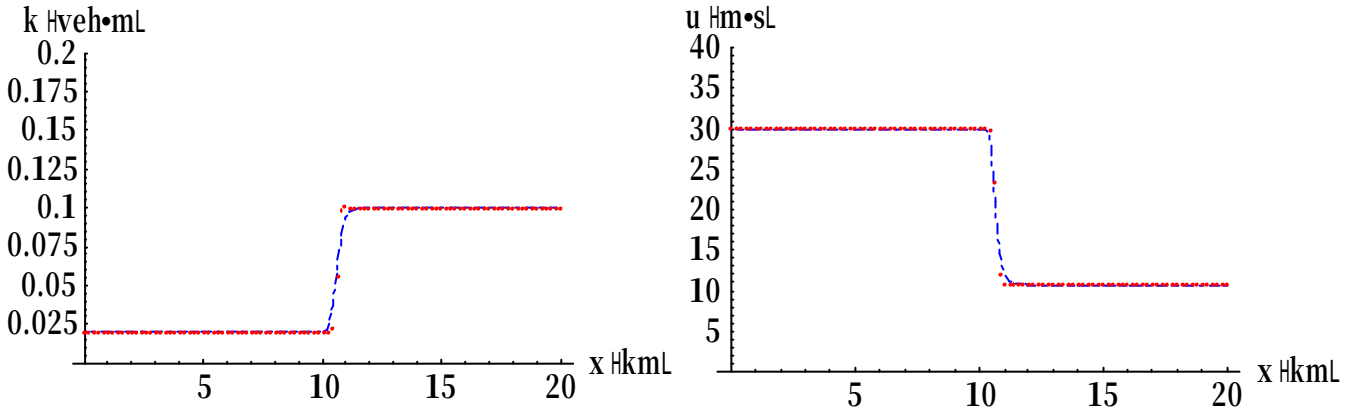

Figure 5.86. The density and velocity profiles at t = 2 min for condition (a) in case II of shock problems simulated with Jiang' s improved model (Dashes: solution of Jiang' s FD scheme; Dots: solution of WENO FV scheme).

Condition (b)

$$k(x,0)=\begin{cases}0.02, & 0\le x<10\\ 0.04, & 10\le x\le 20\end{cases}$$

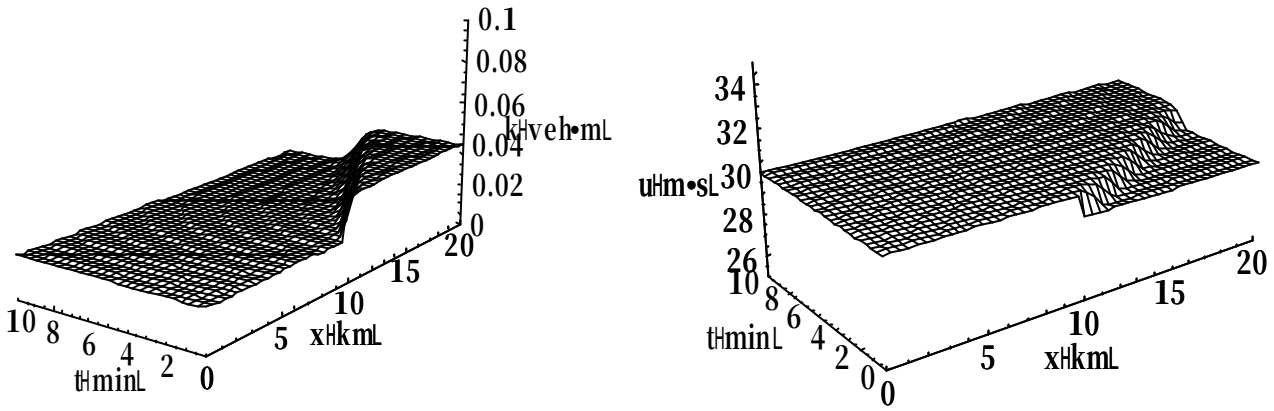

Figure 5.87. The density and velocity behaviors for condition (b) in case II of shock problems simulated by Jiang' s FD scheme with PW model.

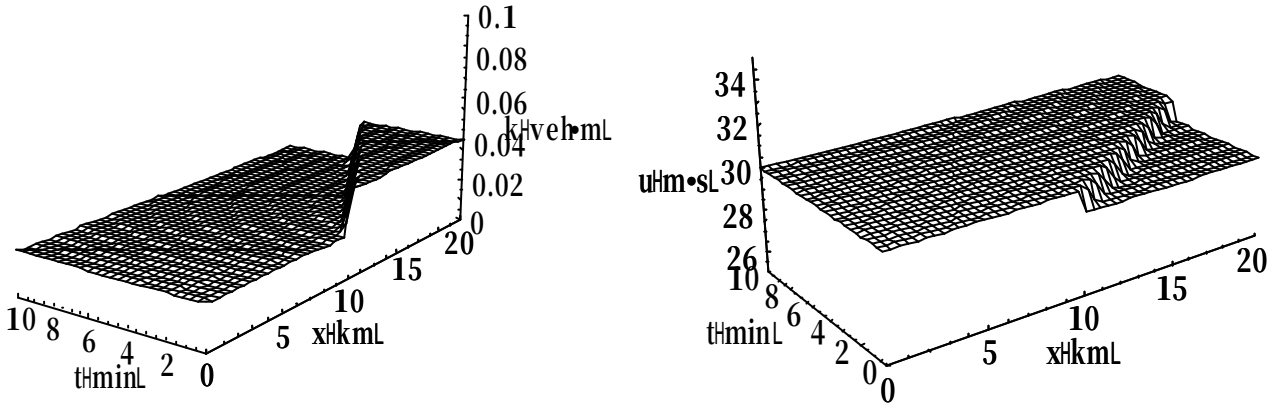

Figure 5.88. The density and velocity behaviors for condition (b) in case II of shock problems simulated by WENO FV scheme with PW model.

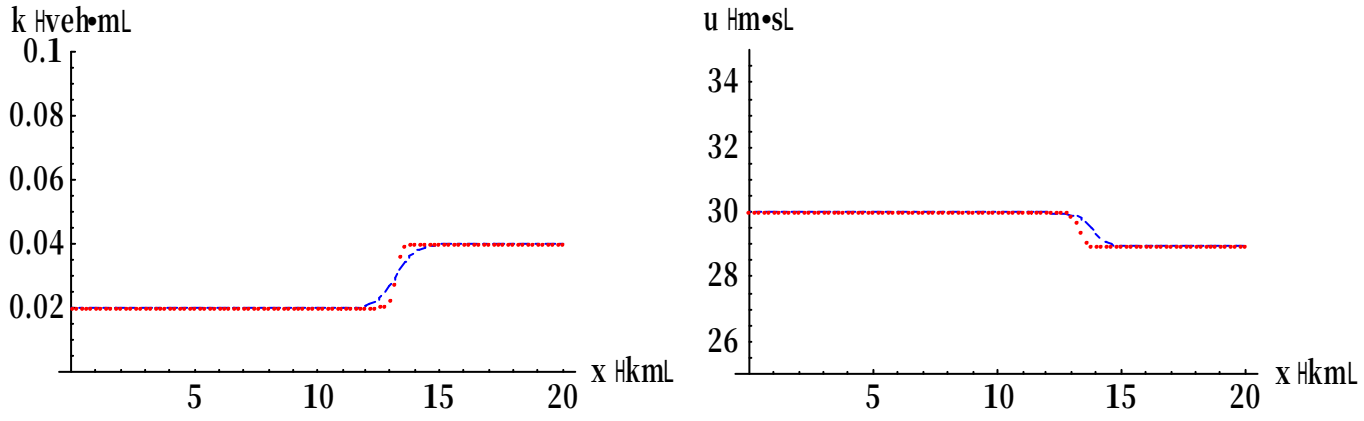

Figure 5.89. The density and velocity profiles at t = 2 min for condition (b) in case II of shock problems simulated with PW model (Dashes: solution of Jiang' s FD scheme; Dots: solution of WENO FV scheme).

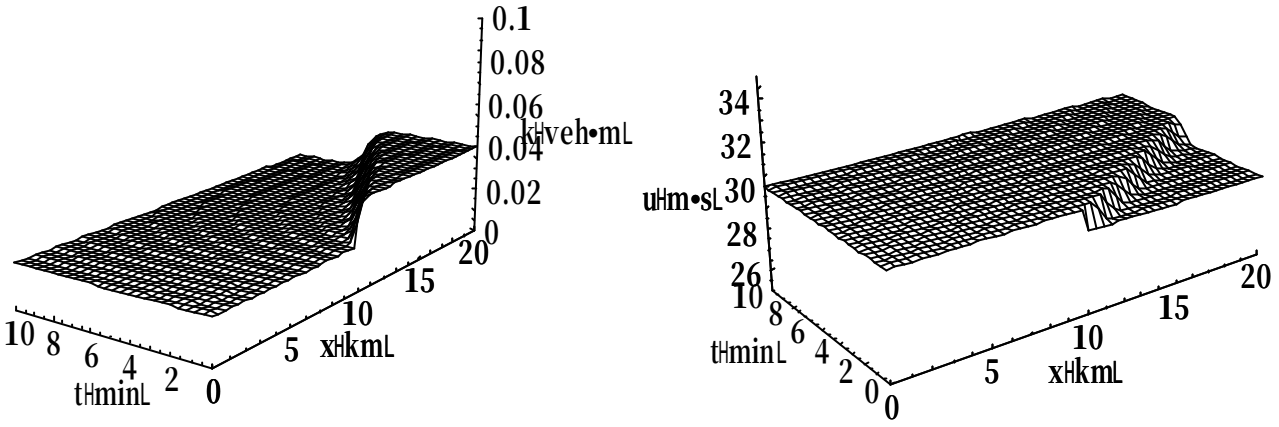

Figure 5.90. The density and velocity behaviors for condition (b) in case II of shock problems simulated by Jiang' s FD scheme with Jiang' s improved model.

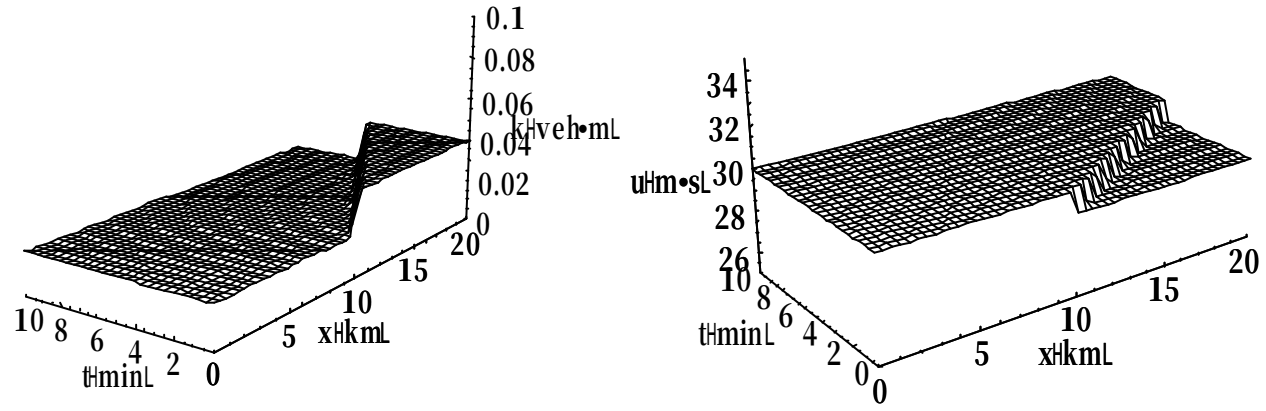

Figure 5.91. The density and velocity behaviors for condition (b) in case II of shock problems simulated by WENO FV scheme with Jiang' s improved model.

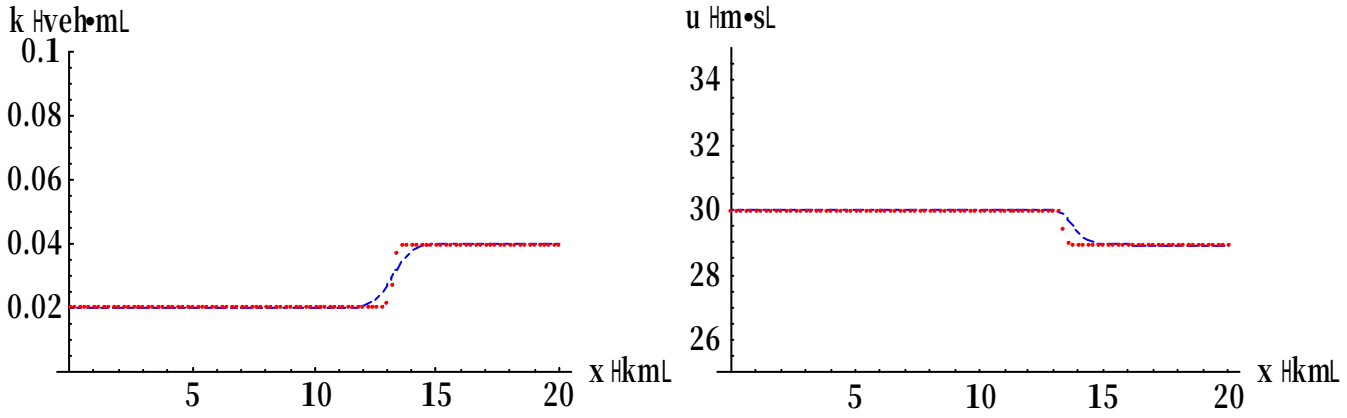

Figure 5.92. The density and velocity profiles at t = 2 min for condition (b) in case II of shock problems simulated with Jiang' s improved model (Dashes: solution of Jiang' s FD scheme; Dots: solution of WENO FV scheme).

5.2.1.3 Case III

In case III of the shock problems, the situation $k_l < k_r$ and $q_l = q_r$ was considered, as shown in Figure 5.93.

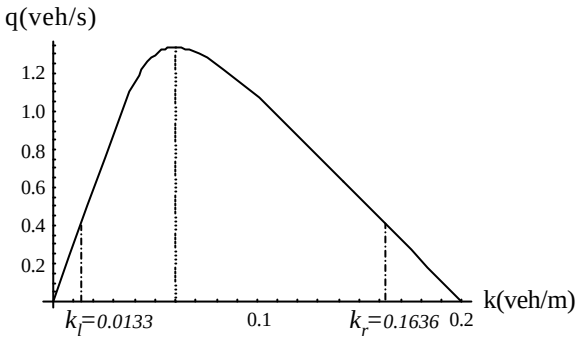

Figure 5.93. Case III of shock problems: k_l = 0.0133 veh/m and k_r = 0.1636 veh/m.

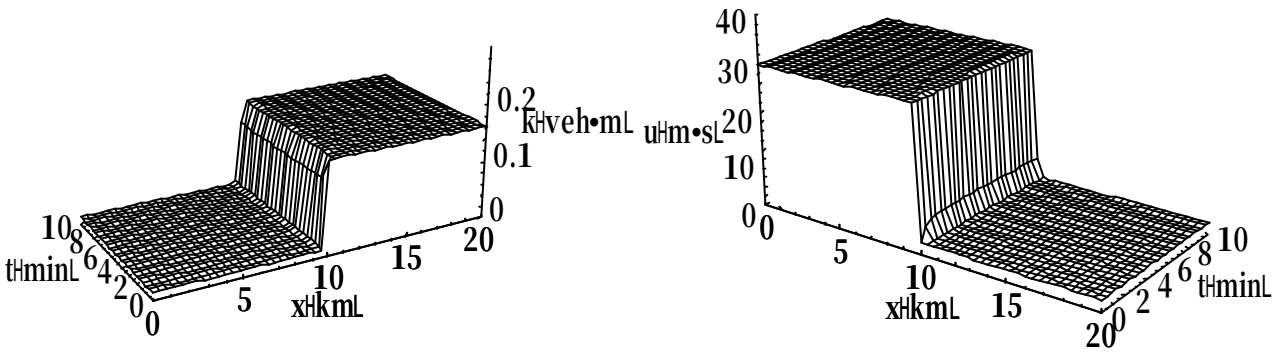

Figure 5.94. The density and velocity behaviors for case III of shock problems simulated by Jiang' s FD scheme with PW model.

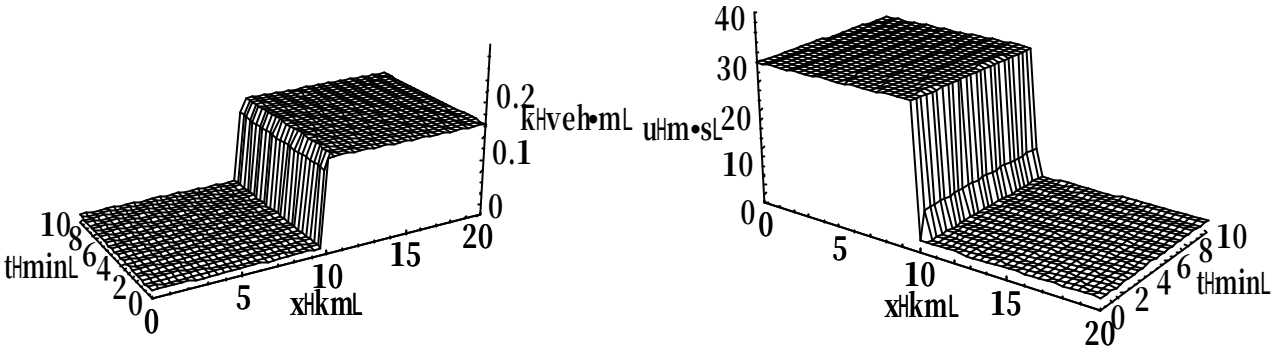

Figure 5.95. The density and velocity behaviors for case III of shock problems simulated by WENO FV scheme with PW model.

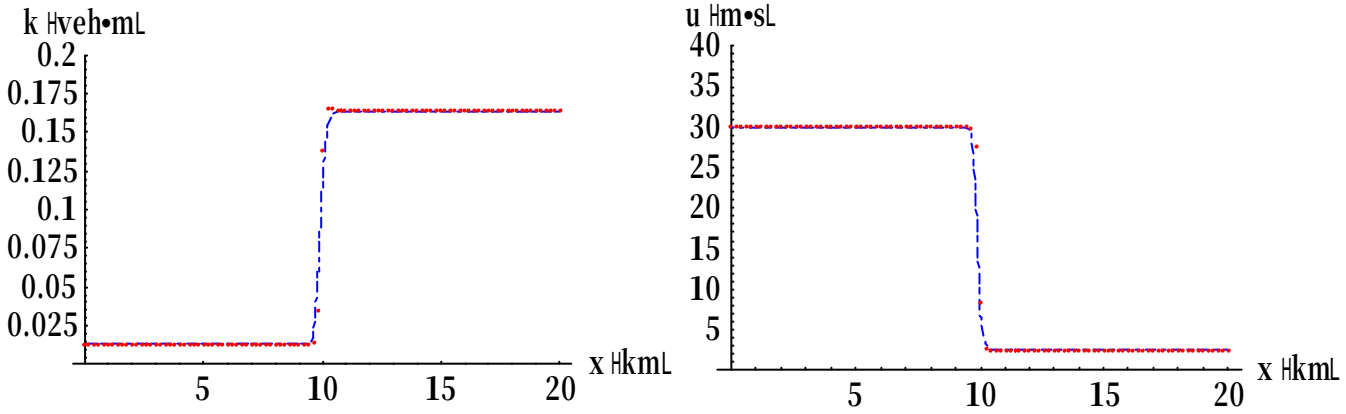

Figure 5.96. The density and velocity profiles at t = 2 min for case III of shock problems simulated with PW model (Dashes: solution of Jiang' s FD scheme; Dots: solution of WENO FV scheme).

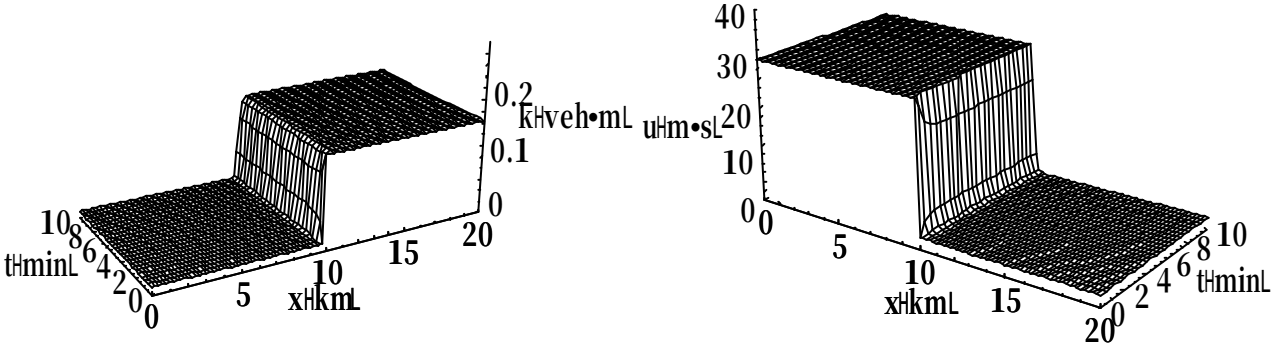

Figure 5.97. The density and velocity behaviors for case III of shock problems simulated by Jiang' s FD scheme with Jiang' s improved model.

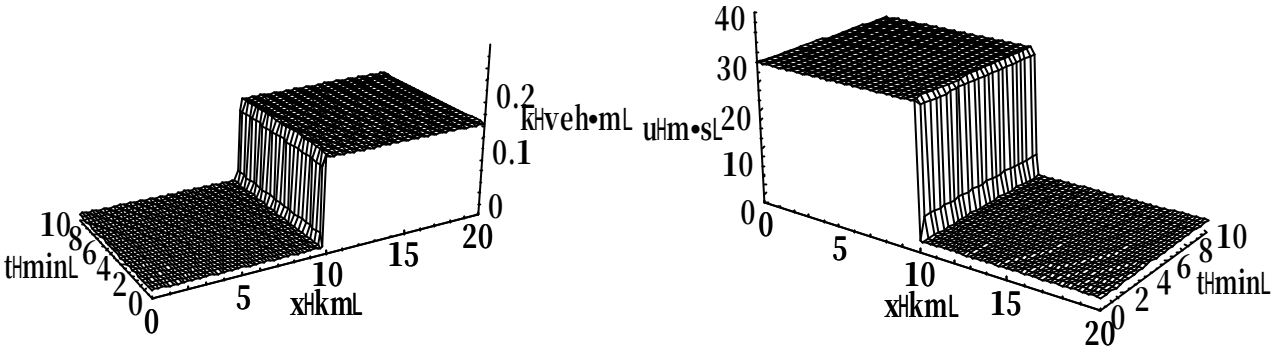

Figure 5.98. The density and velocity behaviors for case III of shock problems simulated by WENO FV scheme with Jiang' s improved model.

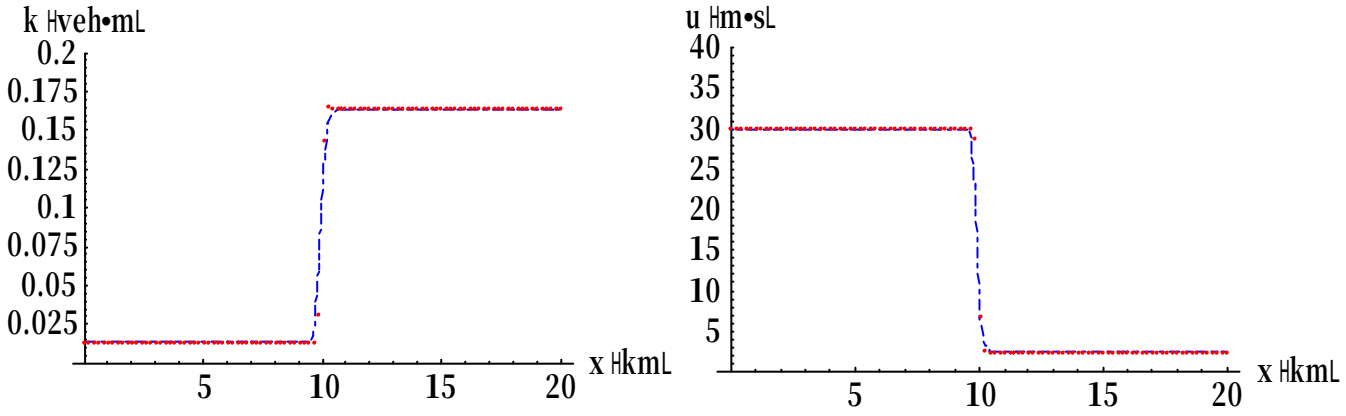

Figure 5.99. The density and velocity profiles at t = 2 min for case III of shock problems simulated with Jiang' s improved model (Dashes: solution of Jiang' s FD scheme; Dots: solution of WENO FV scheme).

5.2.2 Rarefaction Wave Problems

5.2.2.1 Case I

In case I of the rarefaction wave problems, the situation $k_l > k_r$ and $q_l > q_r$ was considered. There are two conditions satisfying the situation, as shown in Figure 5.100.

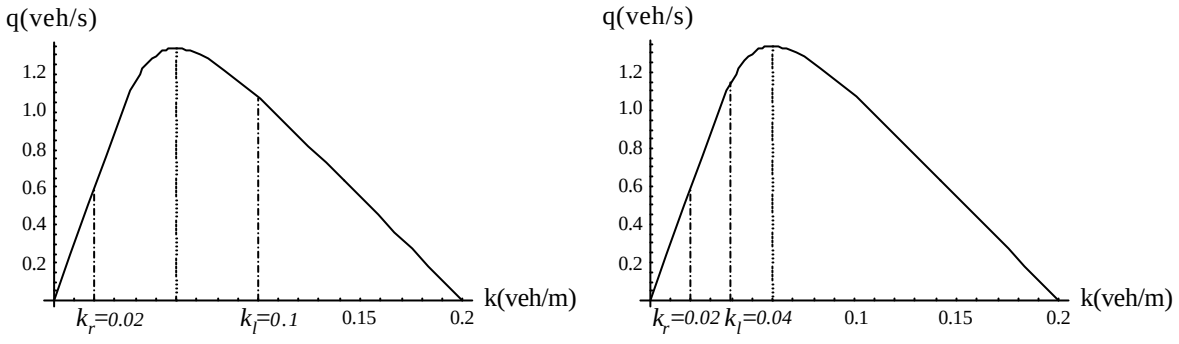

(a) (b)

Figure 5.100. Two conditions in case I of rarefaction wave problems: (a) k_l = 0.1 veh/m and k_r = 0.02 veh/m; (b) k_l = 0.04 veh/m and k_r = 0.02 veh/m.

Condition (a)

$$k(x,0)=\begin{cases}0.1, & 0 \le x < 10\\ 0.02, & 10 \le x \le 20\end{cases}$$

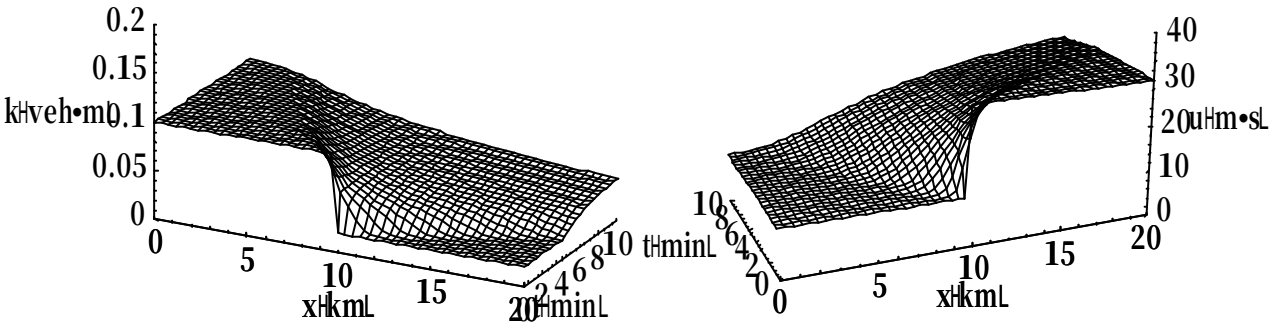

Figure 5.101. The density and velocity behaviors for condition (a) in case I of rarefaction wave problems simulated by Jiang' s FD scheme with PW model.

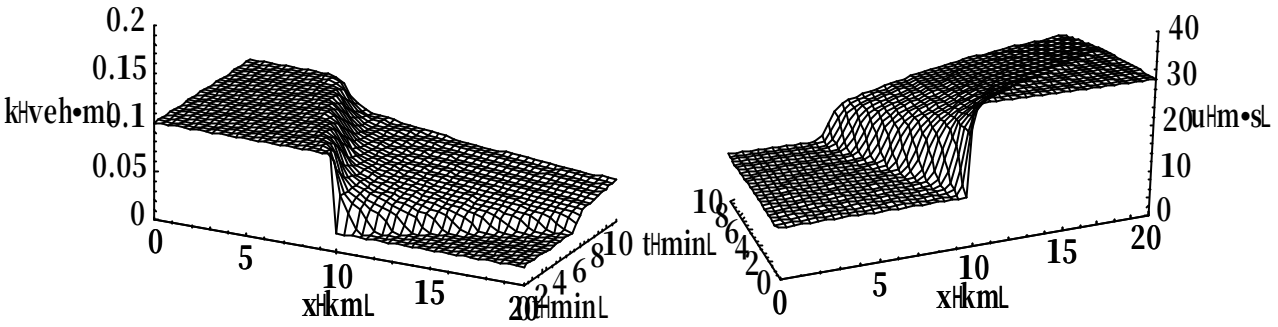

Figure 5.102. The density and velocity behaviors for condition (a) in case I of rarefaction wave problems simulated by WENO FV scheme with PW model.

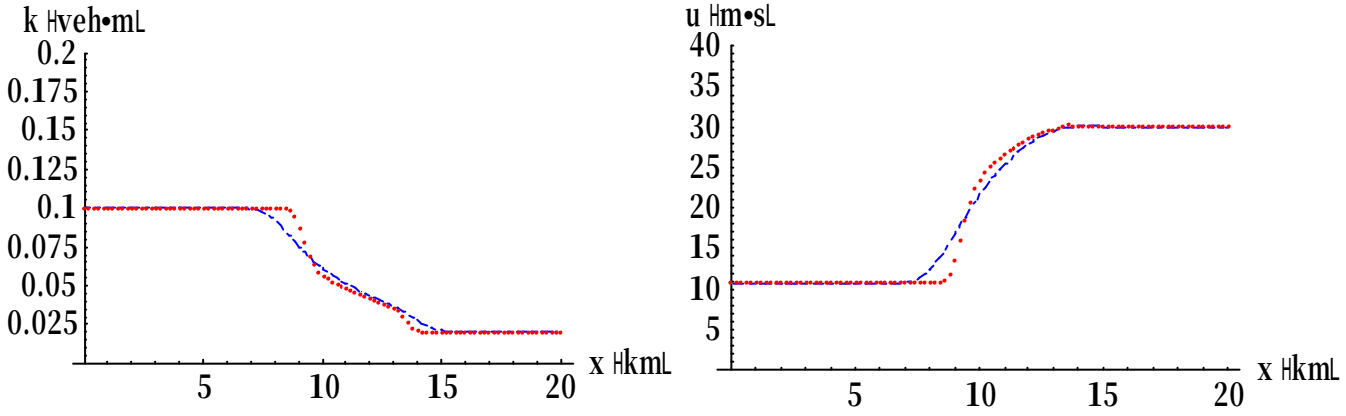

Figure 5.103. The density and velocity profiles at t = 2 min for condition (a) in case I of rarefaction wave problems simulated with PW model (Dashes: solution of Jiang' s FD scheme; Dots: solution of WENO FV scheme).

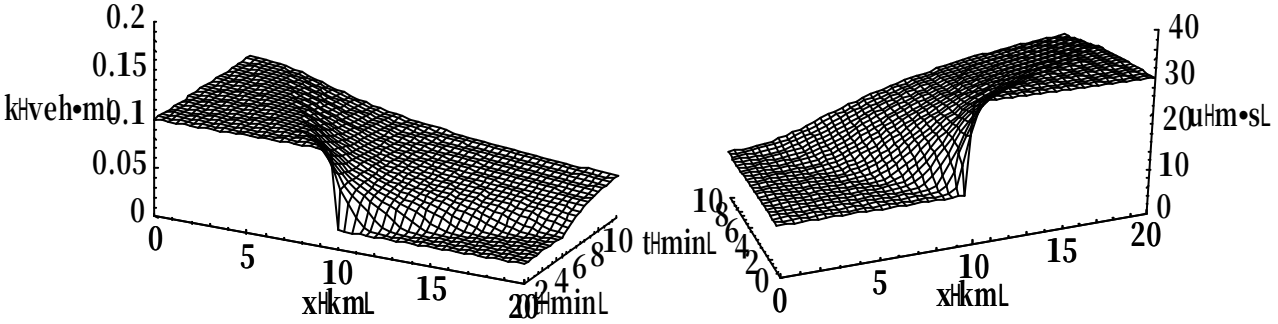

Figure 5.104. The density and velocity behaviors for condition (a) in case I of rarefaction wave problems simulated by Jiang' s FD scheme with Jiang' s improved model.

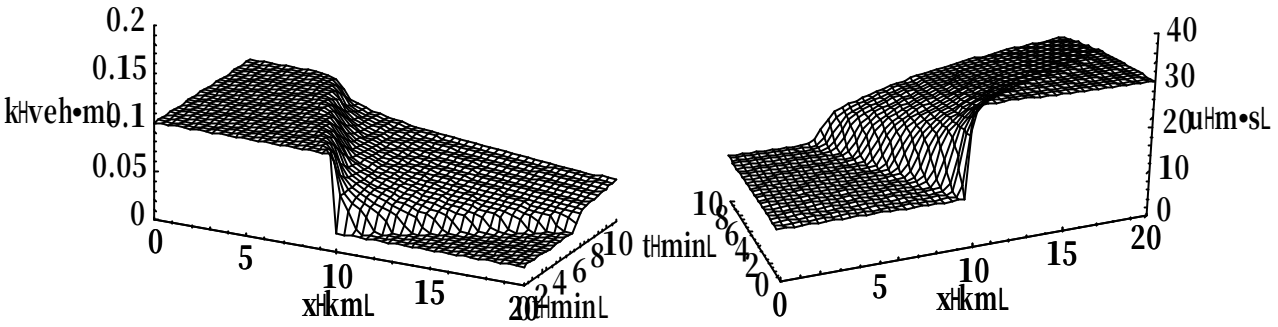

Figure 5.105. The density and velocity behaviors for condition (a) in case I of rarefaction wave problems simulated by WENO FV scheme with Jiang' s improved model.

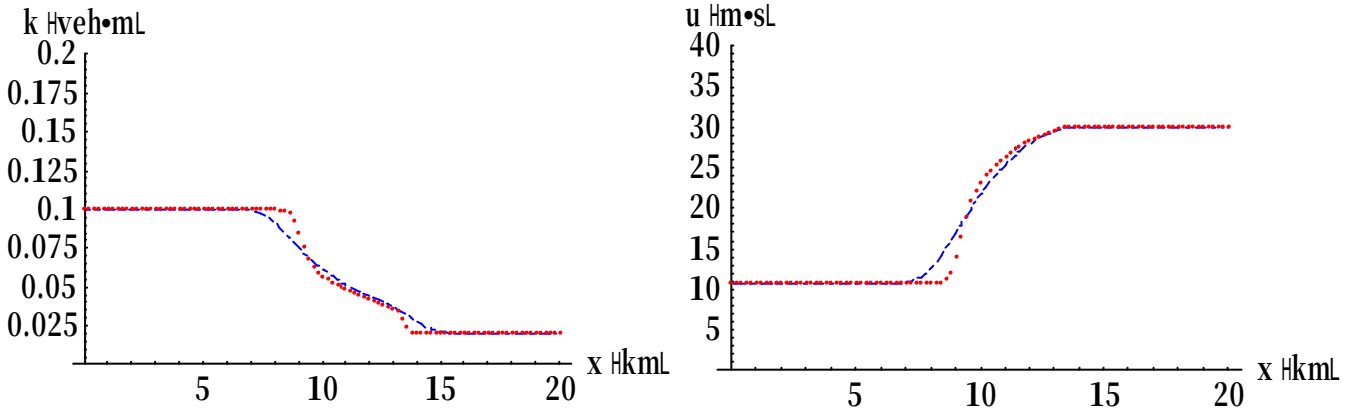

Figure 5.106. The density and velocity profiles at t = 2 min for condition (a) in case I of rarefaction wave problems simulated with Jiang' s improved model (Dashes: solution of Jiang' s FD scheme; Dots: solution of WENO FV scheme).

Condition (b)

$$k(x,0)=\begin{cases}0.04, & 0\le x<10\\ 0.02, & 10\le x\le 20\end{cases}$$

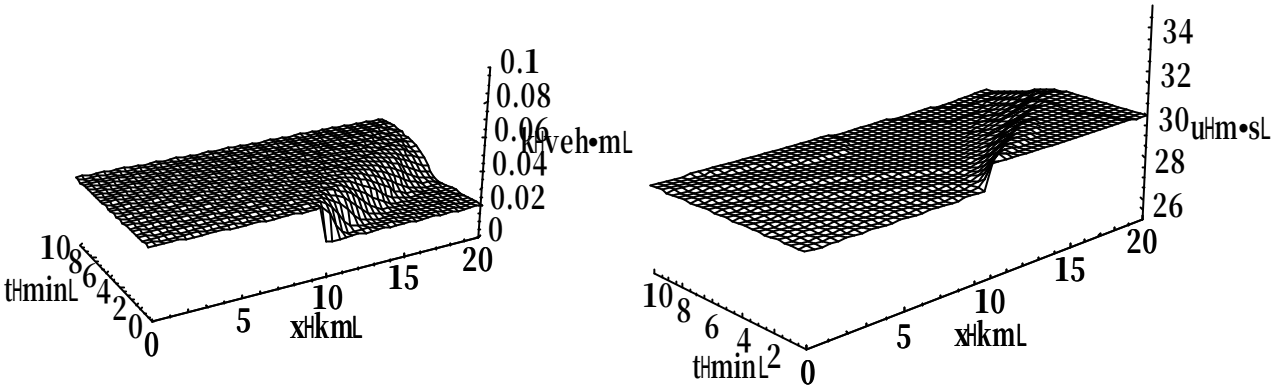

Figure 5.107. The density and velocity behaviors for condition (b) in case I of rarefaction wave problems simulated by Jiang' s FD scheme with PW model.

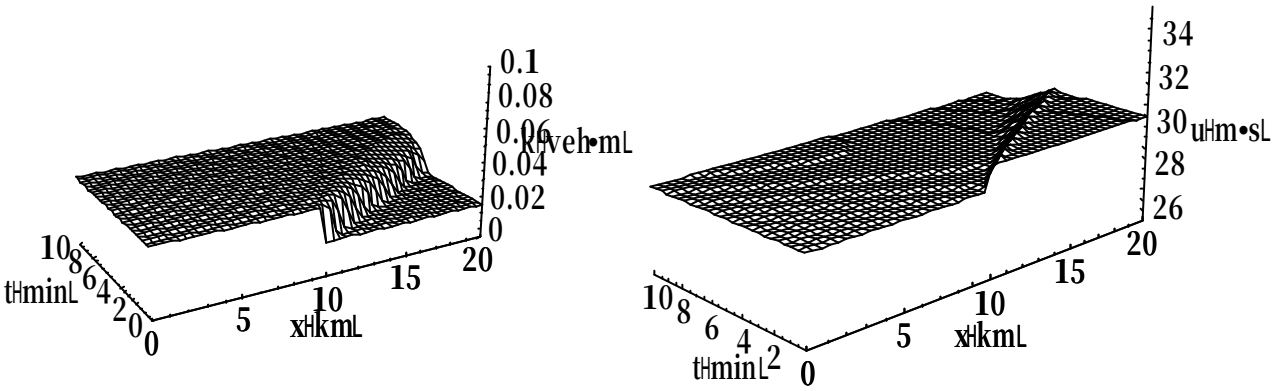

Figure 5.108. The density and velocity behaviors for condition (b) in case I of rarefaction wave problems simulated by WENO FV scheme with PW model.

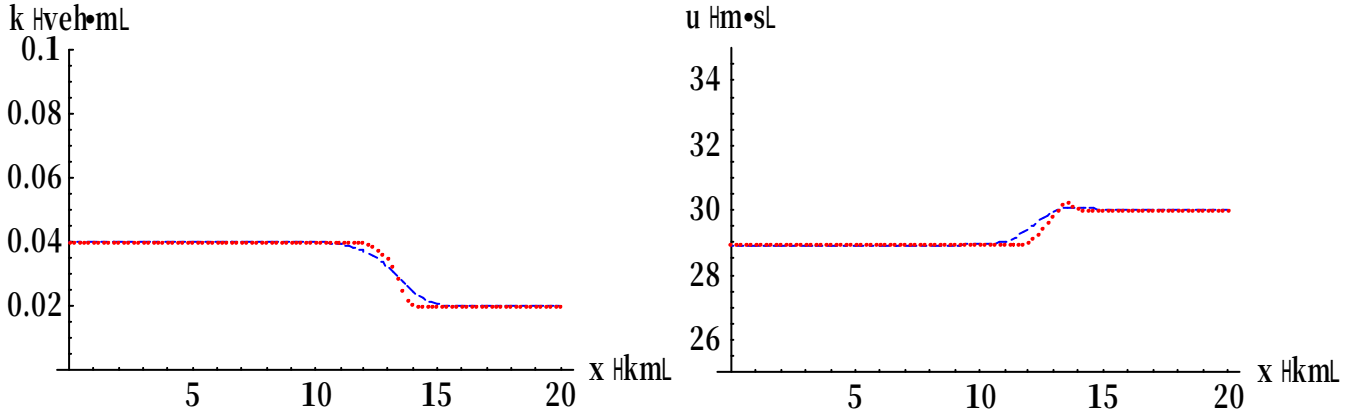

Figure 5.109. The density and velocity profiles at t = 2 min for condition (b) in case I of rarefaction wave problems simulated with PW model (Dashes: solution of Jiang' s FD scheme; Dots: solution of WENO FV scheme).

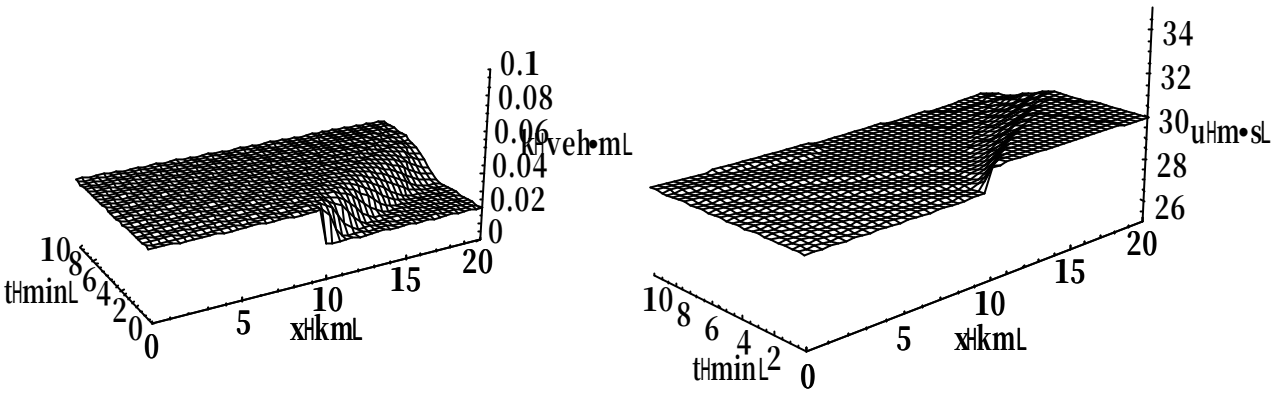

Figure 5.110. The density and velocity behaviors for condition (b) in case I of rarefaction wave problems simulated by Jiang' s FD scheme with Jiang' s improved model.

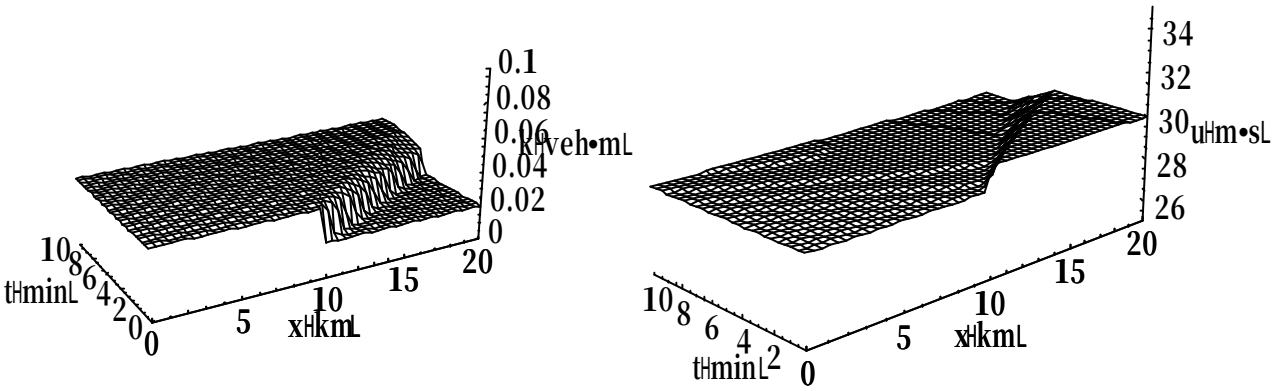

Figure 5.111. The density and velocity behaviors for condition (b) in case I of rarefaction wave problems simulated by WENO FV scheme with Jiang' s improved model.

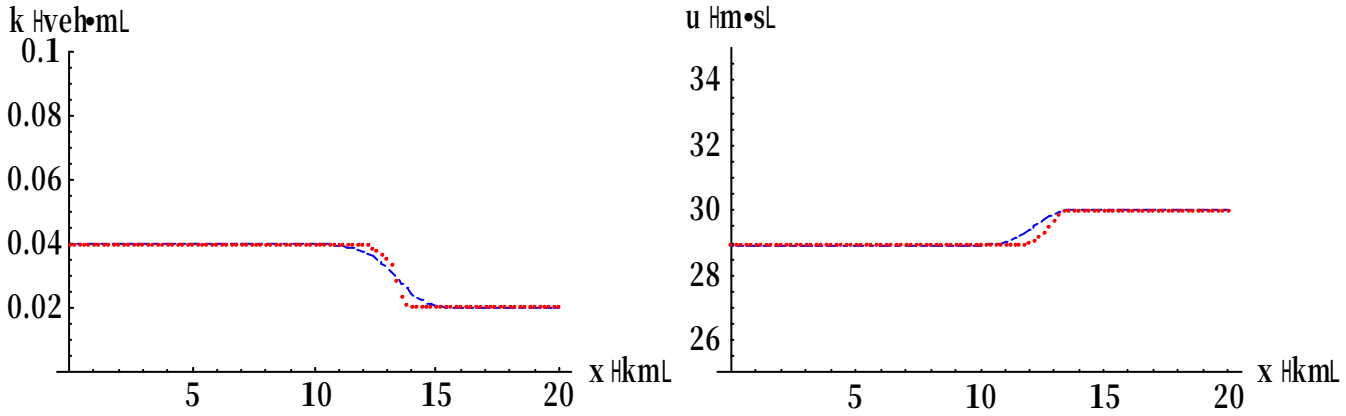

Figure 5.112. The density and velocity profiles at t = 2 min for condition (b) in case I of rarefaction wave problems simulated with Jiang' s improved model (Dashes: solution of Jiang' s FD scheme; Dots: solution of WENO FV scheme).

5.2.2.2 Case II

In case II of the rarefaction wave problems, the situation $k_l > k_r$ and $q_l < q_r$ was considered. There are two conditions satisfying the situation, as shown in Figure 5.113.

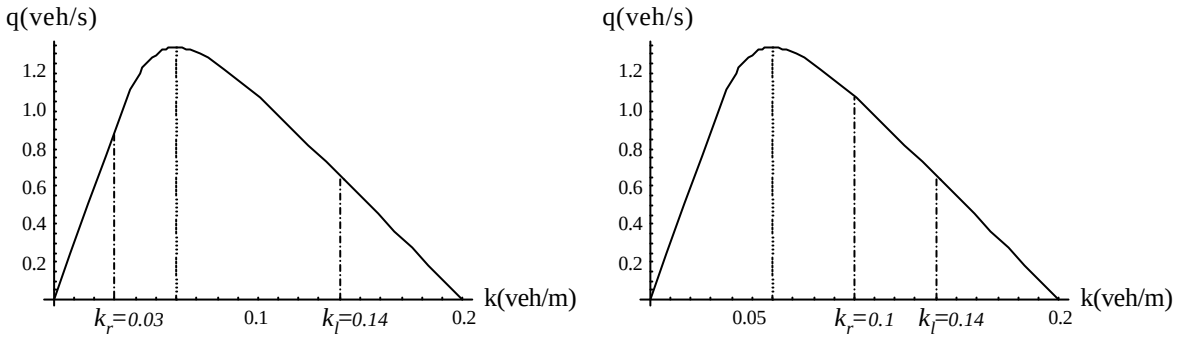

(a) (b)

Figure 5.113. Two conditions in case II of rarefaction wave problems: (a) k_l = 0.14 veh/m and k_r = 0.03 veh/m; (b) k_l = 0.14 veh/m and k_r = 0.1 veh/m.

Condition (a)

$$k(x,0)=\begin{cases}0.14, & 0 \le x < 10\\ 0.03, & 10 \le x \le 20\end{cases}$$

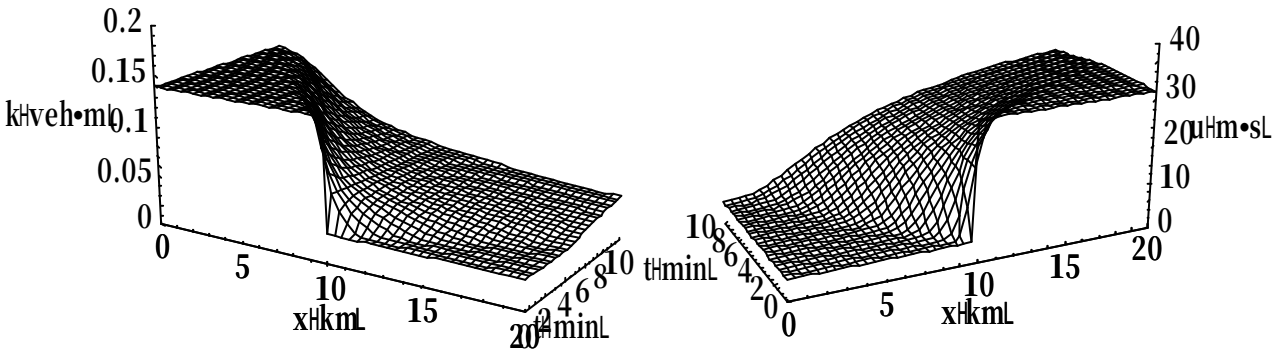

Figure 5.114. The density and velocity behaviors for condition (a) in case II of rarefaction wave problems simulated by Jiang's FD scheme with PW model.

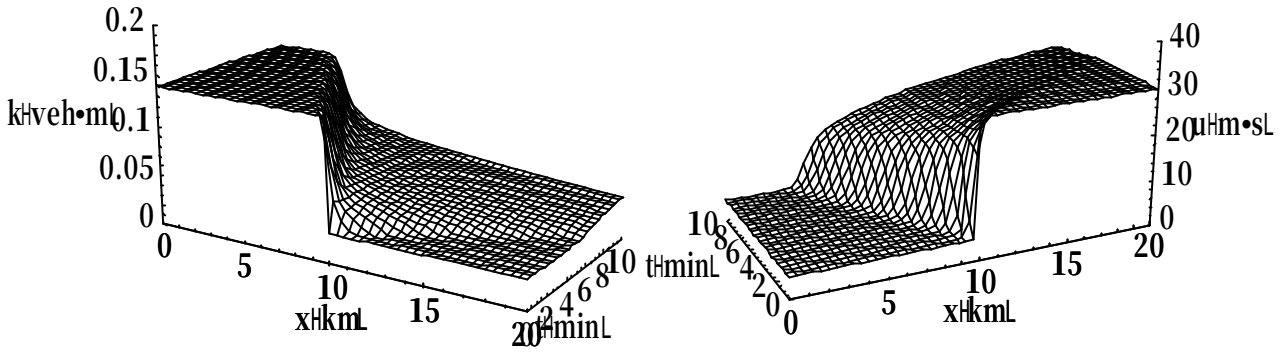

Figure 5.115. The density and velocity behaviors for condition (a) in case II of rarefaction wave problems simulated by WENO FV scheme with PW model.

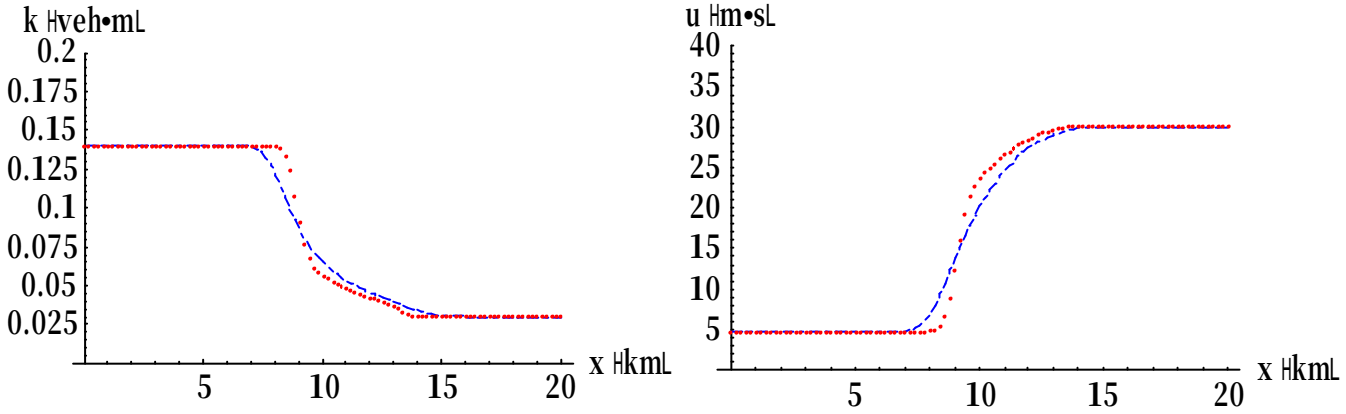

Figure 5.116. The density and velocity profiles at t = 2 min for condition (a) in case II of rarefaction wave problems simulated with PW model (Dashes: solution of Jiang' s FD scheme; Dots: solution of WENO FV scheme).

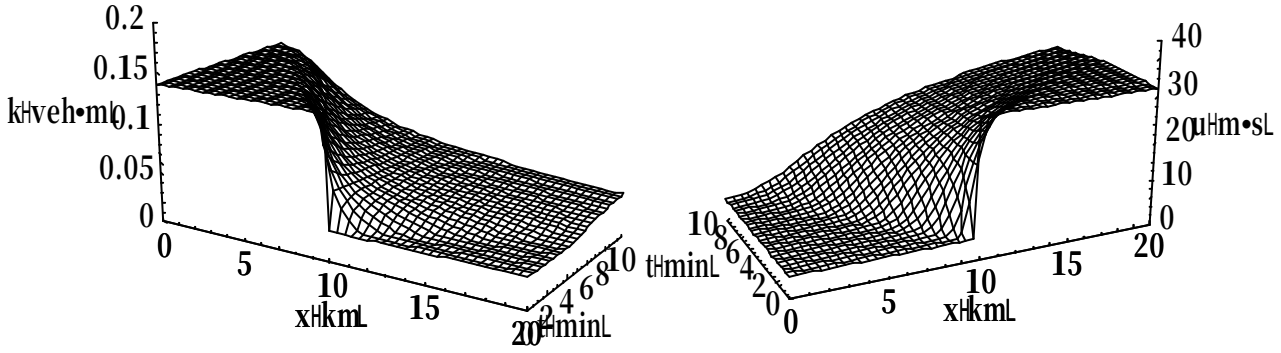

Figure 5.117. The density and velocity behaviors for condition (a) in case II of rarefaction wave problems simulated by Jiang' s FD scheme with Jiang' s improved model.

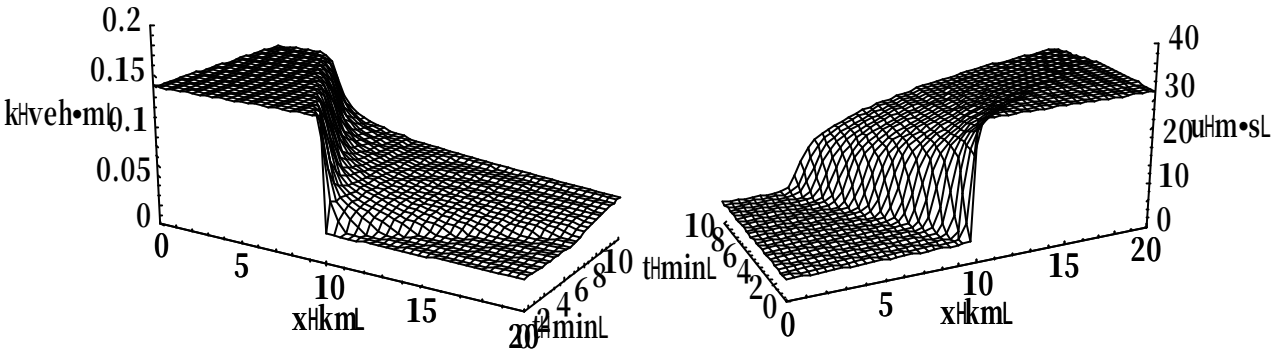

Figure 5.118. The density and velocity behaviors for condition (a) in case II of rarefaction wave problems simulated by WENO FV scheme with Jiang' s improved model.

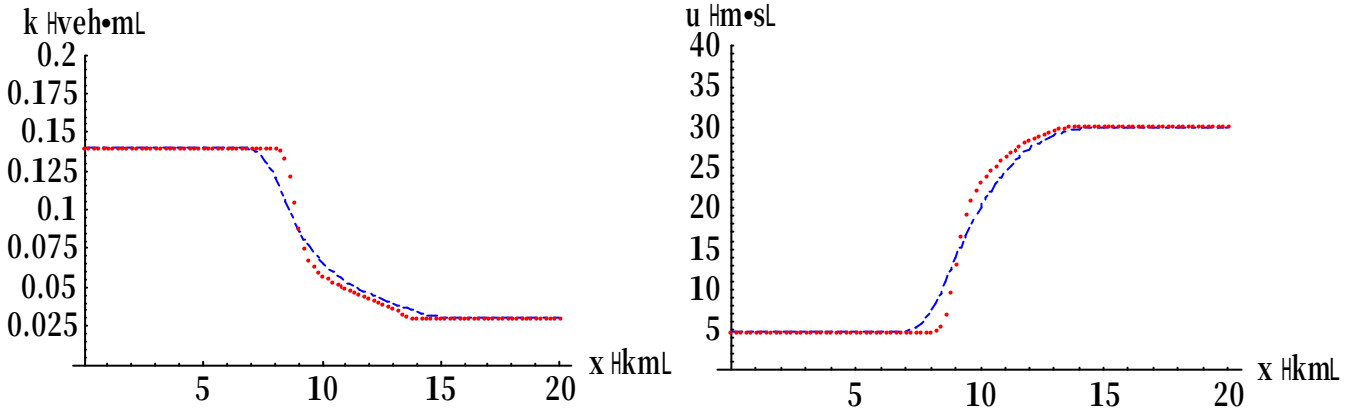

Figure 5.119. The density and velocity profiles at t = 2 min for condition (a) in case II of rarefaction wave problems simulated with Jiang' s improved model (Dashes: solution of Jiang' s FD scheme; Dots: solution of WENO FV scheme).

Condition (b)

$$k(x,0)=\begin{cases}0.14, & 0\le x<10\\ 0.1, & 10\le x\le 20\end{cases}$$

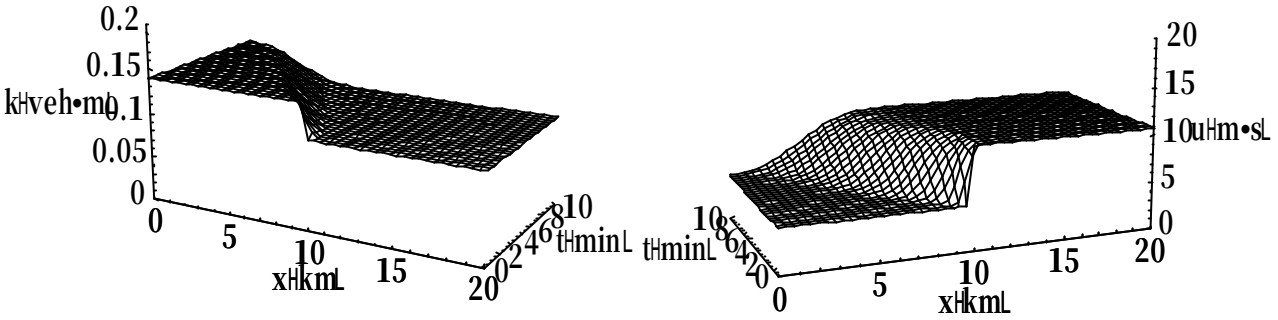

Figure 5.120. The density and velocity behaviors for condition (b) in case II of rarefaction wave problems simulated by Jiang' s FD scheme with PW model.

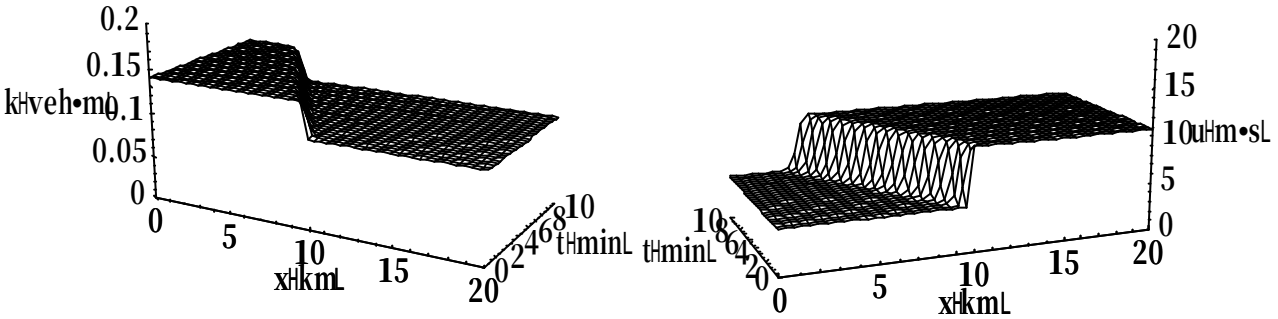

Figure 5.121. The density and velocity behaviors for condition (b) in case II of rarefaction wave problems simulated by WENO FV scheme with PW model.

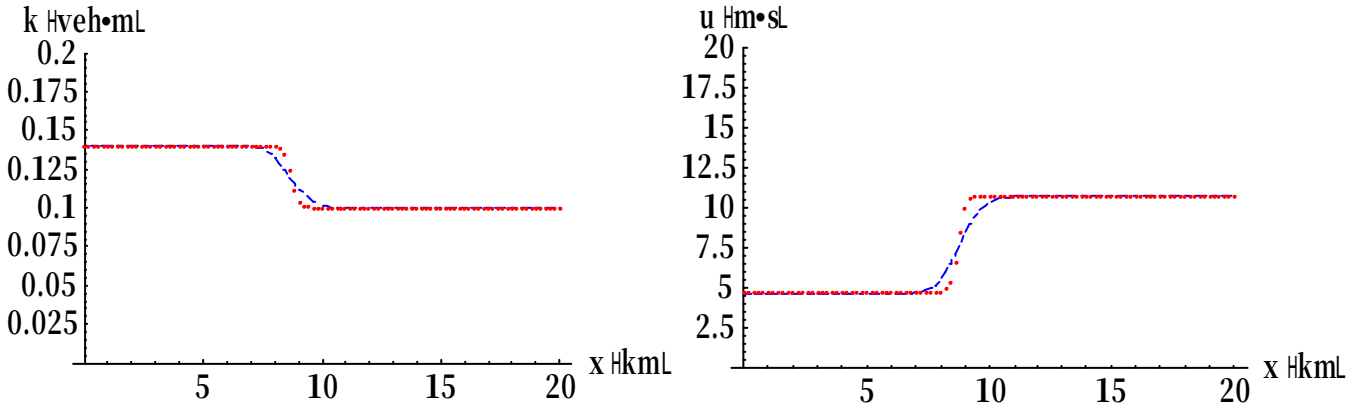

Figure 5.122. The density and velocity profiles at t = 2 min for condition (b) in case II of rarefaction wave problems simulated with PW model (Dashes: solution of Jiang' s FD scheme; Dots: solution of WENO FV scheme).

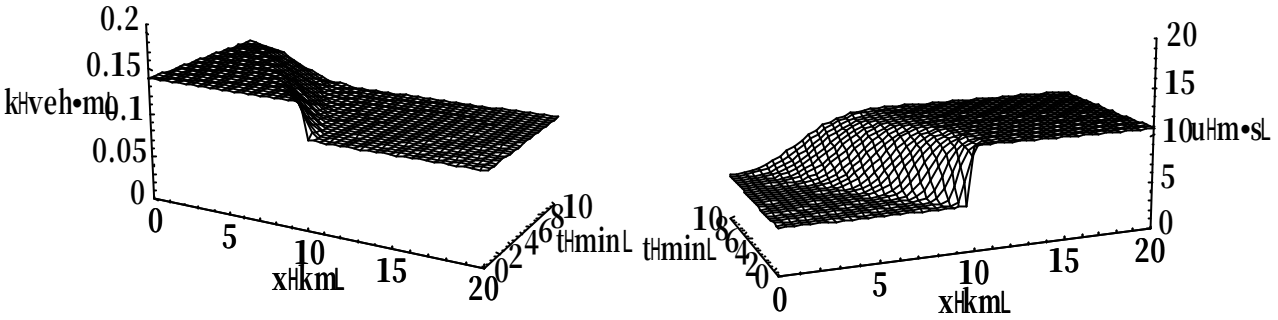

Figure 5.123. The density and velocity behaviors for condition (b) in case II of rarefaction wave problems simulated by Jiang' s FD scheme with Jiang' s improved model.

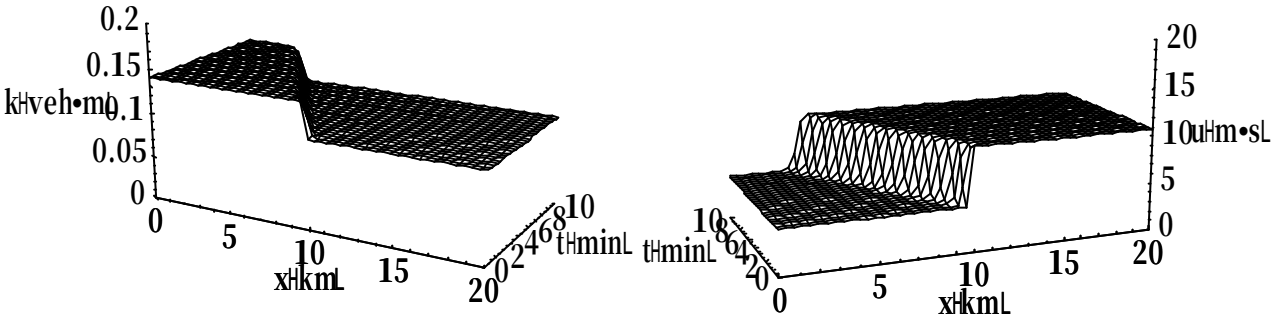

Figure 5.124. The density and velocity behaviors for condition (b) in case II of rarefaction wave problems simulated by WENO FV scheme with Jiang' s improved model.

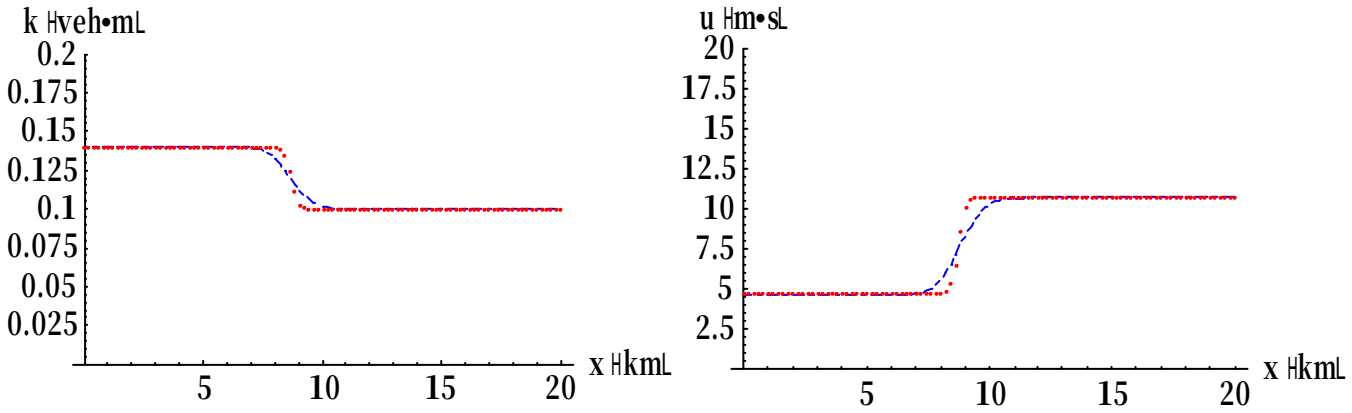

Figure 5.125. The density and velocity profiles at t = 2 min for condition (b) in case II of rarefaction wave problems simulated with Jiang' s improved model (Dashes: solution of Jiang' s FD scheme; Dots: solution of WENO FV scheme).

5.2.2.3 Case III

In case III of the rarefaction problems, the situation $k_l > k_r$ and $q_l = q_r$ was considered, as shown in Figure 5.126.

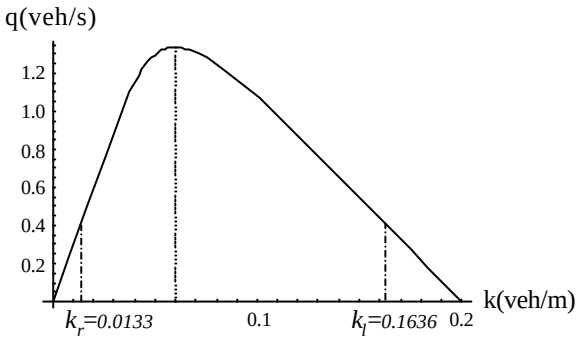

Figure 5.126. Case III of rarefaction wave problems: k_l = 0.1636 veh/m and k_r = 0.0133 veh/m.

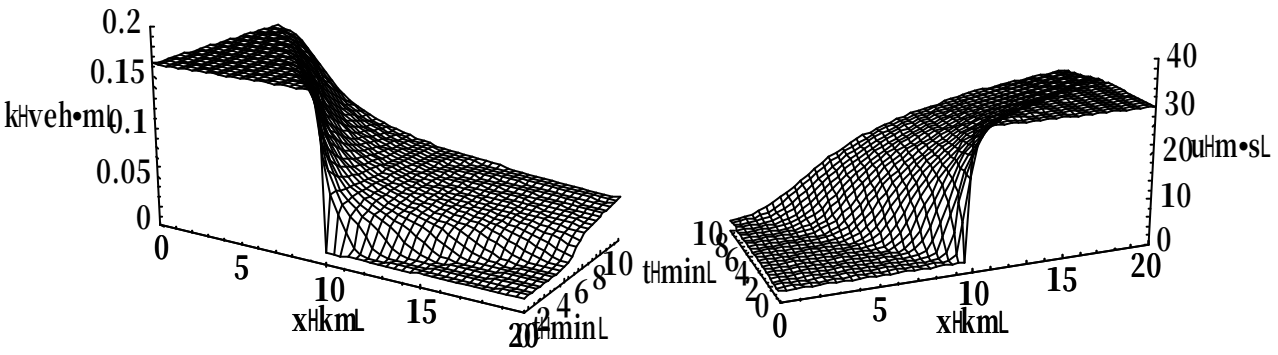

Figure 5.127. The density and velocity behaviors for case III of rarefaction wave problems simulated by Jiang' s FD scheme with PW model.

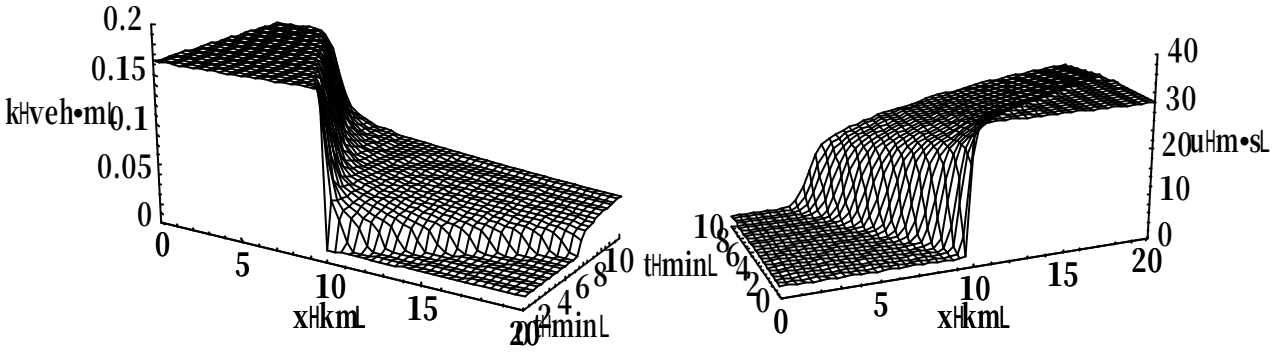

Figure 5.128. The density and velocity behaviors for case III of rarefaction wave problems simulated by WENO FV scheme with PW model.

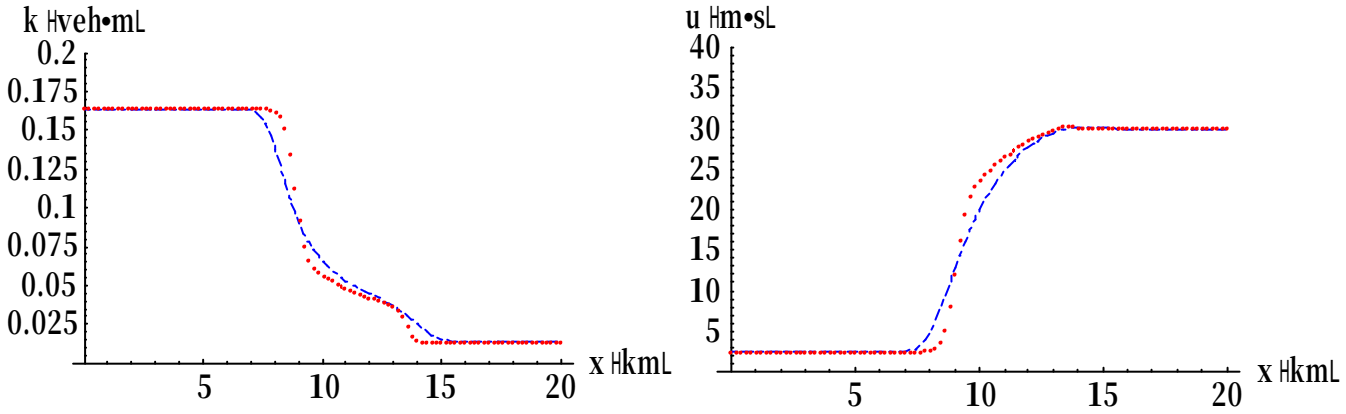

Figure 5.129. The density and velocity profiles at t = 2 min for case III of rarefaction wave problems simulated with PW model (Dashes: solution of Jiang' s FD scheme; Dots: solution of WENO FV scheme).

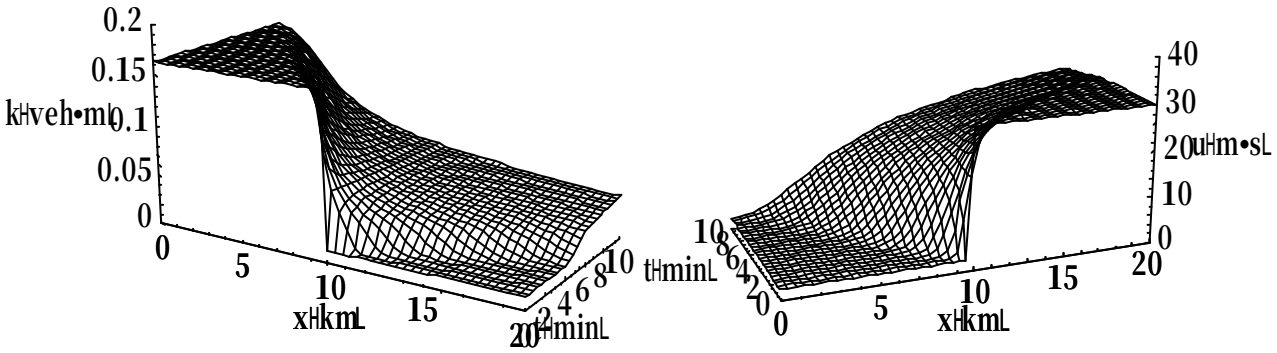

Figure 5.130. The density and velocity behaviors for case III of rarefaction wave problems simulated by Jiang' s FD scheme with Jiang' s improved model.

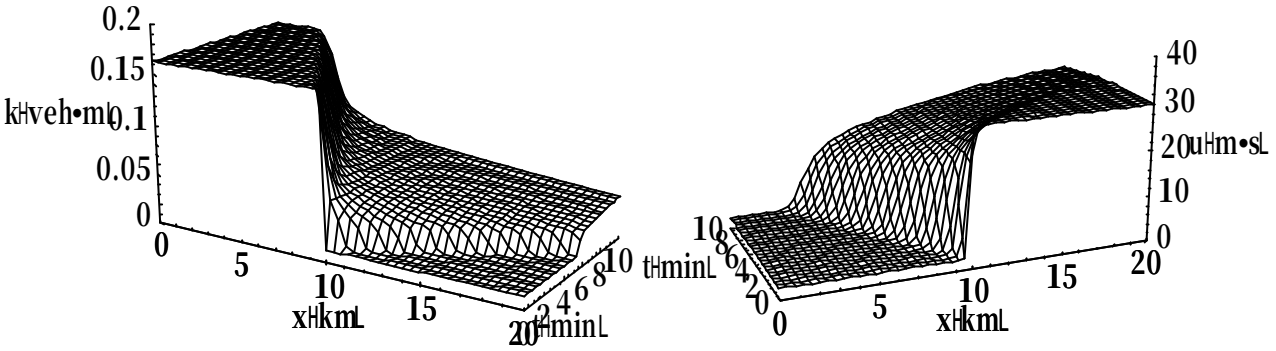

Figure 5.131. The density and velocity behaviors for case III of rarefaction wave problems simulated by WENO FV scheme with Jiang's improved model.

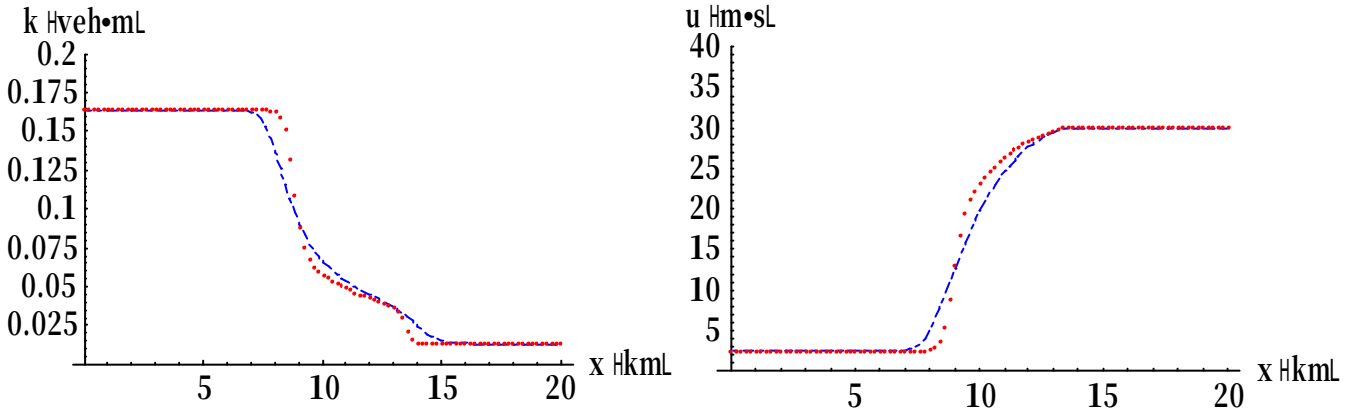

Figure 5.132. The density and velocity profiles at t = 2 min for case III of rarefaction wave problems simulated with Jiang's improved model (Dashes: solution of Jiang's FD scheme; Dots: solution of WENO FV scheme).

5.2.3 Local Cluster Effect

In this section, the local cluster effect with respect to a localized perturbation in an initial homogeneous condition was simulated. Jiang (2002) demonstrated that his improved model can describe the amplification of a small disturbance, known as the local cluster effect of traffic flow (Kerner and Konhäuser, 1993, 1994; Herrmann and Kerner, 1998). The local cluster effect corresponds to the stop-and-go phenomena observed in the field due to a small disturbance (Jiang, 2002). The following initial variation of the average density k_0 proposed by Hermann and Kerner (1998) was applied in this section:

$$k(x,0) = k_0 + \Delta k_0 \left\{ \cosh^{-2}\left[\frac{160}{L}(x - \frac{5L}{16}) \right] - \frac{1}{4}\cosh^{-2}\left[\frac{40}{L}(x - \frac{11L}{32}) \right] \right\},$$

where L is the length of the road section. The equilibrium speed-density relationship presented by Kerner and Konhäuser (1993):

$$u_e = u_f \left(1/\left(1 + \exp(\frac{k/k_j - 0.25}{0.06}) \right) - 3.72\times10^{-6} \right)$$

was also used, as shown in Figure 5.133.

As the condition Jiang (2002) assumed, L = 32.2 km, Äk$_0$ = 0.01veh/m, the space interval Äx = 100m, the time interval Ät = 1sec, and the periodic boundary conditions was adopted as follows:

$k(L,t) = k(0,t),\ \ u(L,t) = u(0,t)$.

Moreover, the initial flow was supposed to be in local equilibrium everywhere:

$u(x,0) = u_e(k(x,0))$,

Other parameter values are the same as in Section 5.2.

Jiang (2002) derived the stable condition and found out the traffic would be unstable when

$k_d < k_0 < k_u$,

where down-critical density k_d = 0.031 and up-critical density k_u = 0.084. The results simulated by Jiang's FD scheme illustrated how the unstable traffic developed, as shown in Figure 5.135(a)-(j). In Figure 5.135(a)-(b), due to the low traffic density, the perturbation is dispersing without any amplification. As the initial density increases, small perturbations can be amplified, leading to traffic instability (Jiang, 2002). A single local cluster forms while the density is just above k_d, as shown in Figure 5.135(d). As the density becomes higher, Figure 5.135(e) illustrates the structure of multiple clusters which corresponds to a stop-and-go traffic. In Figure 5.135(f), a dipole-like structure is observed. When the density becomes

larger than k_u, a stable regime is reached again as shown in Figure 5.135(h).

Therefore, provided that the initial density is below k_d or above k_u, the traffic would be stable, and vice versa. The theoretical values of k_d and k_u derived by Jiang (2002) are 0.031 and 0.084, respectively. When simulating by Jiang's FD scheme, the two values are 0.04 and 0.077. Figure 5.136(a)-(j) demonstrates that WENO FV scheme produces the two values with 0.035 and 0.08. The numerical comparison between Jiang's FD and WENO FV schemes is given in Figure 5.137 and Table 5.5. It is shown again that WENO scheme really has the dominant numerical accuracy.

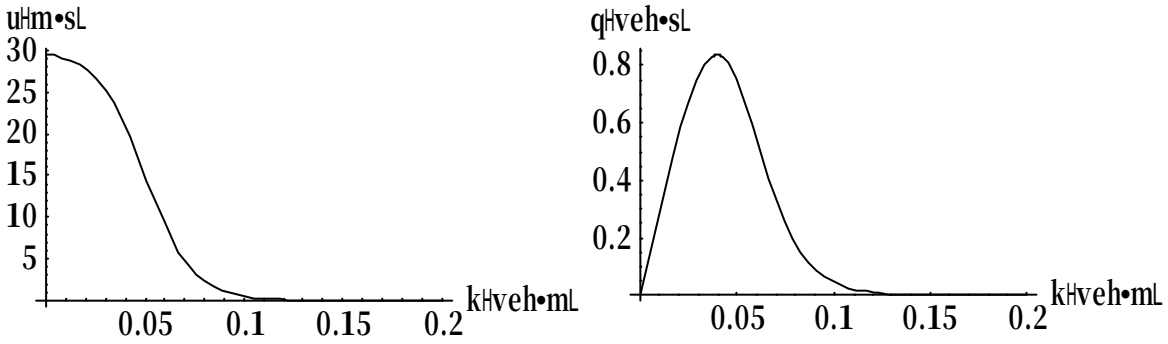

Figure 5.133. The equilibrium speed-density and flow-density relationship presented by Kerner and Konhäuser (1993).

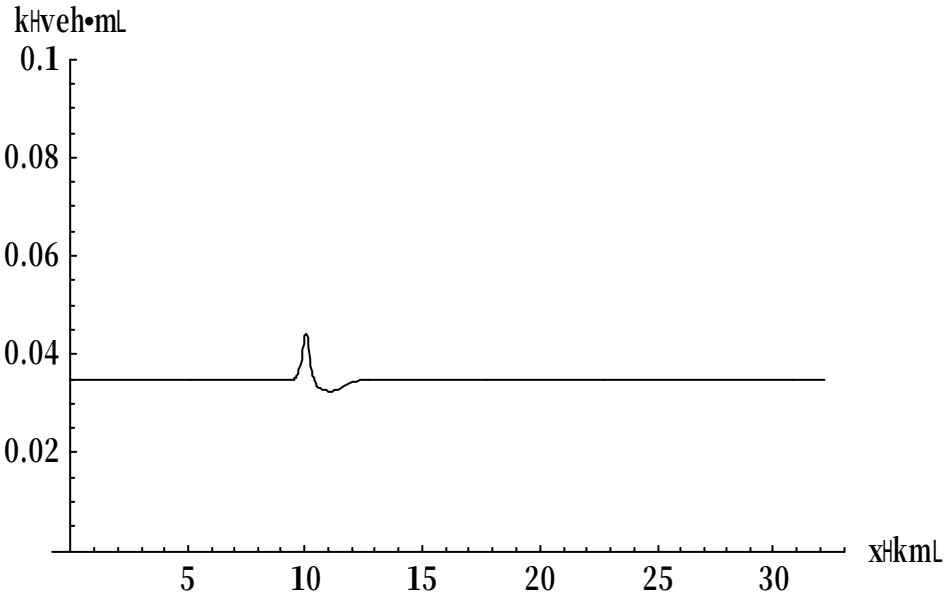

Figure 5.134. The initial variation of the average density k_0 = 0.035 veh/m.

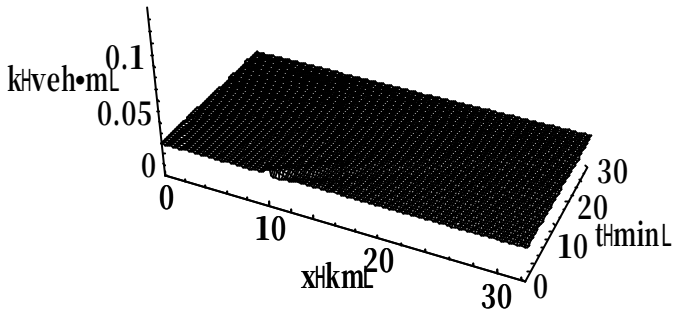
k[veh•m]
0.1
0.05
0
0
10
20
30
x[km]
0
10
20
30
t[min]

(a)

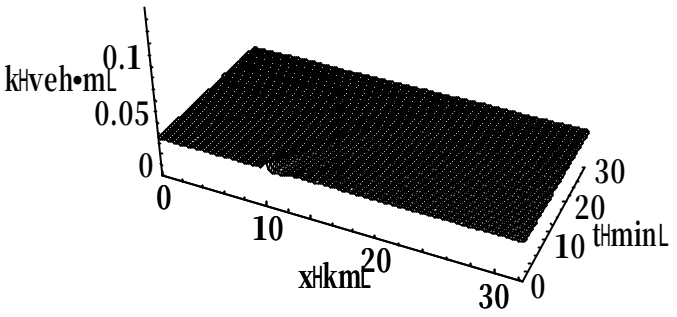
k[veh•m]
0.1
0.05
0
0
10
20
30
x[km]
0
10
20
30
t[min]

(b)

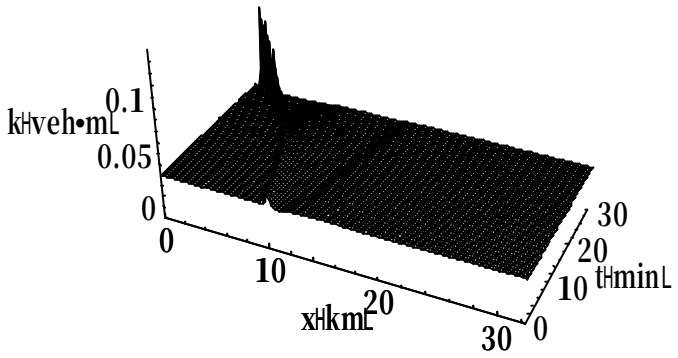
k[veh•m]
0.1
0.05
0
0
10
20
30
x[km]
0
10
20
30
t[min]

(c)

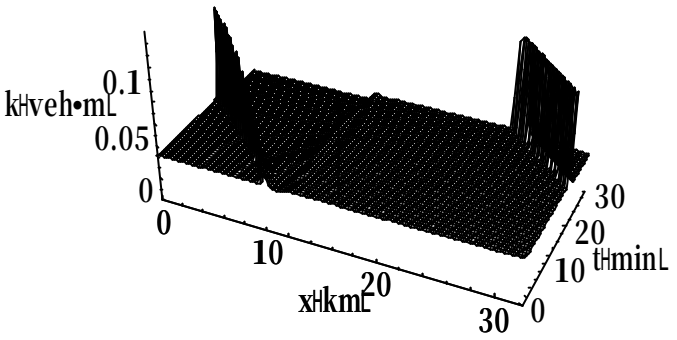
k[veh•m]
0.1
0.05
0
0
10
20
30
x[km]
0
10
20
30
t[min]

(d)

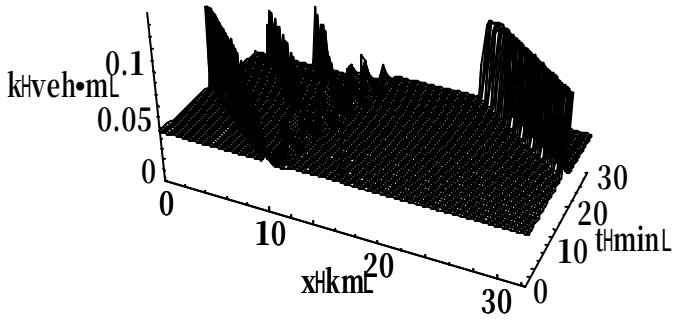
k[veh•m]
0.1
0.05
0
0
10
20
30
x[km]
0
10
20
30
t[min]

(e)

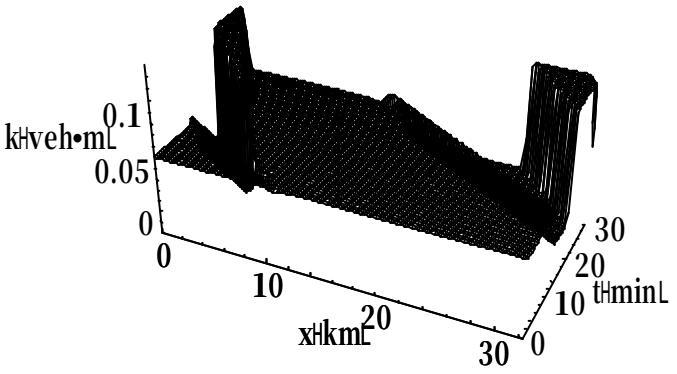
k[veh•m]
0.1
0.05
0
0
10
20
30
x[km]
0
10
20
30
t[min]

(f)

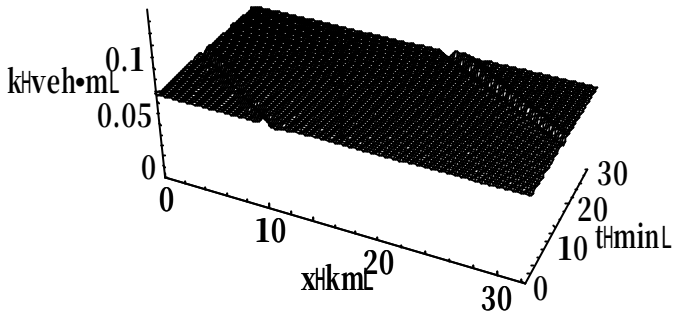

(g)

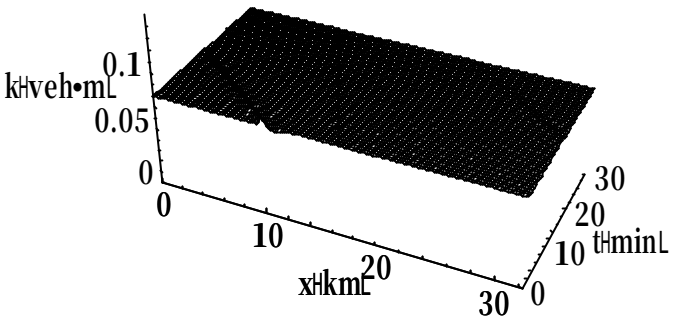

(h)

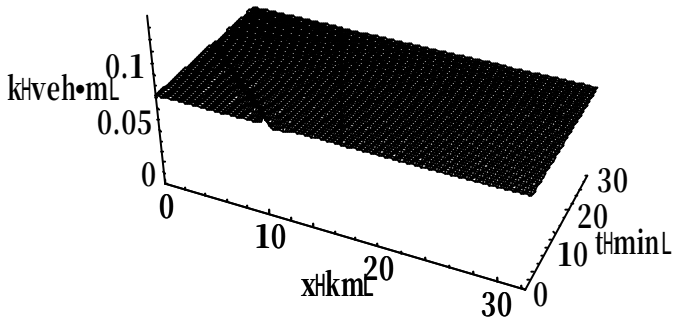

(i)

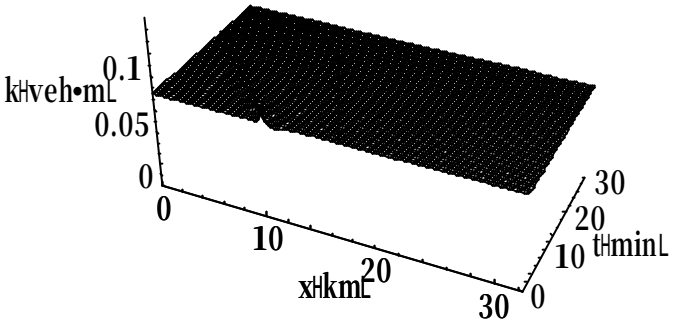

(j)

Figure 5.135. Temporal evolution of traffic on a ring of 32.2 km circumference with a homogeneous initial traffic and a localized perturbation of amplitude Δk_0 = 0.01 veh/m simulated by Jiang's FD scheme for: (a) k_0 = 0.03 veh/m; (b) k_0 = 0.035 veh/m; (c) k_0 =0.04 veh/m; (d) k_0 = 0.042 veh/m; (e) k_0 = 0.046 veh/m; (f) k_0 = 0.07 veh/m; (g) k_0 =0.077 veh/m; (h) k_0 = 0.08 veh/m; (i) k_0 =0.082 veh/m; (j) k_0 = 0.085 veh/m.

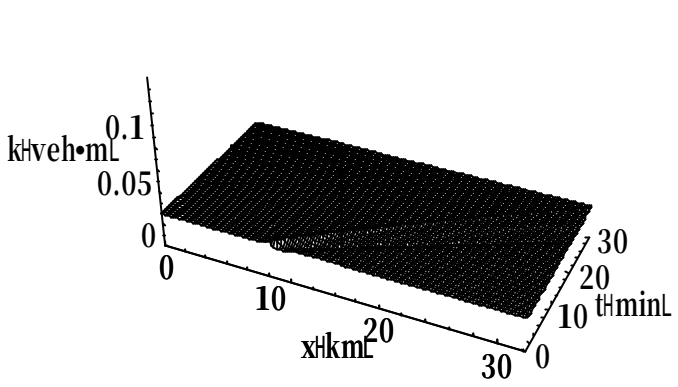
k[veh•m]
0.1
0.05
0
0
10
20
30
x[km]
0
10
20
30
t[min]

(a)

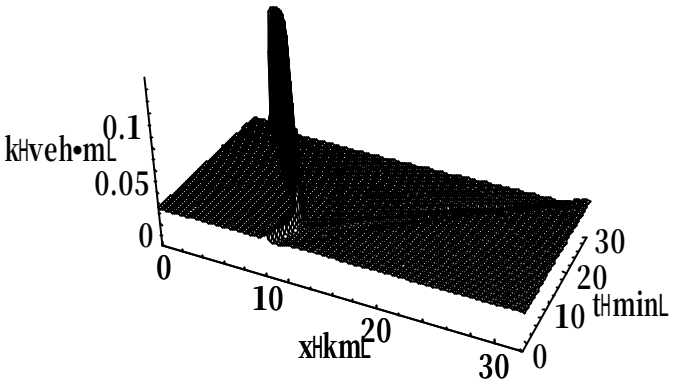
k[veh•m]
0.1
0.05
0
0
10
20
30
x[km]
0
10
20
30
t[min]

(b)

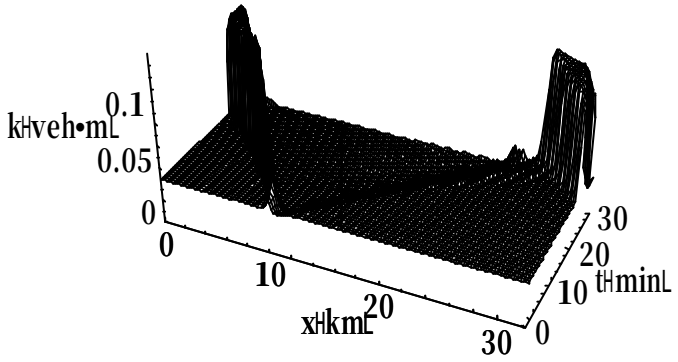
k[veh•m]
0.1
0.05
0
0
10
20
30
x[km]
0
10
20
30
t[min]

(c)

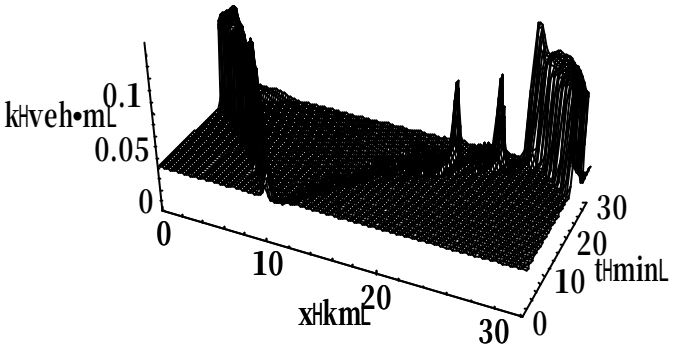
k[veh•m]
0.1
0.05
0
0
10
20
30
x[km]
0
10
20
30
t[min]

(d)

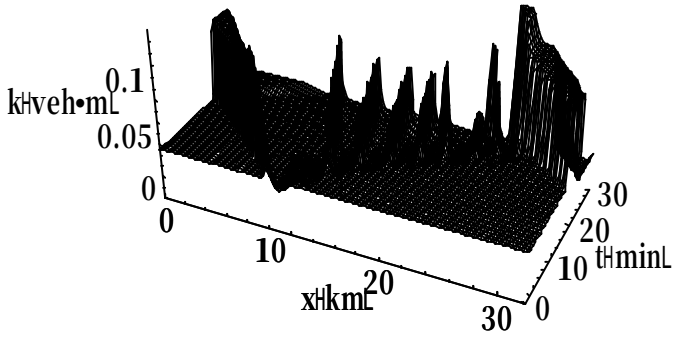
k[veh•m]
0.1
0.05
0
0
10
20
30
x[km]
0
10
20
30
t[min]

(e)

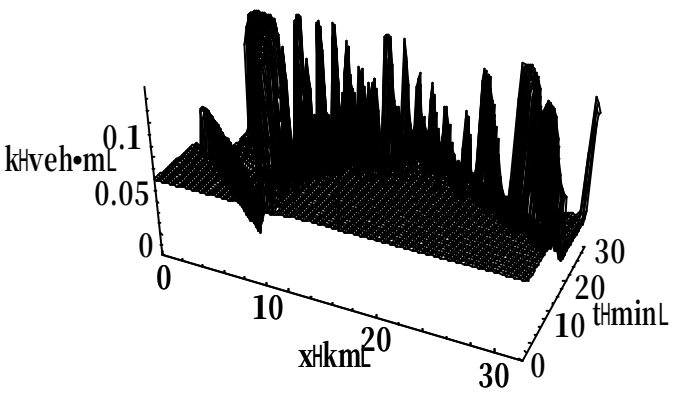
k[veh•m]
0.1
0.05
0
0
10
20
30
x[km]
0
10
20
30
t[min]

(f)

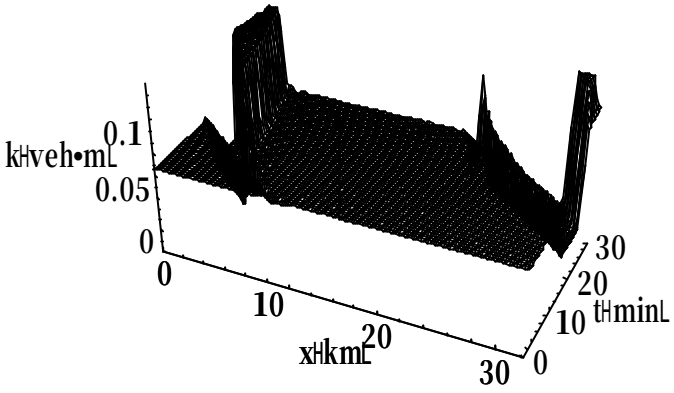

(g)

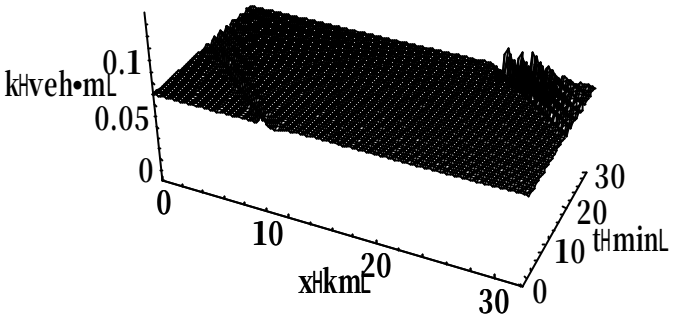

(h)

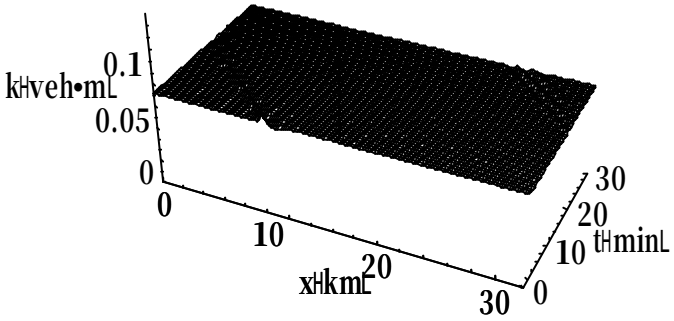

(i)

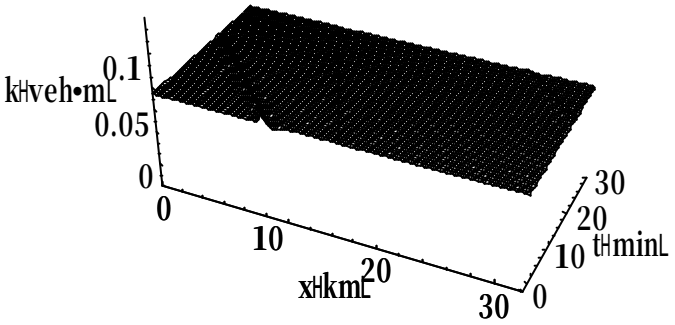

(j)

Figure 5.136. Temporal evolution of traffic on a ring of 32.2 km circumference with a homogeneous initial traffic and a localized perturbation of amplitude Δk_0 = 0.01 veh/m simulated by WENO FV scheme for: (a) k_0 = 0.03 veh/m; (b) k_0 = 0.035 veh/m; (c) k_0 =0.04 veh/m; (d) k_0 = 0.042 veh/m; (e) k_0 = 0.046 veh/m; (f) k_0 = 0.07 veh/m; (g) k_0 =0.077 veh/m; (h) k_0 = 0.08 veh/m; (i) k_0 =0.082 veh/m; (j) k_0 = 0.085 veh/m.

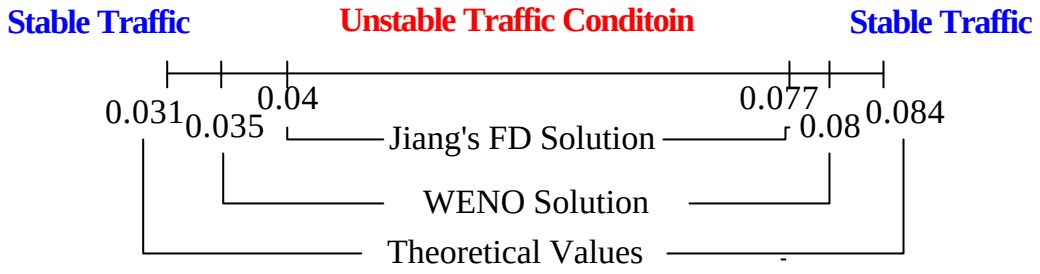

Figure 5.137. Comparison of down-critical density k_d and up-critical density k_u between Jiang' s FD and WENO FV solutions.

Table 5.5. Comparison of down-critical density k_d and up-critical density k_u between Jiang' s FD and WENO FV solutions.

Critical density / Solution	Down-critical	Up-critical
Theoretical	0.031	0.084
WENO FV	0.035	0.08
Jiang' s FD	0.04	0.077